The Role of Biomaterial Interactions in Peri-Implantitis

Fadi Barrak

2023

Submitted in partial fulfilment of the requirements for the degree of Doctor of Philosophy

Department of Materials

Imperial College London

This page intentionally left blank

Declaration of Originality

I hereby declare that the material presented in this thesis is my own work, except where otherwise appropriately referenced.

Part of this work resulted in three publications.

Copyright

Acknowledgement

I would like to take this opportunity to thank Professor Julian Jones for his guidance and support throughout my PhD at Imperial College. I would also like to thank members of Professor Jones's group who helped me with various aspects of my training and learning to use new equipment including Francesca Tallia for the ongoing general support in the lab, Agathe Heyraud, Yu-Chien Lin, Lloyd Zheng and Richard Sweeney with XRD and Mahmoud Ardakani with the SEM and FIB imaging. A special thanks to Siwei Li for his support and patience in assisting with cell culture work. Last but not least, I thank my wife and children for their patience and support which allowed me to fulfil my long term ambition.

Covid-19 impact statement

The covid-19 pandemic laboratory closures, delays in material delivery and wider consequences impacted this PhD project in that some of the follow up experiments were not completed. These include further investigation of the mechanism of the inflammatory process in chapter 5 and a follow up on the strength of cell attachment on the S53P4 bioactive glass surface in chapter 4.

Contents

List of Figures

List of Tables

List of Abbreviations

A – Annealed

AFM - Atomic force microscopy

APC – Antigen presenting cells

ASTM – American society for testing and materials

BAG - Bioactive glass

BCC – Body centered cubic

BH - BioHorizons® grade 5 titanium alloy implant

BL – Bone level

BLT-R – Bone level tapered Roxolid®

BLT-S – Bone level tapered grade 4

BME - β-mercaptoethanol

BMZ – basement membrane zone

BSA - Bovine serum albumin

CO - carbonyl

COOH - carboxyl

CP - Commercially pure

DAPI - 4′,6-diamidino-2-phenylindole

DI - Deionised water

DLS - Dynamic Light Scattering

DMEM - Dulbecco's Modified Eagle's Medium

DMSO – Dimethyl sulfoxide

DNA - Deoxyribonucleic acid

ECM – Extracellular matrix

EDTA – Ethylenediaminetetraacetic acid

EDX - Energy dispersive x-ray spectroscopy

EHT – Electron high tension

ELISA – Enzyme-linked immunosorbent assay

FBGC - Foreign Body Giant Cells

FBS - Foetal Bovine Serum

FDA – Food and Drug Administration

FITC - Fluorescein 5(6)-isothiocyanate

GAG - Glycosaminoglycans

HA - Hydroxyapatite

HBMSC – Human bone marrow derived stromal cells

HCA - Hydroxycarbonate apatite

HCP – Hexagonal close packed

HGF - Human gingival fibroblast

HMDS - Hexamethyldisilazane

ICP – Inductively coupled plasma spectrometry

ICP – OES – Inductively coupled plasma optical emission spectrometry

ISO – International organisation for standardisation

LPS – Lipopolysaccharides

MEM - Minimum Essential Medium

MMP - Matrix Metalloproteinases

MTT - 3-(4,5-dimethylthiazol-2-yl)-2,5-diphenyltetrazolium bromide

NC - Network connectivity

NFkB – Nuclear factor kappa B

NH - amine

NODLR-P3 - Nucleotide oligomerisation Domain Like Receptors-P3

OD – Optical densities

OH - hydroxyl

PAMP – Pathogen associated molecules

PBS – Phosphate buffered saline

PDGF - Platelet derived growth factor

PDL – Periodontal ligament

PE - Polyethylene

PET - polyethylene terephthalate

PMA - Phorbol 12-myristate 13-acetate

PMMA - polymethyl methacrylate

PTFE - Polytetrafluoroethylene

PU - Polyurethane

RGD - arginine-glycine-aspartate sequence

RNA - Ribonucleic acid

RNS – Reactive nitrogen species

ROS – Reactive oxygen species

RPMI - Roswell Park Memorial Institute medium

S100 - Pure SiO_2 glass

SBF - Simulated body fluid

SEM – Scanning electron microscopy

SiOH - Silanol

SLA – Sand blasted, large grit, acid etched

SO_3H - sulfonate

TE - Trypsin ethylenediaminetetraacetic acid

TEC - Thermal expansion coefficient

Tg - Transition temperature

Ti-CP4 - Grade 4 commercially pure titanium

TLR – Toll like receptors

TMB - 3,3’,5,5’ tetramethylbenzidine

TNT – Titanium nanotube

TTT - Time-temperature-transformation

Tx - onset temperature of crystallisation

UA – Unannealed

WD – Working distance

XRD – X-ray diffraction

Y-TZP - Yttrium-stabilized tetragonal zirconia polycrystals

ZDEC - Zinc diethyldithiocarbamate

μ-CT - Micro-computed tomography

This page intentionally left blank

Abstract

Dental implant treatment for the replacement of missing teeth has become mainstream in the dental industry today. The increase in the number of implants placed has also presented an increase in the number of complications seen in practice, such as peri-implantitis. Possible causes of peri-implantitis include foreign body reaction to implant particles released in the adjacent tissues, or bacterial invasion due to weak connective tissue attachments to implants. The aim of this PhD is to investigate particle release from implant fixtures and their potential effects on local cells *in vitro* and bioactive glass S53P4 (SiO_2 53.8 mol%, Na_2O 22.70 mol%, CaO 21.80 mol%, P_2O_5 1.70 mol%) as a potential substrate for achieving collagen attachment with a view to develop a clinically applicable modification to the implant abutment.

In vitro investigations of commonly used titanium alloys revealed significant toxicity and increased inflammatory response from local cell lines to grade 5 titanium alloy particles when compared to grade 4, Roxolid® (Ti15Zr) and zirconia. An ex vivo study confirmed particle release during implant insertion from all test implants, which was significantly higher with grade 5 tapered implants. Grade 5 particles demonstrated an ability to influence macrophage polarity towards the M1 phenotype. When the particles were cultured with S53P4 bioactive glass dissolution product the inflammatory response to grade 5 particles from local cell lines was suppressed and the macrophage polarity was affected towards the M2 phenotype. This indicates a potential anti-inflammatory property of S53P4 not previously described. An initial investigation of S53P4 as a potential substrate for collagen attachment was carried out using scanning electron microscopy (SEM) imaging. Further studies on the anti-inflammatory properties and collagen attachment on S53P4 are needed to understand the mechanism of cellular response to S53P4 and to identify its possible clinical application as a substrate on dental implants.

This page intentionally left blank

1. Introduction

Dental implant treatment is widely available as an effective means of replacing missing teeth with long term predictability(1, 2). Several factors have been suggested to influence implant success and there are various theories for the aetiology of late implant failure. In this chapter a literature review will provide an overview of the natural dentition in health and disease, relate this to the dental implant as a replacement for the tooth and present competing theories for the aetiology of peri-implantitis as the main cause of late failure. The emphasis of this project will be on the potential role of particle release from implant biomaterials in the onset of peri-implantitis, and possible materials that can provide resistance to implant failure. The subsequent four chapters will be on the experimental work carried out with the concluding remarks in the final chapter. This work has resulted in three publications.

The rational for this research is to improve the gap in knowledge with regards to the role of dental implant biomaterials in the onset and progression of peri-implantitis, and to investigate preventative strategies. This can have clinical, manufacturing and future research implications.

1.1 Literature review

1.1.1 Human dentition in health and disease

In health, the tooth has an intact periodontal ligament which securely holds the tooth in the alveolar bone of the jaw. The transmucosal anatomy, where the tooth emerges from the alveolar bone through the mucosa into the environment of the oral cavity consists of connective tissue attachments between the tooth cementum and the adjacent alveolar bone and gingivae (gums), followed by the more superficial junctional epithelium with hemidesmosomal attachments between the tooth enamel and the adjacent gingivae Fig. 1 (3). The healthy tooth will have no carious cavities, no inflammation within the pulp of the tooth or in tissues supporting the tooth and there will be no loss of supporting gum and bone.

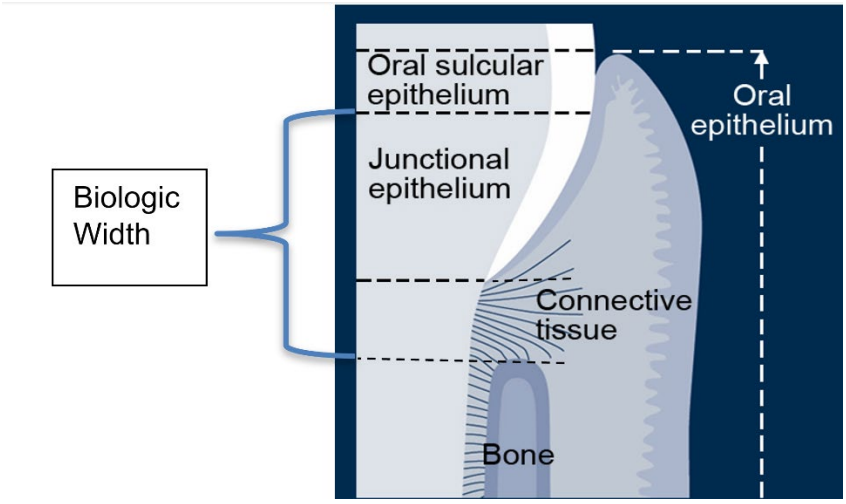

Figure 1. Dental gingival (gum) anatomy at the point of emergence into the oral cavity. Adapted from ITI speaker's library.

1.1.1.1 The transmucosal anatomy of a tooth

In nature, whenever a structure communicates between the deep tissues of the body, beyond the basal membrane zone (BMZ) of the skin or mucosa and the external environment, there is a potential for pathogens to invade. Hairs, nails and horns are structures that emerge from the dermis and do not penetrate the BMZ. Whereas teeth emerge from the jawbone into the hostile oral environment with its associated chemical, physical and microbial insults.

The anatomy of the junction between the tooth and the oral mucosa as the tooth emerges from the jaw into the oral cavity is depicted in Fig. 1. As the tooth emerges from the bony socket into the oral cavity there is a connective tissue attachment just above the crest of bone, which is then covered by the junctional epithelium. The collective name for the connective tissue attachment and junctional epithelium is the Biologic Width.

In healthcare, various devices that need to be implanted deep into tissues communicate with the external environment for various periods of time. The short-term use of intravenous catheters for a few hours to days does not need a strong connective tissue connection as that would complicate their removal. However, prostheses for replacing limbs, dental and maxillofacial implants, cochlear implants and long-term catheters for renal dialysis for example would

benefit from having collagen fibres from adjacent tissues inserting into the prosthesis at the entry point to provide a protective barrier against the external environment, as seen with natural teeth (Fig. 1).

Several processes or mechanisms are involved in the attachment process of the connective tissue fibres to the teeth and bone. Understanding these processes or mechanisms is paramount for the attempt to mimic this around artificial prostheses. The roots of teeth are held in place inside the jawbone via a fibrous joint (gomphosis) called the periodontal ligament (PDL), which is rich in blood supply and stem cells, with an important role in repair and regenerative processes around the tooth. The periodontal ligament allows tooth movement of 50-80 μm under occlusal load (biting) (4). This movement is possible due to the wavy pattern of the PDL fibres, which allow for elongation. Also, the PDL ground substance consists of 70% water allowing for a ‘shock absorbing’ property. Collagen fibres in PDL (mainly type I and III) have a high turnover compared to those in tendons and are therefore less mature and thinner in diameter (55 nm)(3). Type V collagen is found in the interstitial fibrils and between the fibril bands. Collagen IV, VI and XII are thought to play a role in remodelling of the PDL(3).

The PDL fibres insert in cementum at one end and bone at the other. The insertion is thought to be achieved via connections to non-collagenous proteins in the corresponding matrices which then calcify and ‘lock’ the fibres in. The calcified ends are referred to as Sharpey’s fibres. During bone remodelling, osteopontin and bone sialoprotein play an important role in detaching and reattaching of the fibres to the new bone laid down(3). Glycoproteins are thought to be of importance in the PDL attachment include fibronectin and tenascin, which is concentrated at the alveolar bone and cementum insertion sites. The rest of the ground substance consists of non-collagenous matrix proteins such as alkaline phosphatase, hyaluronate, glycosaminoglycans (GAG), proteoglycans and glycoproteins. These may play a role in the organisation of the ligaments(5). The main GAG is dermatan, a polysaccharide with anionic charge that can covalently bond to proteins to form proteoglycans. Therefore, there are important non-collagenous proteins (bone sialoprotein, osteopontin, fibronectin, tenascin)

and extra cellular matrix (ECM) ground substances (dermatan GAG) that play an important role in the PDL fibre attachment to the cementum and bone.

Fig. 2 depicts the junctional epithelium's very unusual anatomy in that there are 2 epithelial layers, a supra-basal layer connecting to the tooth via the internal basal membrane zone (epithelial attachment against the tooth) and basal layer with an external basal membrane zone separating epithelium from the underlying connective tissue.

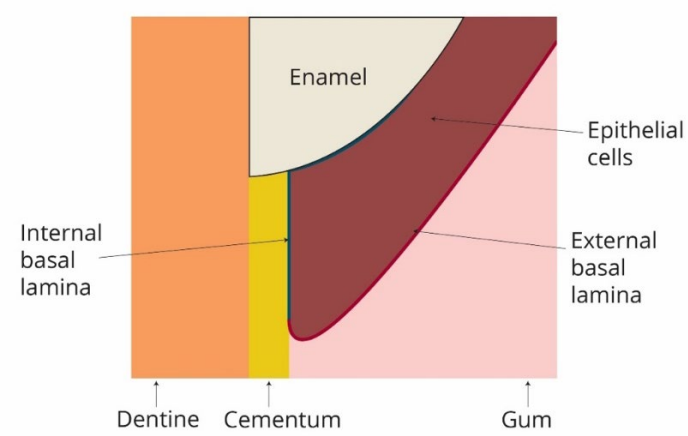

Figure 2. Junctional epithelium. Adapted from Kobayashi, K.(6).

The internal BMZ differs in its anatomy from other BMZ's in that hemidesmosomes attach to the tooth surface, the Lamina Reticularis is missing, and the ECM consists mainly of Collagen VIII and Laminin 332 (Fig. 3).

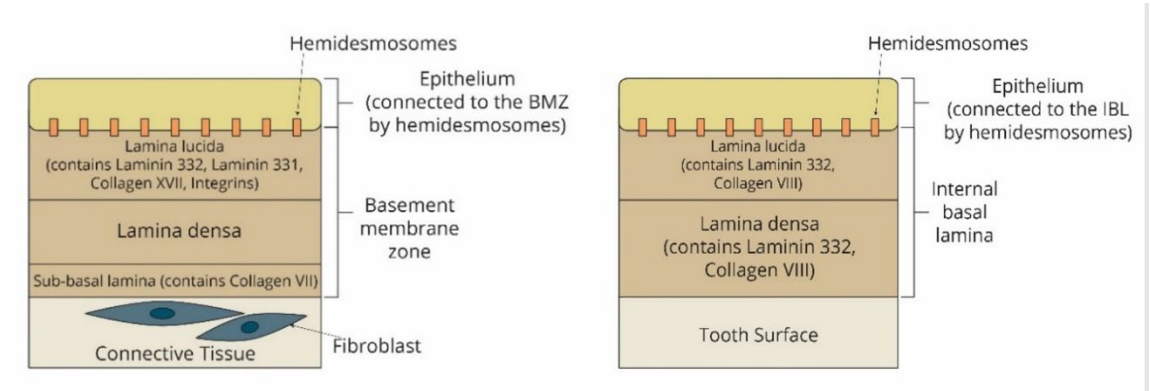

Figure 3. Left: Diagram of basement membrane zone in skin. Right: Diagram of basement membrane zone of gingival junctional epithelium. Adapted from Abdallah, M. N. et al 2017(7).

Laminin 332 is thought to be important in the soft tissue attachment mechanism; the ECM seems to play an important role in this (7). The collagen attachments between the root of the tooth and the gingival tissues (above the crest of bone) have a mechanical protective role for prevention of bacterial invasion as well as providing stability of the gum's position. This has important implications for dentists in the control of the cosmetic appearance of the gums around the tooth. If this barrier is disrupted by bacteria, inflammation and bone loss can result. The inflammatory process can cause release of matrix metalloproteinases (MMP) from macrophages and bacteria, resulting in the breakdown of collagen in the PDL and bone matrix, with subsequent tissue loss and pocketing around the teeth. This process is better known as periodontal disease.

Tooth loss can occur for a number of reasons including tooth decay, chronic periodontal disease (gum disease), trauma, and pathology such as cysts and head and neck cancer. Chronic periodontal disease will be expanded on further below due to its relevance to this research topic of peri-implantitis.

1.1.1.2 Chronic periodontal disease

Chronic inflammation of the gingivae (gingivitis) and the periodontal ligament (periodontitis) is caused by the buildup of plaque on teeth, restorative material such as fillings or crowns and dentures. Plaque is a bacterial biofilm in which stable communities of bacteria can be established when it forms on hard surfaces of the dentition as there is no shedding from the dental surface, unlike the oral mucosa (8).

The biofilm formation starts with the adsorption of salivary proteins and mucins on intraoral hard surfaces to form a pedicle onto which bacteria can directly attach. As the bacterial colony grows an extracellular polymer matrix is synthesised and deposited, allowing further attachment of microbes without direct access to the pedicle and the development of a thicker biofilm.

As the thickness of the biofilm increases, the diffusion of oxygen becomes limited due to the matrix which results in an increasingly anaerobic condition in deeper aspects of the biofilm. This results in an increasingly gram negative and anaerobic species which utilise periodontal tissues, blood supply and other microorganisms for nutrients, compared to the surface bacteria which tend to be more gram positive, aerobic or facultative anaerobic (such as streptococci), which utilise products in saliva as nutrients. Gram negative, anaerobic species that have been associated with periodontal disease progression include: Porphyromonas gingivalis, Prevotella intermedia, Tannerella forsythia, Treponema denticola, Fusobacterium nucleatum and Campylobacter species.

Prevention of plaque biofilm build up is the basic principle underlying oral hygiene protocols, such as brushing teeth in order to disrupt the biofilm and transition of bacterial species to the more gram negative and anaerobic species which are believed to be involved in the advanced periodontal disease. If the plaque buildup continues undisturbed tissue damage can take place as a result of direct bacterial action as well as the indirect host response, such as the release of proteolytic enzymes, pro-inflammatory cytokines (IL1β, IL6, TNFα) and complement activation. These can result in the loss of the periodontal collagen fibres and bone resorption. In an inflamed PDL, stem cells may have an impaired immunomodulatory function which can lead to an imbalanced immune response with an acceleration of osteoclastogenesis, inflammation and bone loss (9).

The loss of supporting tissue around the tooth gives rise to areas of pocket formation between the tooth and adjacent gums, resulting in micro-environments which are protected from the disruptive cleaning by tooth brushing. Other local factors such as poor restorative margins with an overhanging filling which the patient cannot access to clean also provide a micro-environment for undisturbed plaque buildup. This can cause tissue damage and further periodontal pocket formation, which in itself is a protected environment for the plaque and therefore allows for the propagation of the disease with further tissue loss until the eventual loosening and loss of the tooth (8).

The natural barriers around a tooth usually slow down or limit the pathological process through the physical collagen attachment barrier and the immune

response from the well vascularised periodontal ligament. The result of this protective mechanism is to create fibrous encapsulation of the inflammatory process (10) and limit the spread of infection. Hence, in patients with periodontal disease there can be isolated pockets around the root of the tooth where there has been an invasion of the barrier and tissue loss, but then the barrier is re-established lower down; this can slow the invasive process down.
The rate of disease progression is dependent on several factors, including the host's inflammatory response which can be an overreaction in individuals who are highly susceptible to periodontal disease. Other factors that affect the rate of disease progression include the patient's general health, smoking, oral hygiene, and immune status.

1.1.2 Dental implants in health and disease

1.1.2.1 Demand for dental implants

The demand for dental implant treatment as a means of replacing missing teeth is likely to grow with the ever-increasing population age and public awareness of this treatment modality(1). A general dental practitioner today cannot avoid dealing with dental implants in their day-to-day practice. Global figures for the number of implants placed per 10,000 population is summarised Fig. 4.

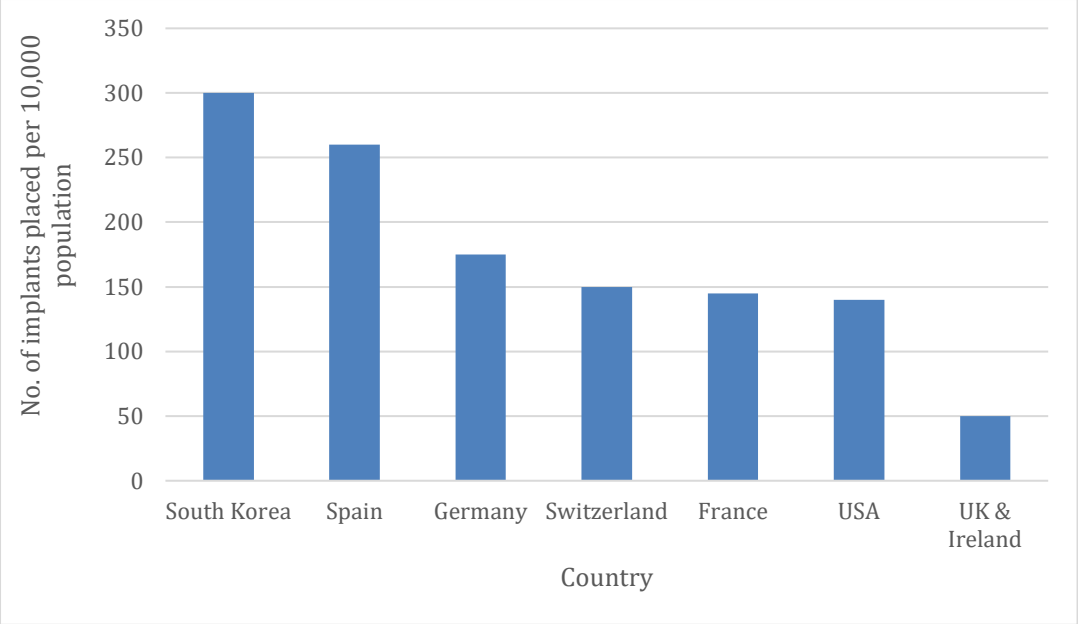

Figure 4. Dental implant placements per 10,000 population. Adapted from Straumann report 2016 (11).

The trend in the percentage of population over 65 years of age has increased dramatically and is forecasted to increase exponentially in the coming decades (Fig.5).

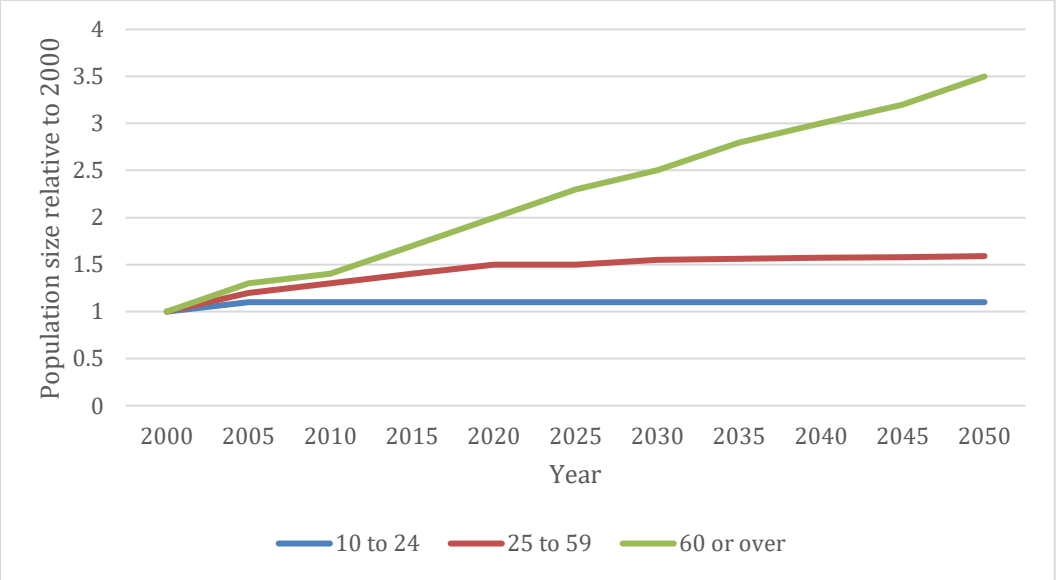

Figure 5. Increase in world population relative to 2000, by broad age group, 2000-2050. Adapted from United Nations (2015). World population Prospects: the 2015 revision (12).

The significance of the above projections includes:

1. As the percentage of the population over sixty is increasing, so is the need for implant treatment due to higher edentulism in the elderly.
2. Implant longevity is becoming more significant as patients are living longer.

Dental implant treatment can improve the quality of life for people with missing teeth. The improvement in chewing, speaking and patient satisfaction from placing two implants in the lower jaw to support the denture has been well demonstrated over the years (13, 14).

1.1.2.2 What is a dental implant?

A dental implant consists of two major components: the implant fixture which is designed to replace the root of a tooth and sits in the jawbone, followed by the crown which is the tooth part. The crown itself consists of the abutment, which is secured inside the implant with a screw, and the ceramic (or metal-ceramic) cover/ crown, which has the appearance of a natural tooth.

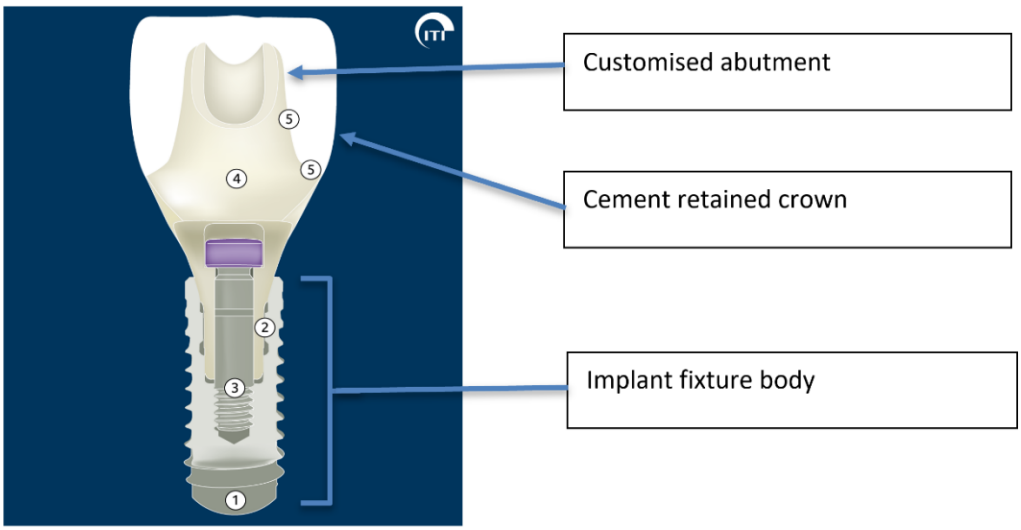

Figure 6. Implant components. Adapted from ITI speaker's library. 1. Implant fixture 2. Implant/ abutment interface (micro-gap) 3. Abutment screw 4. Abutment 5. Abutment fit surface.

Fig. 6 depicts a bone level implant which is the most commonly used implant; this refers to the fact that the implant fixture is set in bone, with the implant-abutment junction at bone level. This contrasts with the tissue level implant (Fig. 7 and 8) where the implant-abutment junction is at gum level and remote from the bone.

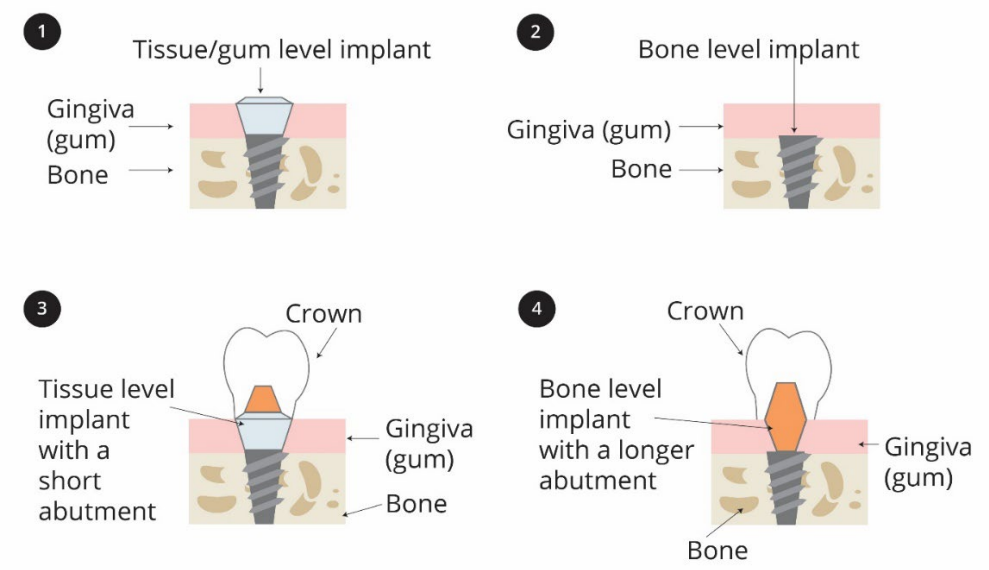

Figure 7. Schematic of a tissue level versus bone level implant: 1. Tissue level implant 2. Bone level implant 3. Restored tissue level implant with a short abutment 4. Restored bone level implant with longer abutment. Designed by Dr F Barrak, illustration by Kitty Lungley.

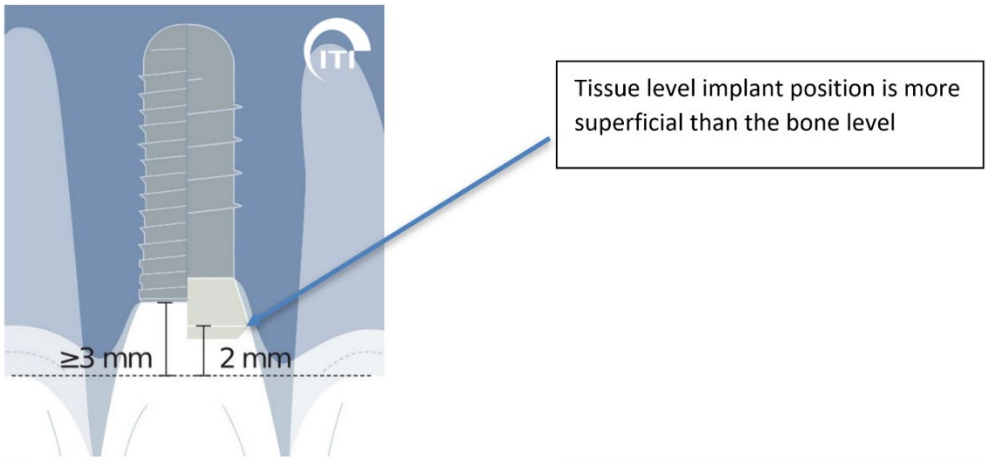

Figure 8. Bone level implant on the left half and tissue level on the right half of the image. Adapted from ITI speaker's library.

Bone level implants are much more widely used and available commercially

because their deeper position below the gum allows for adjustment in angulation of the crown where necessary to improve the aesthetic and functional position. The tissue level implant positioning must be exact, as there is less room to compensate for the fixture angulation as depicted by the green ‘safe’ and red ‘danger zones’ in Fig. 9.

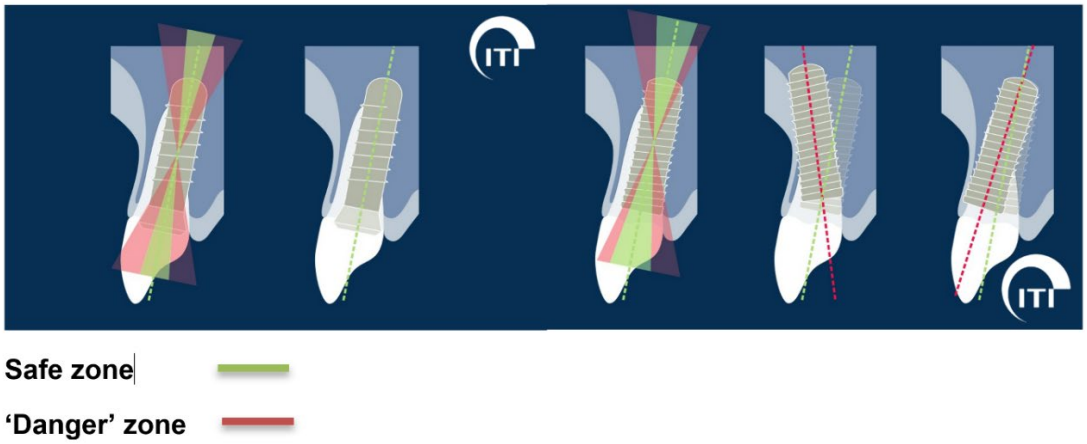

Figure 9. . Tissue level implant (left) has a much smaller ‘safe’ zone of varying angles of placement depicted in green, compared to a bone level implant (right). Tissue level implant placement needs to have more precise placement. Adapted from ITI speaker’s library.

Dental Implants have high survival rates over a 10 year period in which patients have been followed up for (15). However, implants are still susceptible to failure secondary to inflammation in the supporting tissues, referred to as peri-implantitis (15). There has been a considerable amount of clinical research carried out on peri-implantitis, ranging from aetiology and risk factors to its management. Despite the sizable volume of work on the subject there are still no conclusively effective treatment modalities (16). There is still controversy on the aetiological origin of the onset of peri-implantitis (17).

1.1.2.3 Bone healing around dental implants.

Surgical trauma to the bone during the osteotomy drilling process causes bleeding from the alveolar bone marrow due to damage to the vasculature within the bone marrow. On insertion of the implant, its surface becomes impregnated with a fibrin coagulum, neutrophils and macrophages. Subsequently, fibroblasts

infiltrate the site, forming granulation tissue and angiogenesis commences. Sequestrated, non-viable bone fragments from the surgery are then removed by osteoclasts migrating into the site; this starts the process of new bone formation mediated by factors released from bone matrix breakdown by the osteoclasts. Mesenchymal stem cells and fibroblasts from the adjacent alveolar bone differentiate into osteoblasts which lay down immature bone matrix, known as osteoid. This is subsequently mineralised to form immature woven bone. Some of the woven bone is formed directly on the implant surface through differentiation of pre-osteoblasts to active osteoblasts, while some of the bone is generated by extension from local trabecular bone, referred to as distance osteogenesis. In humans, woven bone formation takes approximately twelve weeks and mature lamellar bone can takes six months to form (18).

At the time of implant placement, achieving stability of the fixture is required to ensure a stable surface on which new bone can grow. If the implant is mobile, fibrous tissue is likely to form rather than bone. This initial stability of the implant at the time of surgery is termed primary stability and is achieved through mechanical engagement of the implant threads in the alveolar bone. However, this stability is reduced during the healing process as a result of bone remodelling which involves resorption of the bone in contact with the implant and deposition of new bone. Formation of new bone and osseointegration of the implant brings about the secondary stability, which is long lasting in a healthy implant. Fig. 10 demonstrates the temporal relationship between primary and secondary stability of the implant graphically and highlights a period of dip in implant stability at approximately 3 weeks post-surgery when the stability is compromised as the primary stability is lost due to remodelling and the secondary stability is being established with new bone formation (18).

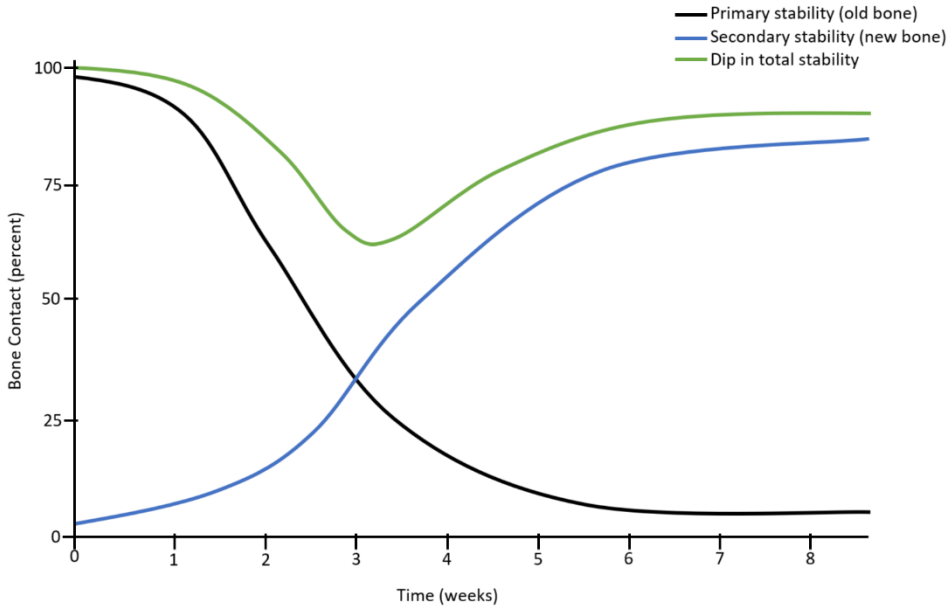

Figure 10. Graphical representation of the temporal relationship between primary mechanical stability (black line) and secondary osseointegration stability (blue line) of a dental implant. The period of drop in total stability when primary stability is reduced and secondary stability in still being established is depicted with the green line showing a dip in stability at 3 to 4 weeks post placement of implant. Adapted from Villar C.C (18).

1.1.2.4 Healthy implant

In health the peri-implant tissues will be free from inflammation, swelling, suppuration (pus discharge), the alveolar bone will be integrated with the implant surface and the transmucosal section will have weak hemidesmosomal connections with the implant surface. Clinically, there would be no distinguishing features between the gums around the tooth or implant. However, on examination the probing depths around the implant may be deeper than around the tooth and the papillae (gum between adjacent teeth) may be blunted (19).

1.1.2.5 Early and late implant failure

Implant failures that occur before the crown is fitted and loaded in occlusal function are referred to as early failures and are likely to be due to the failure of the implant to integrate following surgery. The causes of early implant failure include post-operative infection, the risk of which may be reduced with a prophylactic dose of antibiotics; there is some evidence to suggest a reduced rate of infection with the use of single dose of pre-operative antibiotics, however, there are conflicting opinions on this (2). Poor surgical technique with overheating damage to the bone resulting in osteonecrosis, and a lack of bone implant contact following implant placement can result in fibrous encapsulation as opposed to osseointegration (2). These can subsequently result in early implant failure. Systemic predisposing factors for early implant failure include smoking, immunocompromised patient, and medications such as selective serotonin reuptake inhibitors (20).

Late implant failure refers to the loss of an implant after successful integration has taken place. This research is in relation to late implant failures as a result of peri-implantitis which is the main cause of late implant failure and will be the focus of the rest of this work.

Comparative anatomy and disease progression of teeth and dental implants

As dental implants emerge from the jawbone through the mucosa into the oral cavity, the soft tissue surrounding the per-mucosal aspect follows the same sequence of having connective tissue over the bone, followed by epithelium (the biologic width) as in teeth. However, the key differences are that implants do not have a periodontal ligament and the connective tissue covering the bone does not attach to the implant (Fig.11) but runs parallel or circumferentially around the neck of the abutment in a bone level implant (or the smooth collar of the tissue level implant) (10, 21).

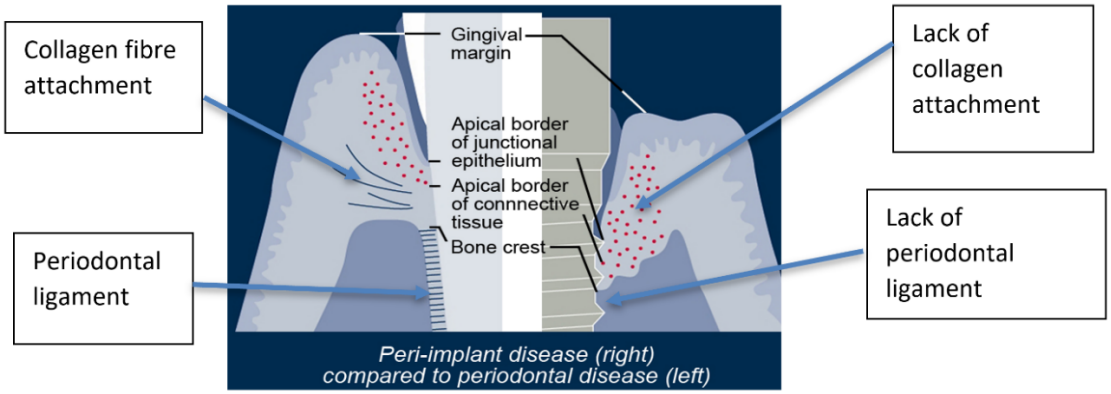

Figure 11. Comparative anatomy of tooth and implant. Adapted from ITI Speaker's library.

The lack of collagen attachment around the neck of implants means that the physical barrier against bacterial invasion, advancing inflammation and recession is missing (10). The rich blood supply and stem cells normally found around the natural tooth are also reduced due to the lack of the periodontal ligament (3). Fig. 12 shows the contrast between the natural tooth where inflammation is encapsulated in pockets and an implant where the physical barrier of collagen attachment is lacking thereby allowing rapid spread of inflammation to the bone. Therefore, inflammation around an implant can progress much faster and spread around its circumference with significant bone loss. This process is referred to as peri-implantitis and can result in catastrophic bone loss as shown in Fig. 13 (10, 15, 21-23). The aetiology and clinical features of peri-implantitis are similar to that of periodontitis, in that inflammation as a result of bacterial colonies and the local host response results in the damage and loss of soft and hard tissue support for the implant (10). However, the disease onset and progression in peri-implantitis is different with an earlier onset of bone loss and a non-linear progression (15).

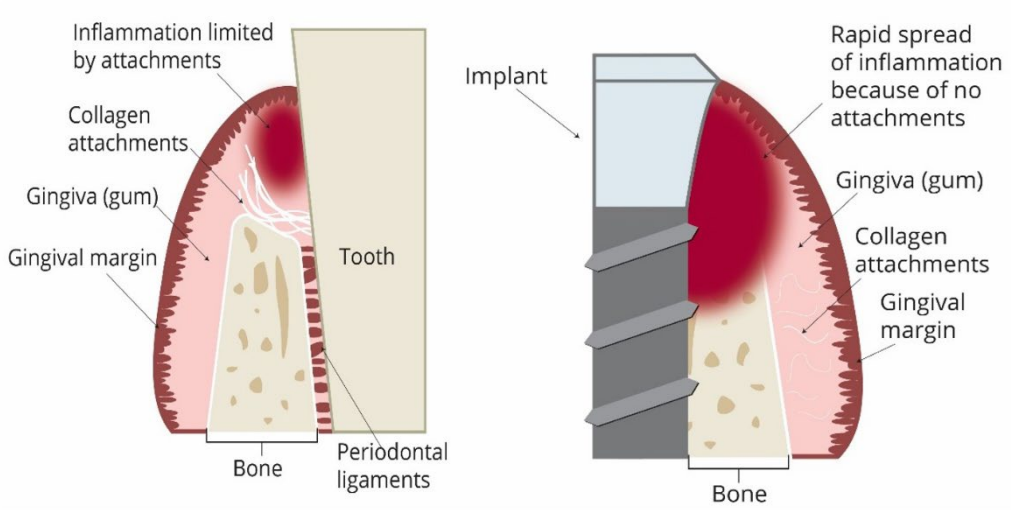

Figure 12. Diagrammatic comparison of the inflammatory infiltrate extension on a tooth surface (left) and an implant surface (right). Adapted from Salvi, G.E. (10).

(10)

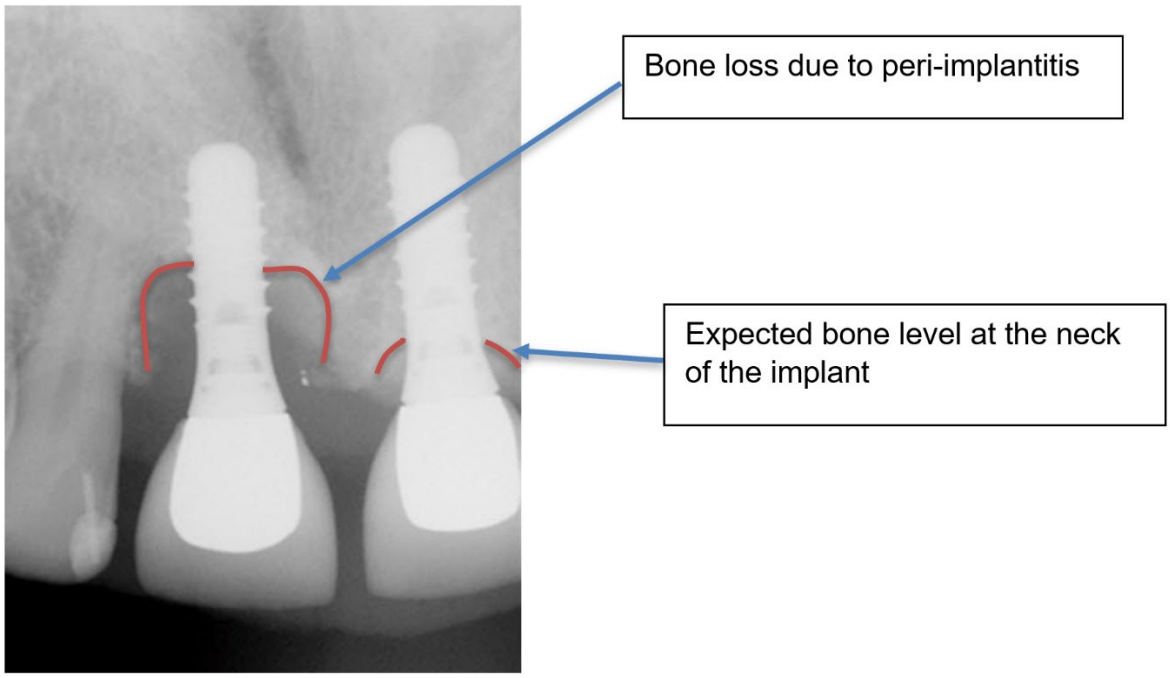

Figure 13. Radiograph of dental implants depicting the vertical bone loss appearance pathognomonic of peri-implantitis. Adapted from ITI Speaker's library.

Further complications with dental implants develop when there is bone loss around the neck of the fixture, including aesthetic compromise, further tissue loss with the advancement of the inflammatory process and increased risk of implant

fracture secondary to the loss of the bone support. This loss of bone can be very dramatic with significant consequences to the patients where they can become worse off from where they started as further reconstruction or restoration will be more complicated with compromised results, if at all possible (10, 15, 21-23).

1.1.2.6 Aetiology of peri-implantitis

The current consensus for the aetiology of peri-implantitis is that it is plaque associated implying a bacterial origin (19).

Some researchers believe that peri-implantitis may start as a foreign body reaction, which then develops into an infection with secondary bacterial invasion (24), as opposed to having a primary bacterial aetiology. There is, however, a consensus agreement that a history of periodontitis makes the individual more susceptible to peri-implantitis (19). There may be a complex interaction between the materials used, the bacterial biofilm and the patient's immune response, which may be over-reacting to the stimulus.

Other suggested causes of peri-implantitis include the presence of peri implant cement adjacent to the implant below the gum level which results in an inflammatory reaction to the cement material with subsequent bone loss. This would occur following restoration of the implant crown using any of the various dental cements to secure the crown on the implant abutment. Many clinicians use screw retained crowns in order to avoid cement, partly for this reason but also as the screw retained crown can make crown retrieval, if required, easier than with a cemented crown. Limited evidence has also been linked peri-implantitis to poorly positioned implants that hinder oral hygiene measures. The evidence for occlusal overload and peri-implantitis is inconclusive. Although he evidence for the link to bio corrosion and particle release as a cause of peri-implantitis is considered as yet to be determined (19), there is some evidence to suggest that particles emanating from implants are deposited into the surrounding tissues, which may play a role in implant failure because of the tissue reaction (25, 26). This could be significant as one must consider the implant material and its constituent metals such as the presence of vanadium in titanium alloy (Ti6Al4V), termed Grade 5 titanium alloy. The Grade 5 alloy has been shown to cause a tissue inflammatory

reaction in contrast to the grade 4 commercially pure (CP) Ti, or the Roxolid® alloy of Ti (85%) and Zr (15%) (Fig. 14) (27).

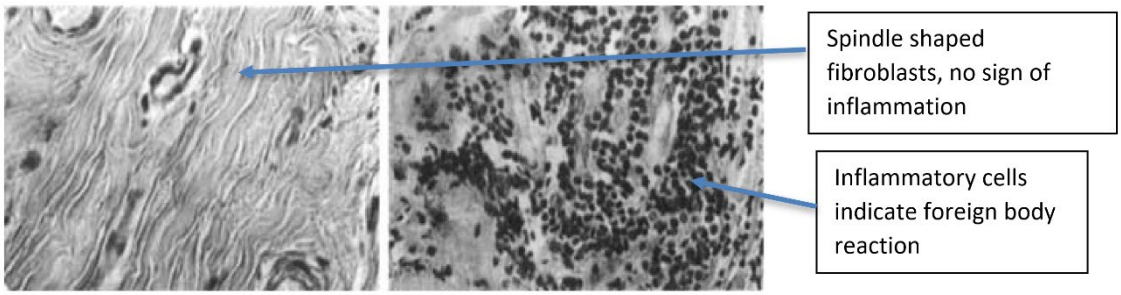

Figure 14. Micrograph of tissue in contact with implants made of commercially pure titanium (left) and Ti6Al4V alloy (right). Scale not available. Adapted from Steinemann 1998 (27).

Studies have demonstrated that fibroblasts proliferate successfully on Ti, Zr, Ta, Nb, but not when in contact with Cu, Mo and V. There was complete inhibition of osteoblast growth when cultured on pure discs of V, Ag, Zn and Fe and partial inhibition with Sn and Al. There was no inhibition on contact with Ti and Zr (27).

Although the consensus opinion for the aetiology of peri-implantitis is of a bacterial origin (19), it is important to consider other theories and the emerging evidence. Hence the importance of this research to investigate the potential role of particle release in peri-implantitis and the influence of the various materials currently used in implant fixtures.
The various theories put forward above have been summarised in Fig. 15 (17).

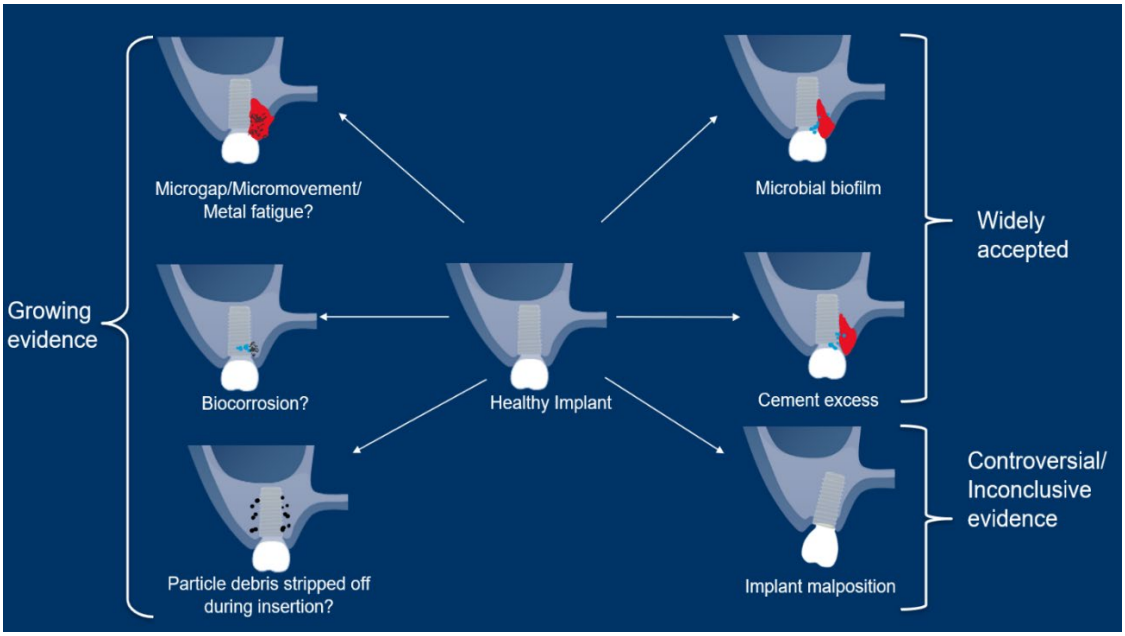

Figure 15. . Diagram summarising the theories for the aetiology of peri-implantitis. Adapted from Fretwurst et al. 2017 (17).

Although implants are considered to have very high survival rates, 94% with 10 years or longer follow up periods (28), increasing numbers being placed globally is causing a growing awareness of their limitations: the lack of connective tissue attachment in the biologic width and peri-implantitis.

There is no agreed or effective protocol for the treatment of peri-implantitis which, once established, has a high rate of recurrence (16). Derks and Tomasi's (15) epidemiologic review revealed that 1 in 5 implants placed develop peri-implantitis after 3.4 to 11 years in functional loading. However, the definition of peri-implantitis has historically been inconsistent; this was due to disagreement on the threshold bone loss before a diagnosis of peri-implantitis can be made (varied from 0.5 mm to 4 mm of bone loss between different groups). More recently a consensus was reached for the diagnosis of peri-implantitis (19). Future studies on peri-implantitis will hopefully be more standardised with the agreed diagnostic criteria, even though the aetiology is still debated.

1.1.3 Titanium properties

Titanium is found naturally as an oxide in either the stable Rutile phase, or a metastable phase such as Anatase or Brookite. Irreversible phase transformation from Anatase to Rutile takes place at 600°C as a result of reconstructive breaking and reforming of bonds, which results in 8% volume contraction and hence higher density of Rutile phase. Ti is a transition metal with a hexagonal closed packed (HCP) crystal structure (alpha phase) up to 882.5°C (the transus temp) beyond which it is transformed to the body centered cubic (BCC) (beta phase). Titanium's melting point is 1678°C. Due to its incomplete d-shell Ti is able to form solid solutions with certain elements such as Zr (15).

In implant dentistry titanium is used as an alloy, or in its commercially pure grade 4 form containing traces of Fe, C, O, N, which provide more yield strength compared to lower grades, without changing the Young's modulus which is dependent on the chemical bonds rather than the microstructure. Grade 4 commercially pure titanium (Ti-CP4) mainly consists of the alpha phase with spontaneous TiO_2 layer formation, rendering it biocompatible.

The most commonly used Ti alloys are the Ti6Al4V (Grade 5) and Ti15Zr (Roxolid® Straumann Group). Ti6Al4V has dual alpha and beta phases, with Al as an alpha phase stabiliser and V as a beta phase stabiliser, which improves the strength and physical properties. Ti6Al4V has higher strength with a lower coefficient of elastic mismatch with bone, however, it is more prone to corrosion due to the reduced surface oxide layer (15, 17, 29).

Zr is a transition metal with phase transition temperature similar to Ti. Ti15Zr has a binary alpha phase with smaller grain size, thereby increasing the surface area for layer of oxides, which enhances the material's corrosion resistance when compared to Ti6Al4V, but has reduced strength (30). Table 1 summarises the properties of the currently commonly used materials in dental implants.

Table 1 - 1. List of dental implant material properties (31-33)

Material	Modulus of elasticity (GPa)	Tensile strength (MPa)	Yield strength (MPa)	Reference
Ti-CP4	104	550	483	(31-33)
Ti6Al4V	113	930	860	(31)
Roxolid	98	850	849	(32, 33)
Zirconia (Y-TZP)	200	>1200	900	(32, 33)

Some metals are susceptible to corrosion, following interaction with tissue fluids resulting in hydrolysis (decomposition of a substance by water). An electrochemical reaction which results in ion release can give rise to hydroxides, hydrous oxides and oxides, which can result in a foreign body reaction, giving rise to tissue loss. With CP titanium, an oxide layer (3-10 nm thickness) forms within seconds of being exposed to air or tissue fluid; this oxide layer may inhibit Ti dissolution (27).

Titanium particles have been shown to start an inflammatory response with the release of IL1β, IL6 and TNFα from macrophages. This inflammatory reaction is accompanied by increased bone loss through osteoclastic activity and reduced osteoblastic activity (34). The inflammatory response results in macrophage recruitment with their subsequent release of MMP and activation of the complement cascade. Particles can be released for various reasons, including friction during fixture insertion, wear between the implant and abutment interface, corrosion and following use of metal instruments on the implant surface for cleaning and debridement (35, 36).

1.1.4 The role of tissue response in peri-implantitis

Consensus opinion suggests a bacterial aetiology for peri-implantitis (19). However, there is a growing school of thought and research efforts to investigate the potential role of titanium and titanium alloy particles in the onset of the inflammatory process in peri-implantitis (37). The orthopaedic community has accepted the role of particle release in aseptic osteolysis around hip replacement implants (38-40). The mechanical and tissue dynamics of orthopaedic prosthesis

are very different to the oral environment, nevertheless this is worth investigating as certain alloys and surface properties may play a significant role. The bacterial involvement could be due to the fact that dental implants are transmucosal, emerging from the alveolar bone through a thin layer of weakly connected soft tissue and into the oral cavity with its rich bacterial flora and the various fluids that moderate the chemistry and pH of the local environment. The orthopaedic and veterinary surgeons encounter similar challenges when they are working with transcutaneous prosthesis for replacement of limbs. This issue of bacterial invasion is also of importance in other fields whenever a prothesis such as a canula or catheter needs to be transmucosal for long periods. Despite the clear bacterial involvement in peri-implantitis, there is a possible foreign body inflammatory reaction as the aetiological origin which then allows bacterial invasion as a secondary, or synergistic factor (41).

In order to understand the potential factors involved in the aetiology of peri-implantitis it would help to consider the tissue response to the fixtures from the time of surgery and implant placement, as this is where the initial tissue response and subsequent healing takes place, both of which may be influenced by the reaction to the materials used. The initial response to surgery and implant fixture placement involves the innate immune system whereby the trauma to the soft tissues and the alveolar bone from the surgical procedure causes damage to blood vessel and ECM. This results in an inflammatory reaction mediated by a cascade of events, the initial part of which is summarised in Fig. 16 (42).

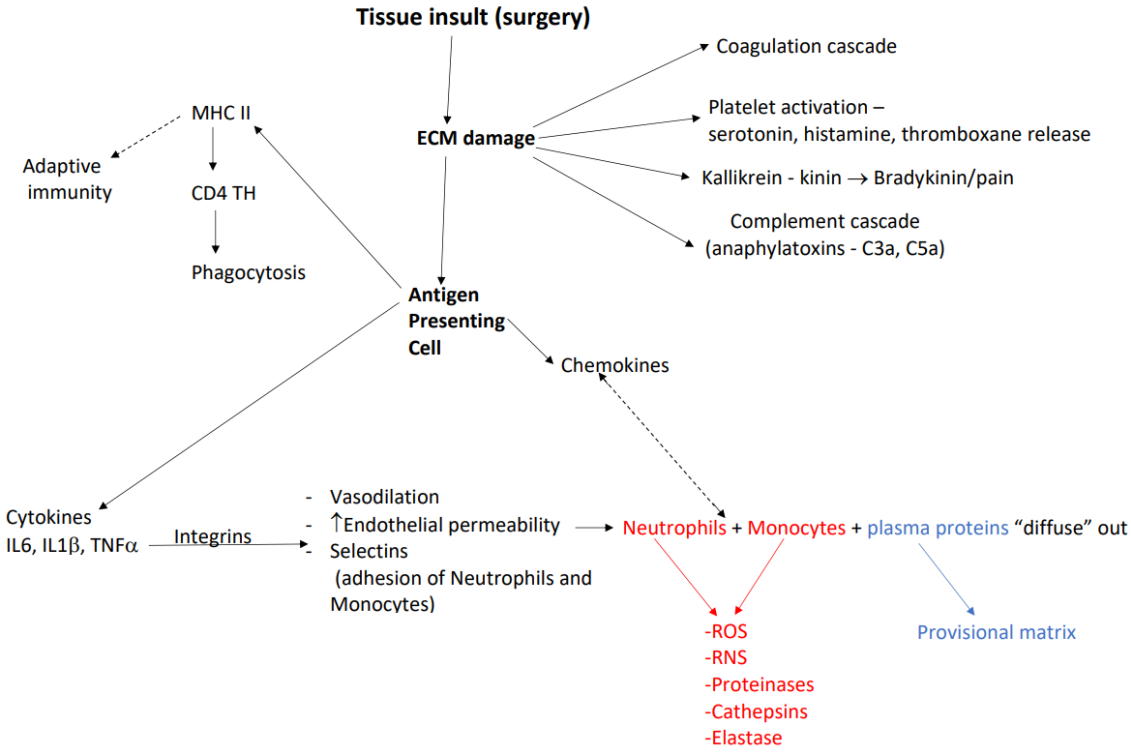

Figure 16. Flow diagram of the initial inflammatory response to implant placement. Design and illustration by Dr F Barrak.

At the time of surgery, the drilling process results in in the exposure and release of matrix proteins which activate the innate immunity cascades including the coagulation pathway, platelet activation, kallikrein - kinin pathway and the complement cascade (37, 42, 43). The latter results in enhanced inflammatory response through C3a, C5a which act as anaphylatoxins by activating histamine and serotonin release from mast cells resulting in vasodilatation, increased permeability, lymphocyte chemotaxis as well as opsonisation of contaminating pathogens during the surgery.

The damaged ECM components and bacterial Lipopolysaccharides (LPS) also activate the Antigen Presenting Cells (APC) locally through Toll-like receptors (TLR). The activated APC will release Cytokines (IL1β, IL6, TNFα) which will cause vasodilation and interact with the local endothelial cell integrins to bring about increased permeability and release of selectins to provide adhesion for circulating neutrophils and monocytes and enable their 'seeping' out into the tissues at the injury site. Once the cells are in the ECM chemokines released by

the APC (CXCC8) will 'guide' neutrophils and monocytes from the blood vessels to the APC at the injured location. The neutrophils and now macrophages will engulf foreign bodies, pathogens and damaged cells by endocytosis.
The APC will also activate the appropriate CD4 cells by presenting the phagocytosed antigens on the MHCII receptors which will result in phagocytosis as well as developing adaptive immunity. The latter can cause release of Reactive Oxygen Species (ROS), Reactive Nitrogen Species (RNS), proteinases and cathepsins.

The increased permeability of the local vessels also allows for proteins from plasma to 'seep' out into the tissues and aid in the formation of a new provisional matrix. Biomaterial surface properties can affect, or through design, guide the subsequent tissue response. The initial phase following the insertion of a device involves the attachment of proteins from the blood stream and local tissues to the substrate surface. The type of protein that is attracted to the surface will, to a large extent, depend on the surface properties of the biomaterial. The initial proteins may be displaced by others with a higher affinity to the surface, the Vorman effect. The surface proteins play an important role in the local cell interactions and can be used to guide this initial response to the implant (37).

The inflammatory process is a complex network involving cross reacting factors which can have positive and negative feedback loops affecting different parts of the network by amplification or limiting the responses. Although certain elements of the inflammatory response are identified and better understood, the overall process is far from being a linear cascade of events which can be systematically worked out and controlled in isolation and we still do not have the complete picture (42). This may partly explain the lack of agreement on the aetiology of peri-implantitis, the potential role of particles in the onset of the inflammatory process around dental implants and the potential influence of the biomaterials we are currently using in our daily clinical practice. Fig. 17 is an outline of some the events that may contribute to the emergence of peri-implantitis, including the potential role of Ti/ Ti alloy particles.

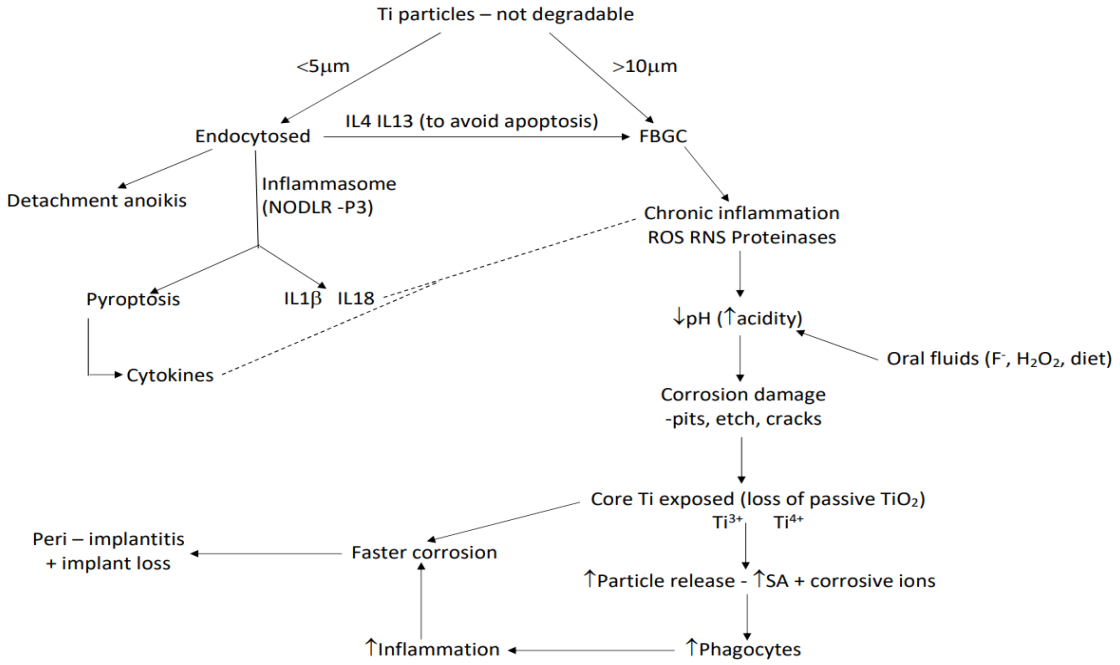

Figure 17. Flow diagram of sequence of events leading to corrosion and inflammation in tissues adjacent to implants. Design and illustration by F Barrak.

At the time of implant placement titanium particles have been shown to be released due to shear forces on the micro roughened implant surfaces (44). Particle release can also take place as a result of wear at the implant – abutment junction and due to corrosion. These particles are not degradable and those of less than 5 µm can be phagocytosed by macrophages in local tissues and on the implant surface. This may result in the disruption of cellular function and the detachment of the phagocyte from the matrix or substrate and the resultant anoikis (cell death as a result of detachment). The lysosome can rupture and release ROS, RNS and proteinases, activating the nucleotide oligomerisation domain like receptor-P3 (NODLR-P3) inflammasome formation and activation of Capsase 1 with the subsequent conversion of pro-IL1β and pro-IL18 to active IL1β & IL18 (Fig. 17). The inflammasome may also result in pyroptosis (inflammatory cell death) which will also result in the release of cellular components including cytokines. The cytokines thus released from the affected cell will result in enhancing the inflammatory response (37, 40, 45).

Phagocytosed particles larger than 10 µm can result in apoptosis, or the cell may avoid apoptosis and instead through the release of IL4 and IL13 promote the

fusion of the cells and formation of foreign body giant cells (FBGC) resulting in chronic inflammation (37).

Particle endocytosis and inflammasome activation, or FBGC formation result in enhancing the inflammatory process and potential chronic inflammation which results in ROS, RNS, proteinase release. The chronic inflammation results in a reduced pH in the local environment, which is often exacerbated by oral fluids including fluoride, H_2O_2 and dietary acids. The chronic drop in pH can cause corrosive damage to titanium resulting in surface damage in the form of pitting, etching and cracks (46, 47). This process can, over time, result in the loss of the passive TiO_2 layer, which can be permanent, exposing the titanium core which become ionised (Ti^{3+}, Ti^{4+}) with reduced potential for osseointegration (47).

The loss of the passive layer can take place at pH 6, very close to the salivary resting pH of 6.3-7.0 which can drop to pH 3.5 for short periods in the presence of acidic drinks (46). Exposure of the core titanium to electrolytes results in further corrosion. Once crevices and cracks develop, the area of stagnant fluid becomes depleted of oxygen with a further drop in pH, resulting in a potential propagation of the corrosive process with pitting and delamination of the surface (47). Macrophages and FBGC (and bacteria) can adhere to the implant surface where they provide a 'protected' environment between the cell membrane and the implant surface for the release of ROS, enzymes and acids which in phagolysosomes can have as low as pH 4 (37).

The corrosion products influence the macrophages to release inflammatory cytokines. Also, the increased number of particles and surface area encourage further phagocytosis. The process of inflammation, corrosion, surface damage and further inflammation can become self-propagating and further amplified in the presence of physical stresses such as the micro motion of the implant and mobility at the micro gap of the implant-abutment junction. This can result in faster corrosion and eventual clinically detectable peri-implantitis, bone loss and implant loss (47).

1.1.5 Possible inflammatory pathway at cellular level

The activation of the inflammasome is thought to be as a result of the APC/ macrophage being primed first via the TLR activation by extracellular pathogen associated molecules (PAMP) such as LPS. Activated TLR will result in nuclear factor kappa B (NFkB) transcription with the resultant synthesis of pro-IL1β, pro-IL18 and TNFα ready for their release which requires caspase 1 activation. Internalisation of material (e.g. Ti particles) directly into the cytosol, or by endocytosis (which results in rupture and release of the lysosome contents) causes disruption and activates the NLR-P3 inflammasome complex assembly and subsequent activation of caspase 1 to convert pro-IL1β and pro-IL18 to their active forms to be released and enhance the inflammatory response. There is a possibility that priming of macrophages can take place by TNFα via cytokine receptors, in addition to the priming via TLR activation by PAMP (Fig.18) (40, 45, 48). An initial inflammatory response in a sterile environment with no bacterial components can still result in priming the cell for inflammasome activation. This is thought to be a possible mechanism for the sterile osteolysis seen in orthopaedic prosthesis loosening.

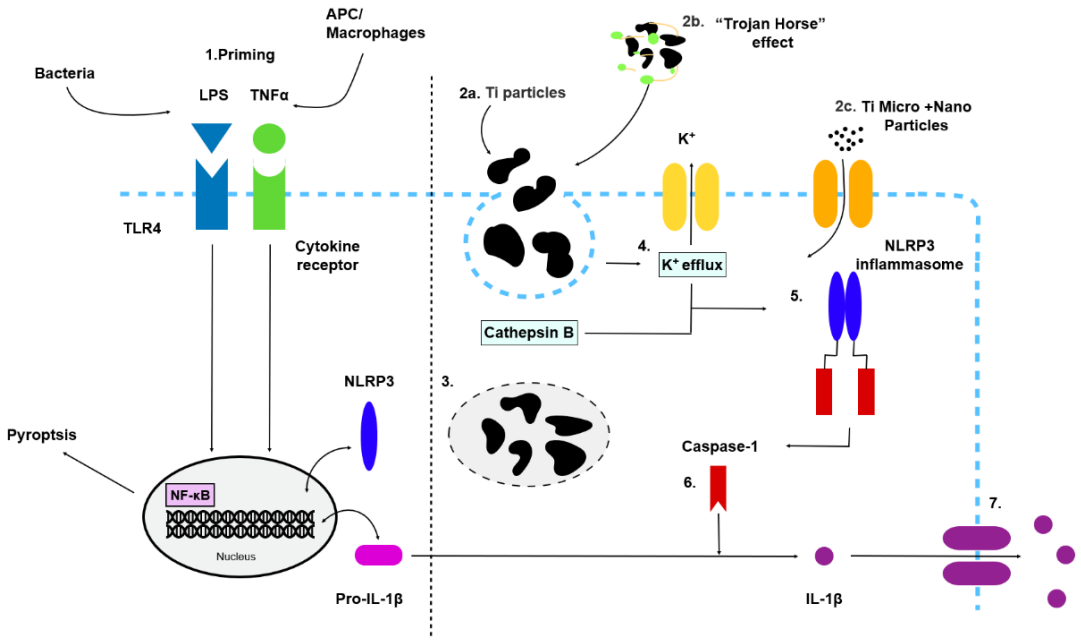

Figure 18. . Particle induced inflammasome activation pathway diagram. 1. Priming of the NFκB transcription via LPS/ TLR4 or TNFα/ cytokine receptor. 2. Particle internalisation pathways a. phagocytosis b. adhesion of proteins, calcium

and other ions from ECM resulting in trojan horse effect c. particles passing into the cytoplasm via membrane receptors. 3. Leakage of cathepsin protease from the lysosome. 4. Outflow of K+. 5. K+ efflux is sensed by NLRP3 receptor leading to Inflammasome component assembly. 6. Caspase-1 is activated by NLRP3 inflammasome; Caspase-1 converts pro IL1β to the active form. 7. IL1β release from membrane pores. Adapted from Jämsen et al. 2020 (48).

The importance of the grade of titanium used in the biomaterial becomes clear when we consider the chemical and physical influences on the surface. It becomes even more important to consider the potential toxicity of certain biomaterials when they are in particles especially if micro and nano sized. Implant companies carry out the standard testing of the materials using the entire fixture, with no current standards available for testing the implant material particles. Grade 5 titanium alloys contain vanadium and aluminium, which are toxic (38). This also raises the question of whether certain grades of Titanium and Ti alloys are more susceptible to corrosion and degradation, and therefore more likely to release particles with potential toxic influence in the tissues. Although some studies have suggested there is no difference between Ti-CP4 and Ti6Al4V (49), the *in vivo* conditions are very different to the experimental models where the many variables cannot be replicated accurately, such as the protein adhesions on the implant surface, the subsequent cellular response, the bacterial contamination in the presence of the occlusal loads and the implant- abutment micromovements, all of which can play a role in the conditions at the implant surface at various sites.

1.1.6 Biomaterial considerations for connective tissue attachment

Whether foreign body reaction or infection is the primary cause of peri-implantitis, having strong connective tissue attachments could be beneficial in disease limitation and maintenance of the soft tissue levels for function and aesthetics. Several attempts have been made to achieve connective tissue attachment for transcutaneous and transmucosal prostheses with the aim of reducing infection rates and their longevity.

Materials used for attempting soft tissue attachment include polymers such as

polyurethanes, polyethylene terephthalate (PET), silicones and polymethyl methacrylate (PMMA). However, these polymers are too weak and have unwanted tissue reactions. Several metals have been used for tissue integration. Metals have free electrons, unlike in living tissue. Gold and silver are resistant to corrosion in air, but not in body fluids. Stainless steel and cobalt-based alloys also become polarised and undergo redox reactions in living tissues. Other metals such as iron and aluminium are more susceptible to corrosion whereas nickel, vanadium, molybdenum and copper can be toxic to cells (27).
Ti has the right combination of the desired properties of strength, being inert and highly resistant to corrosion in living tissue as a result of the oxide layer. This process applies to Ti and Zr in that the oxygen atoms move into the metal oxide layer and the metal ions do not migrate to the surface, unlike other metals e.g. gold and stainless steel which is why they corrode. Water molecules are attracted to the oxide surface, and a hydroxyl group is formed, either as a lone group or as a bridging group. Therefore, the TiO_2 layer has amphoteric and zwitterion properties.

TiO_2 properties allow it to interact with various functional groups in the extracellular matrix, such as hydroxyl (OH), carbonyl (CO), carboxyl (COOH), amine (NH), sulfonate (SO_3H), and have physiological effects. Understanding these interactions may be the key to achieving the desired strong connective tissue attachment, e.g. interactions with ECM molecules such as osteopontin, bone sialoprotein, Dermatan and Fibronectin. The latter is a key ECM protein that enables attachment of cells and substrate via the functional groups on its arginine-glycine-aspartate (RGD) sequence. This sequence interacts with integrins on cells and influences cellular activity.

The question is whether Ti, as the currently preferred metal substrate, can promote connective tissue attachment. Although Ti remains inert in tissues, it can cause allergic reactions (0.6% prevalence), and undergo corrosion and increased oxidation in acidic conditions of bacterial biofilm (27). The oxide layer may not be favourable for soft tissue attachment. CP titanium is graded 1-4 based on the following properties - strength, corrosion resistance, ductility with Grade 1 being the most resistant to corrosion and most ductile while Grade 4 is the least

resistant to corrosion but the strongest and least ductile. Grade 4 is used in dental and orthopaedic implants due its higher strength compared to the other lower grades.

The most commonly used Ti alloy commercially is Ti6Al4V, also known as Grade 5 Ti alloy with 6% Al, 4% V, 90% Ti. This has higher strength than the Ti-CP4 , but has poor wear resistance, and is more expensive. The poor wear resistance is very important in long term prostheses, as it can result in the release of particles in the tissues which can have toxic effects, such as vanadium particles in a Grade 5 implant. Even at 4% vanadium can cause an inflammatory response with a foreign body reaction (Fig. 14) (27). Studies have shown that epithelial cells spread and attach more favourably on Titanium Grade 4 and 5 alloy compared to porcelain and aluminium oxide based on scanning electron microscopy (SEM) and immunofluorescence results; but gingival fibroblast attachment was unfavourable on Grade 5 alloy (Ti6Al4V) compared with grade Ti-CP4, as evidenced with rounded cell shapes indicating lack of attachment (50). This may possibly be due to the toxicity of Al or V.

For the purposes of this study, the main interest is in the positive interaction of the epithelial cells and fibroblasts to the substrate with regards to their proliferation and attachment. As far as metal substrates are concerned, the evidence supports Ti-CP4 over other metals and Ti alloys.

Other materials to consider for transmucosal prostheses include ceramics such as calcium phosphate, aluminium oxide or zirconium oxide, which can be applied as a plasma spray or used as bulk material and are discussed next.

Hydroxyapatite (HA), which is calcium phosphate ($Ca_{10}(PO_4)_6(OH)_2$), has excellent biocompatibility having a similar composition as mineralised bone. However, its brittle mechanical properties with long-term degradation and crack propagation, have resulted in increased complication rates as the HA coatings can shear off during placement or function. There are conflicting reports regarding the effect of HA on soft tissue attachment (7). Different morphologies seem to affect the soft tissue attachment (7). When porous and solid HA, as well

as concave and round surfaces were compared to the solid HA showed better attachment and the concave surface showed more stable attachment of soft tissues. CP Ti has been shown to have superior attachment to HA.

Aluminium oxide has been shown to have good bone and soft tissue integration, both at epithelial and connective tissue level with hemidesmosomal attachments (structures that enable cells to attach to underlying surface such as the basal lamina, ECM) and the presence of BMZ (51). However, failure rates of aluminium oxide implants were high (survival of 65-92%) possibly due to its brittleness, low tensile strength and long-term aging. Hemidesmosomal attachments may not be sufficient for the barrier effect which is achieved with the connective tissue attachment to the cementum of teeth.

Zirconia, yttrium-stabilized tetragonal zirconia polycrystals (Y-TZP), is stronger than aluminium oxide and is thought to have reduced tendency to collect plaque which is another desirable property for dental implants. However, in the presence of water it undergoes ‘low temperature degradation’ from tetragonal to monoclinic phase, which is brittle. The preparation of zirconia is very technique sensitive (52). Zirconia implants are more brittle with less flexion in response to load. Failure rates have been reported to be higher than Ti, however, more studies are required for conclusive results on the long-term survival and success of Zirconia implants compared to Ti. One of the weak points of the Zirconia implants are the threads where high stresses can result in fractures, which can be in response to high torque forces during the implant insertion. Zirconia in thin sections, as is desired on a thread, is weak. Two-piece Zirconia implants have an even higher risk of fracturing due to the internal abutment threads. The evidence for soft tissue integration to Zirconia or Ti and Zr alloys is lacking with some conflicting results.

1.1.7 Attempts at connective tissue attachment

1.1.7.1 Design

Various design modifications have been used to promote soft tissue attachment; these include surface treatments, collars (or flanges), grooves, porous structures, surface roughness manipulation, as well as surface energy and wettability. Current surface treatments attempted include:

- Mechanical e.g. blasting with Ti, Zr, Al;
- Chemical e.g. acid etching, anodisation;
- Physical e.g. sputtering, ion deposition.

Although these rough surfaces increase surface area for bone integration, they do not necessarily enhance soft tissue attachment. The summary of current evidence is (7):

- Epithelial cells attach and proliferate better on smooth surfaces;
- Fibroblast attachment and proliferation is better on rough surfaces;
- There was no difference in connective tissue response to different rough material between Ti, Zr and TiZr alloys;
- Research on the nanoscale roughness is inconclusive so far for soft tissue attachment, although there is evidence for its effectiveness in osseointegration, potentially through affecting direct cell-substrate interactions e.g. via RGD motif.

1.1.7.2 Collars and flanges

Studies have looked at increasing the surface area for soft tissue attachment by adding a mesh collar, nylon hooks, steel springs and solid flanges Fig. 19 (53). These have shown better soft tissue ‘integration’; however they still do not offer strong connections due to the direction of the soft tissue attachment (collagen fibril alignment) not being perpendicular to the implant core. The surgical

technique for positioning of the implant becomes very sensitive to ensure that the collar is at the correct height in relation to the appropriate aspect of the skin or mucosa.

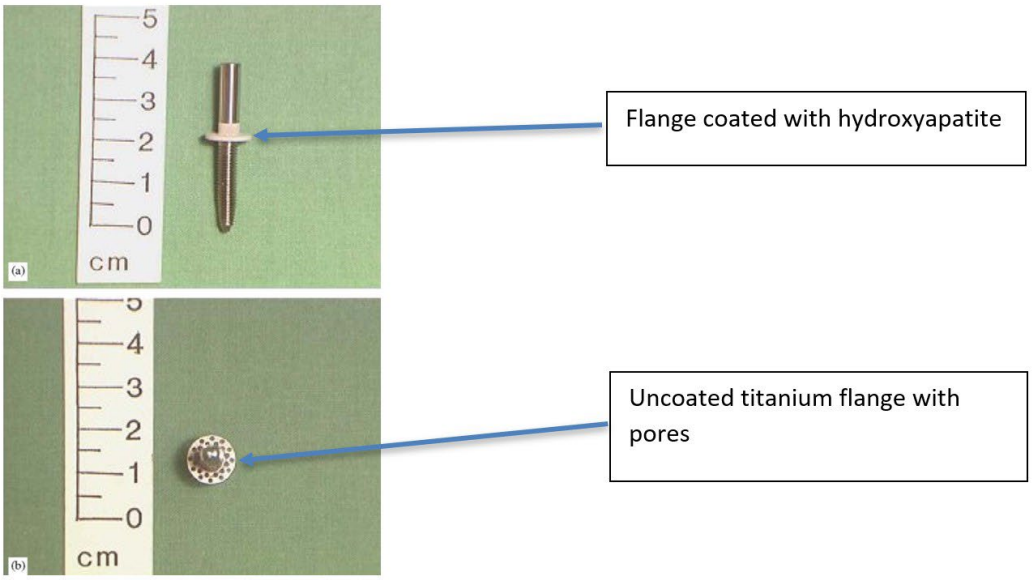

Figure 19. Images depicting transcutaneous implants with pores in flanges (a) coated with hydroxyapatite coating; and (b) plain titanium. Adapted from Pendegrass, C.J. (53).

1.1.7.3 Grooves

Groove orientation, depth and spacing can affect the position and growth of epithelial cells and fibroblast response. Contact guidance is a term to describe the ability of controlling epithelial cell and fibroblast orientation by altering the groove characteristics on an implant (54). Studies have shown that epithelial cell and fibroblast attachment and orientation can be influenced by the titanium surface microgroove morphology (53, 55, 56).

Contact guidance can be seen in studies by Nevins et al. (57) with the histological images (Fig. 20) demonstrating the orientation of the collagen fibres being ‘guided’ towards the implant surface with the grooves created by the Laser Lock technology. However, orientation does not mean attachment, and so far, the

latter has not been demonstrated.

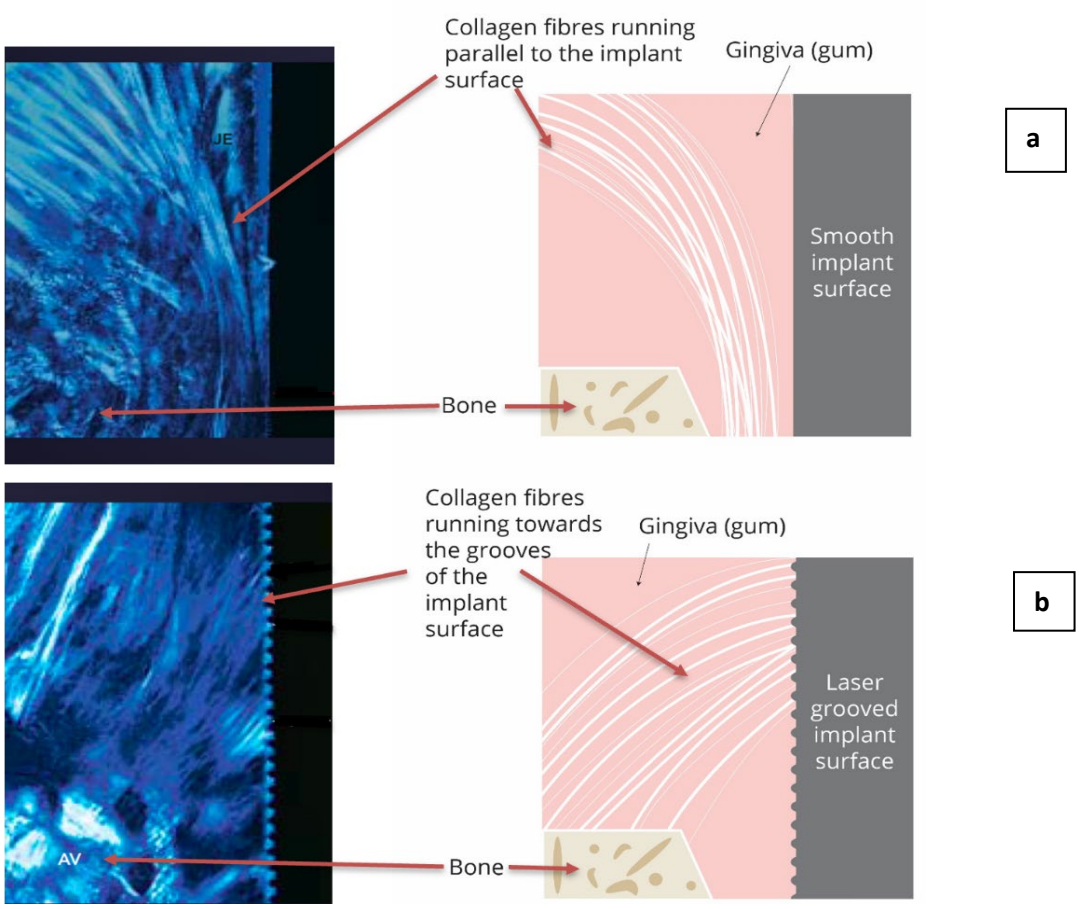

Figure 20. Histology and illustrations depicting connective tissue in contact with BioHorizons® (grade 5 Ti alloy) implant surfaces, (a) smooth surface depicting parallel orientation of collagen fibres to the implant surface and (b) laser grooved surface depicting collagen orientation towards the implant surface. Adapted from Nevins et al. (57) Illustrations designed by Dr F Barrak and drawn by Kitty Lungley.

1.1.7.4 Porosity

Different cell types will need different porosity for the growth and establishment of blood supply for tissue metabolism. Poly(hydroxyethyl methacrylate) has been used as a negative control as its surface does not allow protein attachment and so the results will reflect the pore size effect as opposed to the surface reaction. Results from studies have shown that (7): although the effects of porosity are not fully understood, a pore size of 40 μm and throat size of 16 μm allowed

incorporation of soft tissues predictably irrespective of surface characteristics; pore sizes of > 100 μm demonstrated higher rates of epithelial downgrowth and implant exposure (58).

1.1.7.5 Surface energy and hydrophilicity

Fibroblasts have a positive response to increased hydrophilicity with the highest attachment found at 20-40° water contact angle. Epithelial cells did not respond to wettability, but more to nanotopography of intermediate surface energy compared to the unmodified Ti (with lowest energy) and nanotubular Ti (with the highest energy).

1.1.7.6 Biomolecular coating

Biomolecular coating e.g. peptides, and seeding of mesenchymal stem cells are further techniques being studied for the achievement of connective tissue attachment. The aims of biomolecular coating include:

1. Reduction of non-specific protein attachment and cell adhesion;
2. Enhancement of selective tissue cell attachment;
3. Integrin mediated cell stimulation for healing.

Fibroblasts and epithelial cells have ECM surrounding them with different constituents (e.g. epithelial cells are in contact with laminin) and therefore we can expect them to respond to different proteins. Components of ECM include collagen type I, collagen type IV, laminin, fibronectin, vitronectin. Collagen type I and IV have been shown to improve epithelial attachment (59). Laminin 332 has also been shown to improve epithelial cell attachment and reduce epithelial down growth. Fibronectin, on the other hand, promotes fibroblast attachment and has binding sites for fibrin, thrombin, heparin sulphate and integrins (arginine, glycine, aspartic acid – RGD sequence) which play a role in cellular interaction with the ECM.

Other biomolecular factors to be considered include: platelet derived growth factor (PDGF) which speeds up healing in response to injury physiologically, and as demonstrated in experiments around implants (60); E-Cadherins, which are calcium dependent trans-epithelial adhesion proteins have also been considered for biomolecular treatments (61); and vitamins D and E, which have beneficial effect on fibroblasts *in vitro* (62).

Various methods have been used for coating of medical devices such as implant fixtures and bone substitutes to improve bone healing via targeted cell activation. These include the use of growth factors such as BMP 2, 7 and various peptides with the aim of targeting specific cells and specific functions within them (63). The use of growth factors has had much attention with conflicting results in relation to their effectiveness for the stimulation of bone growth predictably (64). The application of growth factor proteins onto substrate surfaces is via adsorption methods and has disadvantages. The large protein molecules are susceptible to folding and structural changes in response to small environmental fluctuations such as pH and temperature. These can alter the protein's activity by altering the active sites. Also, the adsorption of the protein molecules involves weak forces which results in dissipation of the growth factors with reduced concentrations in the intended target site as well as ectopic bone growth, hence the need for the higher concentrations used in medical devices to compensate for the loss of activity from some of the factors.

In contrast to the use of growth factor proteins which are adsorbed, the application of small peptide chains to medical device surfaces can be attained via covalent bonding which allows a more stable, controlled and targeted approach, both in terms of dosage, site of activity and cellular responses (63). Hence, with small chain peptides lower doses are required and they are also less likely to have undesirable immunogenic effects compared to proteins, while still maintaining their intended targeted cellular action. Reyes et al. 2017 (65) showed the effects of using biomolecular treatment using selective amino acid sequences for stimulating osteoblasts via α2 β1 integrins and Runx2/Cbf1a expression, as demonstrated in Fig. 21 where the bone to implant contact as well as the pull-out forces were much higher with the implants coated with amino acid sequence

(GFOGER) compared to the implants coated with collagen, which in turn were higher than the uncoated implants.

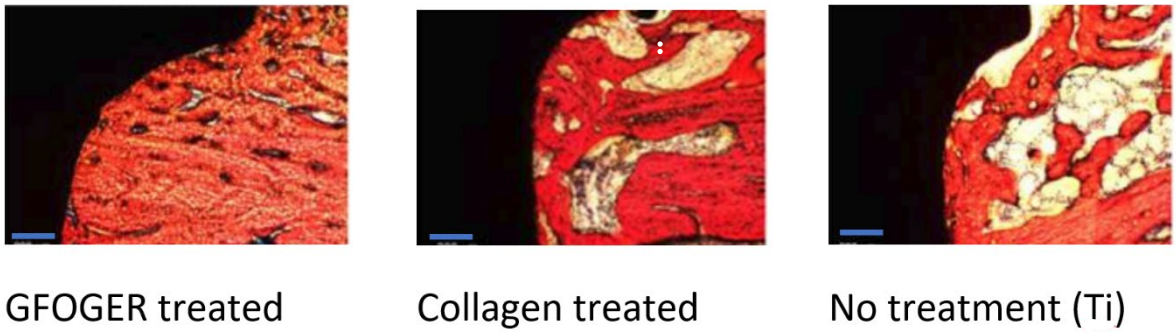

Figure 21. Histology images depicting the difference in bone to implant contact with different coatings - left: GFOGER peptide coating, middle: collagen I and right: no coating. The blue bar depicts scale of 200 µm. Adapted from Reyes, C.D. 2017 (65).

The choice of the peptide chain can influence the cellular interaction for the desired effect. Several peptides have been identified to have different cellular influences. For example RGD, is an amino acid sequence found on fibronectin, vitronectin and collagen, which interacts with integrins on various cells in a non-specific way to enhance adhesion. Other peptide sequences are believed to be important in cell adhesion and spreading such as KRSR and FHRRIKA (Phe-His-Arg-Arg-Ile-Lys-Ala) which was shown to be effective on silanised titanium surfaces (63).

Various scaffolds have been considered for application of small peptide chains. The use of peptides incorporated in hydrogel scaffolds may provide a structure to allow physical and chemical fixation of collagen fibers. Although hydrogels have lower mechanical strength than bone, the transmucosal application would not involve the loading forces encountered in the intra-osseous aspect of the implant. However, a disadvantage of hydrogels is the rate of degradation which would be of significant importance for the desired long-term physical connective tissue attachment.

Other materials considered for the application of small chain peptides include bioactive glasses, as well as direct application to titanium implant surfaces. This

methodology has been focused on bone healing mainly, however, there may be applications for controlling connective tissue attachment.

1.1.7.7 Summary of biomaterial properties required for achieving connective tissue attachment

Based on the above literature analysis and the natural tooth anatomy the suggested criteria for an 'ideal substrate' may have the following characteristics:

- Porosity with pore size of 40 μm and throat size of 16 μm;
- Surface energy with a of 20-40° water contact angle;
- Roughness - micro or possibly at nano level;
- Specific affinity for integrins and cell selectivity for fibroblasts possibly through biomolecular surface treatments;
- Bioactive surface;
- Anti-microbial properties;
- Ability to calcify to 'lock' collagen attachments - mimicking the tooth cementum/ PDL relationship (Fig. 22).

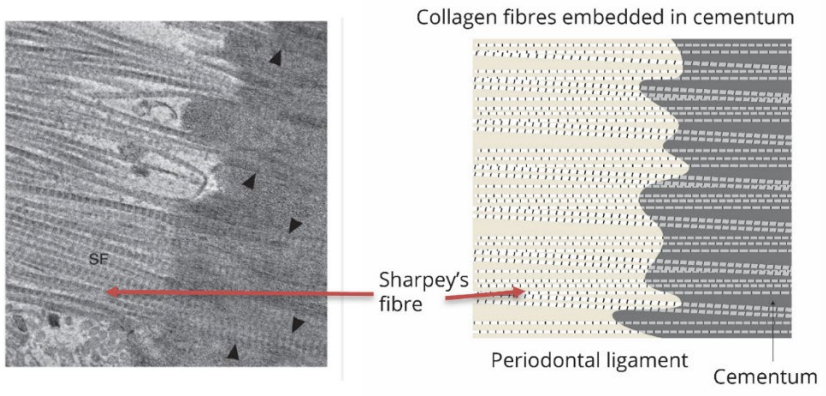

Figure 22. . SEM image and illustration showing the collagen fibres inserted in the calcified cementum matrix. Adapted from Beertsen, W. 1997 (66). Illustration designed by F Barrak and drawn by Kitty Lungley.
(66).

1.1.8 Bioactive glass as a potential substrate for achieving connective tissue attachment

Bioactive glass is a material that comes very close to having many of the desired properties for the ideal substrate to allow connective tissue attachment in a similar way to cementum of the tooth.

1.1.8.1 Bioactive glass structure

Bioactive glass is an amorphous material rich in Si with a tetrahedral structure as shown in Fig. 23.

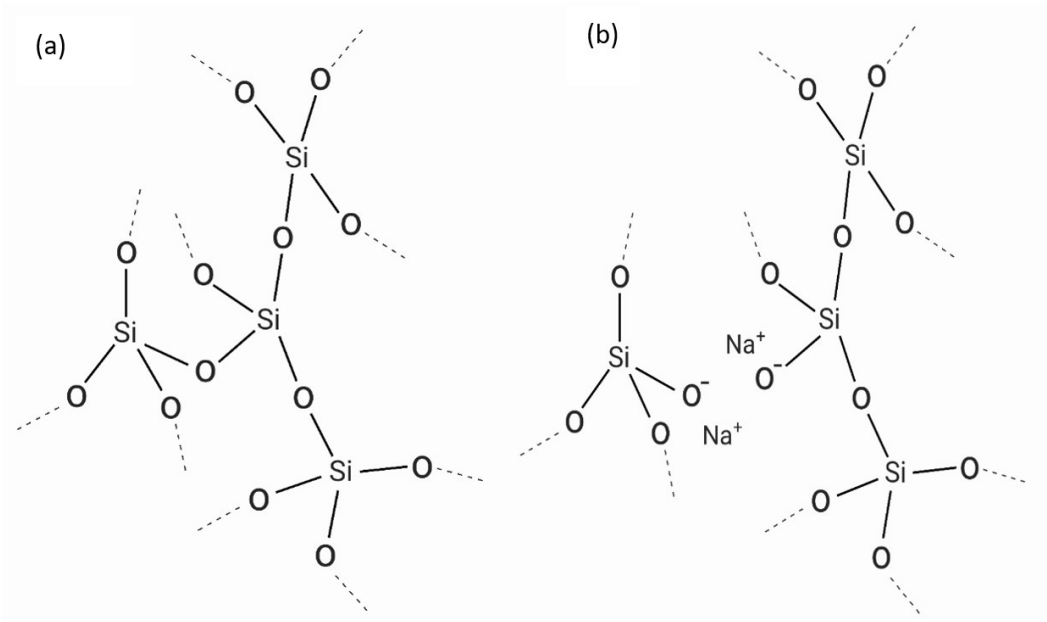

Figure 23. (a) Bridging oxygen (b) Non-bridging oxygen with a network modifier cation. Adapted from Aguiar, H. 2018 (67)

There are two main types of bonds in a glass network: bridging oxygen bonds between neighbouring Si atoms that hold the network together - network forming oxide (SiO_2) and non-bridging oxygen bonds between Si and network modifier atoms that disrupt the network - network modifying oxides (Na_2O, K_2O, CaO,

MgO). The behaviour of bioactive glass depends on the balance of bridging and non-bridging O bonds Fig.23. The bioactive response based on compositional variations in 6% P_2O_5 systems is shown in Fig. 24.

1.1.8.2 Bioactive glass composition and properties

Melt quenched glass needs to be cooled rapidly to avoid crystallisation. If the cooling is slow or if there are insufficient network formers, a crystalline microstructure will form. Base components of the original 45S5 bioactive glass are SiO_2 46.14 mol%, Na_2O 24.35 mol%, CaO 26.91 mol%, P_2O_5 2.60 mol%.

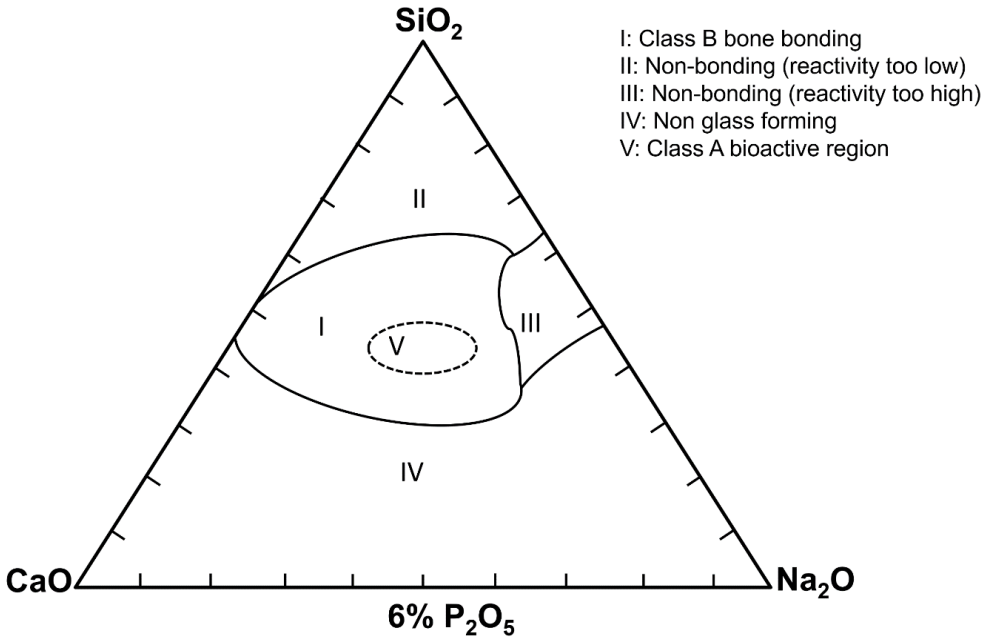

Figure 24. The bioactivity map of CaO, Na_2O and SiO_2 composition systems with 6% P_2O_5 and the bioactive response. Adapted from Jones. J (68).

Much research has been carried out on the properties of bioactive glass and its uses as a bone substitute, however, very little has been done on its potential as a substrate for connective tissue attachment. Bioactive glass has a wide range of possible compositions, which provide a variety of properties to choose from. It may be possible to mimic the mechanism for achieving strong connective tissue attachment seen around teeth, which involves collagen fibre endings aligning on

the tooth surface due to initial ionic attraction followed by calcification which 'locks' the fibres on the surface (69).

One of the important properties of bioactive glass includes the changes that take place at its surface once introduced into tissue fluids. This starts with a leaching, releasing alkaline earth elements (network modifiers) resulting in an increase in pH. This is followed by dissolution of the Si-O-Si bonds due to the OH group action. Silica is released into the tissues and a layer of silanols (SiOH) forms. Calcium phosphate precipitates at the surface and crystallises into hydroxycarbonate apatite (HCA) by incorporating carbonate ions. HCA interacts with collagen and matrix forming cells are activated; this enables bonding of the glass to the surrounding bone and soft tissue. This resembles the incorporation of Sharpey's fibres into the cementum of a tooth. Other desirable properties of bioactive glass include its potential antibacterial properties, as has been suggested for S53P4 bioactive glass with the following composition: SiO_2 79.45 mol%, $CaCO_3$ 53.62 mol%, Na_2CO_3 59.13 mol%, P_2O_5 5.94 mol% (70-72).

S53P4 bioactive glass has been chosen for further study in this PhD not only due to its desirable bioactive and antibacterial properties mentioned above, but also due its low substitution (degradation) rate, which is important in implant dentistry for long term stability of augmented sites. It is also already Food and Drug Administration approved (FDA) approved and in clinical use in orthopaedic and craniofacial surgery, which allows clinical application of the product in implant dentistry.

1.2 Motivation for this PhD project

As a clinician in this growing field of dentistry, the diagnosis of peri-implantitis is extremely challenging with the knowledge of the unpredictability of the current treatments. The patients are advised that the treatment of peri-implantitis is at best a salvage procedure to try and stop disease progression and maintain the implant in function. Patient expectations have to be managed for even this salvage procedure's long-term success, as this is also unpredictable with an unlikely re-establishment of osseointegration in the areas of bone loss (16).

There is therefore a need for further research to better understand the aetiological contributing factors for peri-implantitis and preventing its occurrence or improving the treatment outcomes. This knowledge may have potentially wider benefits in all disciplines involving transcutaneous and transmucosal prostheses.

Based on the above literature review, there are two key areas of gaps in knowledge in relation to the aetiology and prevention of peri-implantitis. These are the potential role of dental implant particles in the aetiology of peri-implantitis which is currently considered to require further evidence (19), and the ability to achieve robust collagen attachment in the transmucosal segment of the implant prosthesis as a barrier to microbial invasion and hence prevention of peri-implantitis.

1.2.1 Aims and objectives

The aims and objectives of this research are to investigate:

a. The potential role of dental implant particles in peri-implantitis

b. The potential use of S53P4 bioactive glass as a substrate for collagen attachment

The specific objectives of the research are to answer the following questions:

1. Are particles released from the implant surfaces during implant placement and if so, is this influenced by implant morphology and grade of Titanium used?
2. Are the particles released from dental implants cytotoxic and behave differently to the bulk material? if so, what is the mechanism of cytotoxicity?
3. Can the grade of Titanium influence tissue response and macrophage polarity? Can the inflammatory response be reduced with biomaterials?
4. Can connective tissue attachment be achieved to reduce the ease of bacterial invasion?

This page intentionally left blank

2. Investigation of particles released from dental implants following mock implantoplasty and their effect on human gingival fibroblasts

2.1 Introduction

The use of titanium dental implants to replace missing teeth has been well documented and accepted as a treatment option (73, 74). Despite the predictability of dental implants there are potential complications such as peri implant inflammation (peri-implantitis), which can result in rapid loss of the bone supporting the fixture with eventual loss of the implant (10, 15, 75, 76). Bone loss around the neck of the implant can be due to bone remodelling and therefore, the diagnosis of peri-implantitis is made when bone loss takes place in the presence of inflammation in the surrounding gums, as demonstrated at clinical examination by bleeding on probing and deepening pockets between the implant and the surrounding tissues.

The aetiology of peri-implantitis has been suggested to be related to plaque and the associated bacterial invasion of the tissues by a consensus report published in 2018 (19). The risk factors for developing peri-implantitis include a history of periodontal disease, uncontrolled diabetes mellitus and smoking. There have also been suggestions about the aetiology being related to an initial foreign body reaction to particle release from the implant surface, resulting in bone loss and subsequent bacterial invasion (24, 37, 41, 77). Particle release from the implant fixtures can take place during implant placement as a result of the shear forces on the roughened surface of the implant, from the implant-abutment interface due to wear and occlusal loading of the implants. The particles released locally may also be found in distant sites (25). Particle release from dental implants can also take place as a result of corrosion due to exposure to fluoride treatments and the acidic environment in the oral cavity (78, 79).

The treatment of peri-implantitis is aimed at stopping the inflammatory process and the progression of disease, and to maintain the implant in function. This involves a range of procedures from debridement and antiseptic application to

surgical and resective treatment which involve the removal of the exposed and contaminated rough surface of the implant to reduce plaque retention. The latter is referred to as implantoplasty and involves the use of rotary instruments to drill the outer superficial rough implant surface including the threads (Fig. 2 - 1). The procedure creates a smooth surface rendering it less plaque retentive. However, the procedure results in particle release in the tissues, which can be very difficult to control.

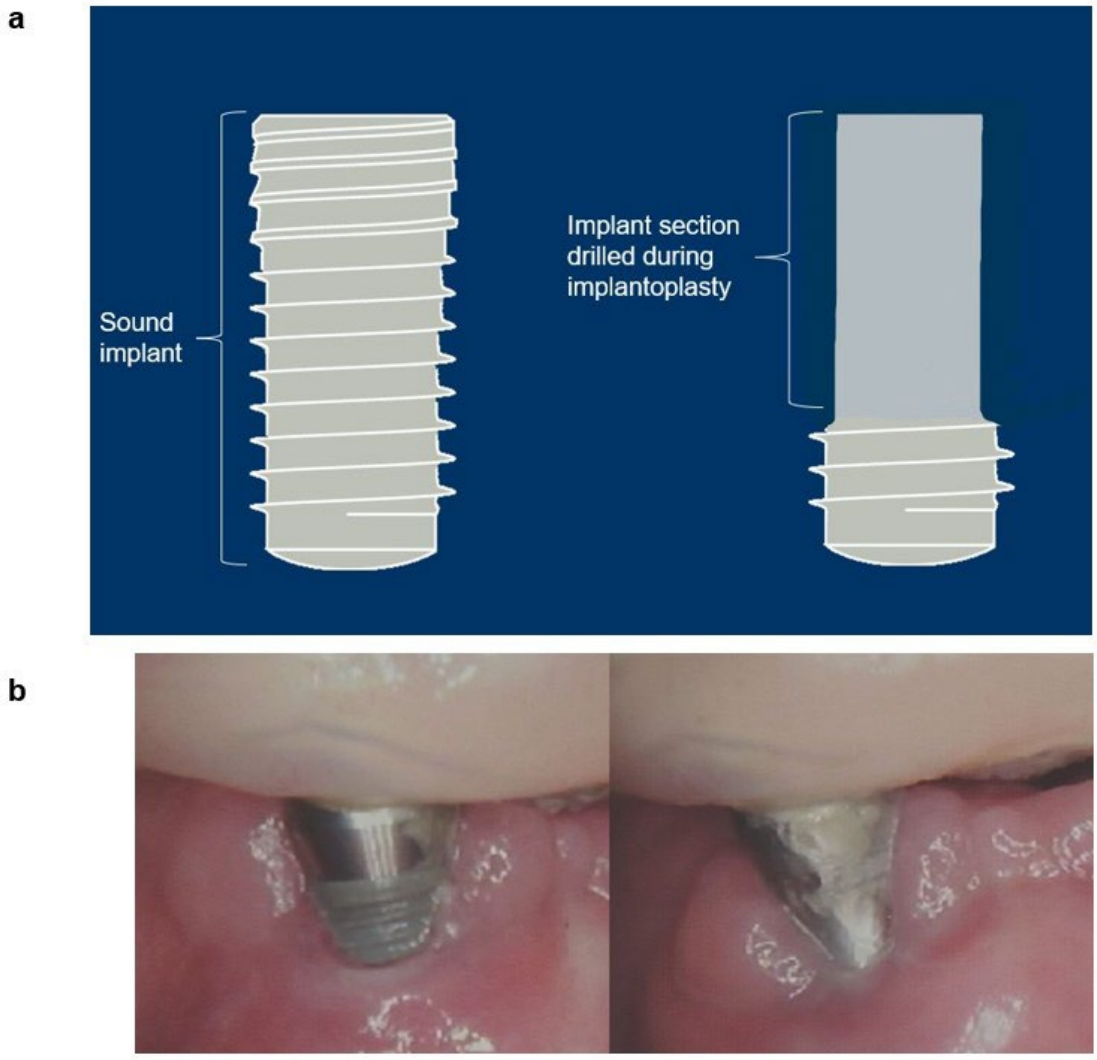

Figure 2 - 1. a Schematic representation of the amount of implant diameter reduction using rotary drilling instruments during the implantoplasty procedure; adapted from ITI speaker's library. b Clinical image of before and after implantoplasty of a small segment of an exposed implant to remove the rough surface and threads and reduce plaque retention; C/o Dr Wail Girgis

The aim of this study was to use simulated implantoplasty on two commonly used titanium implant grades (grade 4 and 5) to investigate the particle characteristics and *in vitro* human gingival fibroblast cellular response.

2.2 Materials and methods

2.2.1 Materials

Six dental implants were purchased, three 4.1 by 12 mm grade 4 commercially pure bone level tapered Straumann implants (Sussex UK) and three 5.0 by 10.5 mm grade 5 titanium alloy bone level tapered Bio Horizon implants (Berkshire UK). The grade 5 titanium alloy consists of 90% Ti, 4% V and 6% Al with trace elements of Fe.
Reagents and solvents were purchased from Sigma-Aldrich (Dorset UK).

2.2.2 Simulated implantoplasty method

The procedure was standardised by using a single operator, dental implants were held using a table clamp, the drilling was carried out using new single use diamond burs (Diatech G856.314.021.9ML-200453AA) in a handpiece (W&H, Alegra dental turbine handpieces TE-98 Led G) at 50,000 rpm for 5 minutes.
The particles released were collected in Falcon tubes to analyse.

2.2.3 Particle size measurement

The particles collected were suspended in 70% ethanol at 5mg.ml^{-1}. Particle size was analysed by using the Malvern Zetasizer and Mastersizer for 3 sub runs of 15 minutes duration each, automatically set by the instrument. The suspended particles were placed in an ultrasonic bath for 15 minutes immediately prior to performing laser diffraction measurement to minimise their settling at the base of the Falcon tubes.

2.2.4 Scanning electron microscopy

The particles were dried in a 60˚C oven, secured using carbon tape on an aluminium sample holder and coated with 10 nm gold. A Zeiss Sigma-300 SEM was used to acquire images with electron high voltage (EHT) of 10 kV, working distance (WD) of 7 mm, and for energy dispersive X-ray spectroscopy (EDX) analysis using samples coated with 10 nm gold using silver conductive paint to make contact with the holder.

2.2.5 Ion release from titanium particles

Simulated body fluid (SBF) was prepared in a 1 L polypropylene beaker containing 700 ml of deionised (DI) water warmed to 37˚C in a water bath, by slowly adding reagents according to the Kokubo method while continuously stirring the solution and monitoring the pH to avoid sudden increase and precipitation. Table 2-1 lists the reagents in order they were carefully added with the amounts used (80, 81). Once the reagents were mixed, the solution was made up to 1 L using DI water, stored at 37˚C and used within 48 hours. The SBF was adjusted to pH 7.4 at 37˚C before use and the particles were suspended in simulated body fluid at three concentrations: 0.75, 1.5 and 3 $mg.ml^{-1}$ in airtight polyethylene containers. In addition to the particles, a whole undisturbed implant fixture was also placed in SBF in a sealed polyethylene container for comparison of the whole implant to its particles. The containers were kept in a 37˚C water bath and placed on an orbital shaker rotating at 120 rpm. Aliquots of 1 ml were taken for pH and ionic analysis at day 0, day 3 and day 10.

Table 2 - 1. List of reagents and their amounts, in order of addition for preparing SBF (73)

Order	Reagent	Amount
1	NaCl	8.035g
2	$NaHCO_3$	0.355g
3	KCl	0.225g
4	$K_2HPO_4.3H_2O$	0.231g
5	$MgCl_2.6H_2O$	0.311g
6	1.0_M-HCl	39ml
7	$CaCl_2$	0.292g
8	Na_2SO_4	0.072g
9	Tris	6.118g
10	1.0_M-HCl	0-5ml

2.2.6 Preparing culture media

Basal Dulbecco's Modified Eagle's Medium (DMEM) containing 1% (v/v) penicillin and streptomycin (100 unit.ml^{-1} penicillin and 100 µg.ml-^{1} streptomycin) and 10% (v/v) Foetal Bovine Serum (FBS) was prepared for culture expansion of human gingival fibroblast (HGF) cell line (PCS-201-018TM, ATCC®, UK). Table 2-2 summarises the DMEM components (Sigma-Aldrich).

Table 2 - 2. List and amounts of components in DMEM (Sigma-Aldrich)

COMPONENTS	g/ L
Inorganic salts	
$CaCl_2$	0.265
$Fe(NO_3)_3.9H_2O$	0.0001
$MgSO_4$	0.09767
KCl	0.4
$NaHCO_3$	3.7
NaCl	6.4
NaH_2PO_4	0.109
Amino Acids	
Vitamins	

Cryopreserved stock HGFs were thawed rapidly in a 37°C water bath. 1 ml of cell suspension was added to 9 ml of basal media and placed in 75 cm^2 flask. Cells were maintained in humidified atmosphere at 37°C, 5% CO_2 and 21% O_2 for 3 days until 70-80% confluence. Culture medium was replaced every 2-3 days.

To passage cells, culture medium was removed and cells were washed with phosphate buffered saline (PBS) 3 times. 1X Trypsin ethylenediaminetetraacetic acid (TE) (1 ml of Trypsin EDTA 0.5% (10X) was added to 9 ml PBS to dilute to 1X TE 0.05%) was added to the culture flask and introduced to the incubator for 1 minute. Cell motility was checked under light microscopy to ensure detachment of most cells and basal medium was added to flask to arrest the TE activity. Cell suspension was added to a Falcon tube and centrifuged for 4 minutes at approximately 400 G (1200 RPM); the supernatant media was carefully discarded into a separate Falcon tube temporarily. Cells were counted using a haemocytometer and resuspended to achieve the desired concentration for the test groups.

Before use in culture, the titanium particles were sterilised using 70% ethanol for 1 minute. Grade 4 and grade 5 particles were suspended in DMEM at concentrations of 0.75, 1.5 and 3 $mg.ml^{-1}$ in airtight polyethylene containers and placed in an orbital shaker at 120 rpm, at 37°C for 72 hours. The test samples were divided into 2 groups: Group 1 - Dissolution product group – Grade 4 and grade 5 particles were filtered using 0.2 µm polytetrafluoroethylene (PTFE) membrane syringe filters following incubation to remove the particles before the cells were cultured with the media; Group 2 – Particle group - the cells were cultured with the particles present in the media. Basal DMEM and DMEM containing whole, unprocessed grade 4 and grade 5 implants were used as controls. 24 well culture plates were used for each time point (3 days, 7 days and 10 days), 12 wells for each test group with 3 repeats for each variable and controls in each group (3 X basal media, whole implant in media, grade 4 and grade 5). Media change was carried out every 2-3 days using the stock media. The effect of the titanium particles on the HGF metabolic activity was investigated by performing a 3-(4,5-dimethylthiazol-2-yl)-2,5-diphenyltetrazolium bromide (MTT) metabolic activity assay with group 1 and group 2 test samples.

2.2.7 Metabolic activity assay

A 24-well plate was seeded with 3000 cells/cm^2 and after 24 hours in DMEM the media was replaced with the test samples with 10% FBS supplement and incubated for a further 3, 7 and 10 days. At each time point the media was removed and replaced with 100 µl MTT (1 $mg.ml^{-1}$) in serum-free medium, freshly prepared) and incubated for 3 hours. MTT solution was removed and the formazan derivatives produced by metabolically active cells were then dissolved with 100 µl dimethyl sulfoxide (DMSO) and introduced into the plate reader to measure luminescence at 570 nm (SpectraMax M5).

2.2.8 Inductively coupled plasma optical emission spectroscopy sample preparation

Samples for Inductively coupled plasma optical emission spectroscopy (ICP-OES/ ICP) (iCaP6300 Duo, ThermoFisher Scientific, UK) were in 3 groups: SBF, dissolution products of particles from immersion in DMEM for 3 days and DMEM samples from culture studies with particles present. Collected samples were filtered through 0.2 µm filter and diluted (1:10 dilution) in nitric acid and stored until all the samples were ready for analysis. ICP standards containing 0, 2, 5, 10, 20 and 40 $\mu g,ml^{-1}$ of Ti, V, Al, Fe were prepared. pH measurements were also taken at all the time points used for the ICP.

Standard solution used (µl):	0	50	125	250	500	1000
Concentration ($\mu g.ml^{-1}$):	0	2	5	10	20	40

Total made up with nitric acid to 25 ml using ICP flasks (2 M nitric acid solution was prepared by adding 127 ml nitric acid to distilled water to make up to 1 L). An acid blank was used as control.

2.2.9 Statistical analysis

Results were presented as mean ± standard deviation (S.D.). Mann–Whitney *U* test (2 groups) or Mann–Whitney *U* test with Bonferroni correction (> 2 groups) was performed using OriginPro 2019. Results were deemed significant if the probability of occurrence by random chance alone was less than 5% (i.e. $p < 0.05$).

2.3 Results

2.3.1 Particle sizing

Particles produced by performing implantoplasty resulted in larger size particles with grade 4 implants when compared to grade 5 implants, 77.4 ± 9.1 μm (modal number 66.3 μm) and 48.4 ± 6.4 μm respectively (modal number 43.1 μm). Nano-sized particles were also detected on laser diffraction analysis; diameters were Grade 4: 125.4 ± 10.9 nm (modal number 109.3 nm) and Grade 5: 57.74 ± 2.66 nm (modal number 52.1 nm).

2.3.2 Particle morphology and composition

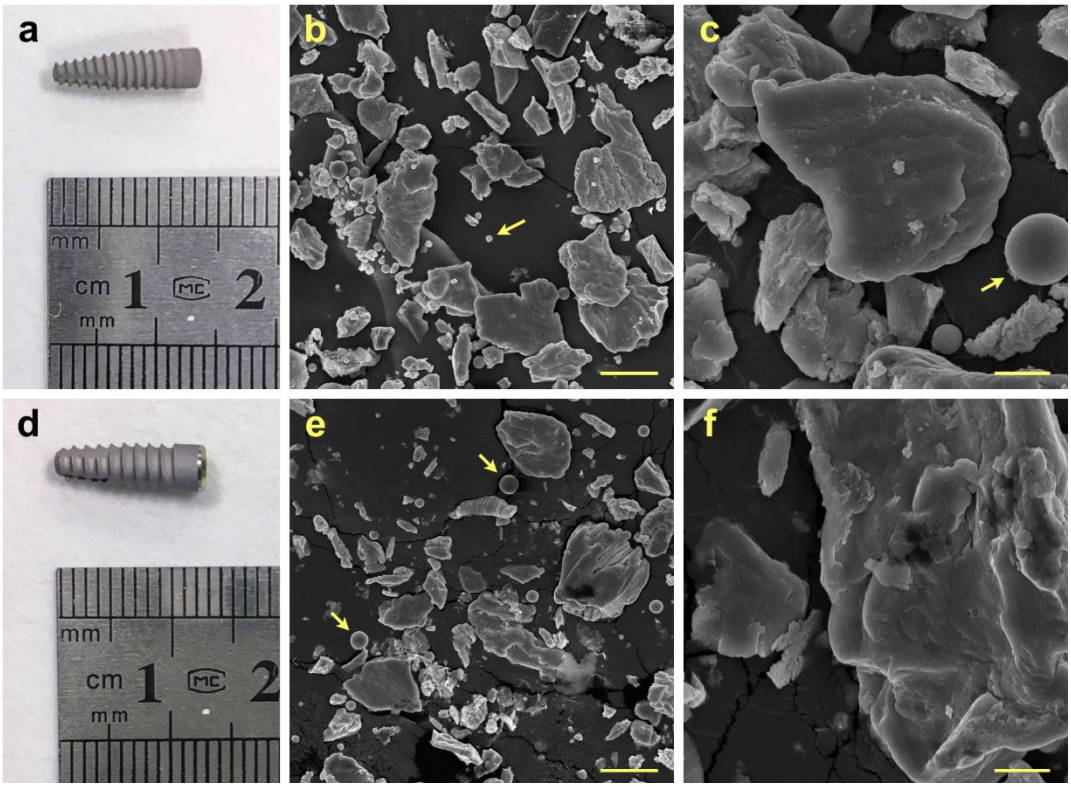

Figure 2 - 2. Images of implants and SEM of particles produced by mock implantoplasty procedure. a–c Straumann implant (commercially pure grade 4 titanium). d–f BioHorizons® (grade 5 titanium alloy). Arrows indicate titanium oxide spheres. Scale bar represents 20 and 5 µm for low and high magnification respectively.

SEM images of the particles produced by implantoplasty showed irregular sizes and shapes for both grade 4 and grade 5 samples with some spherical particles in both groups, indicated by the arrow in Fig. 2 - 2.

EDX analysis confirmed the spherical particles to be titanium oxide and demonstrated the presence of vanadium and aluminium in grade 5 samples only. Titanium and carbon were present in both samples Fig. 2 - 3.

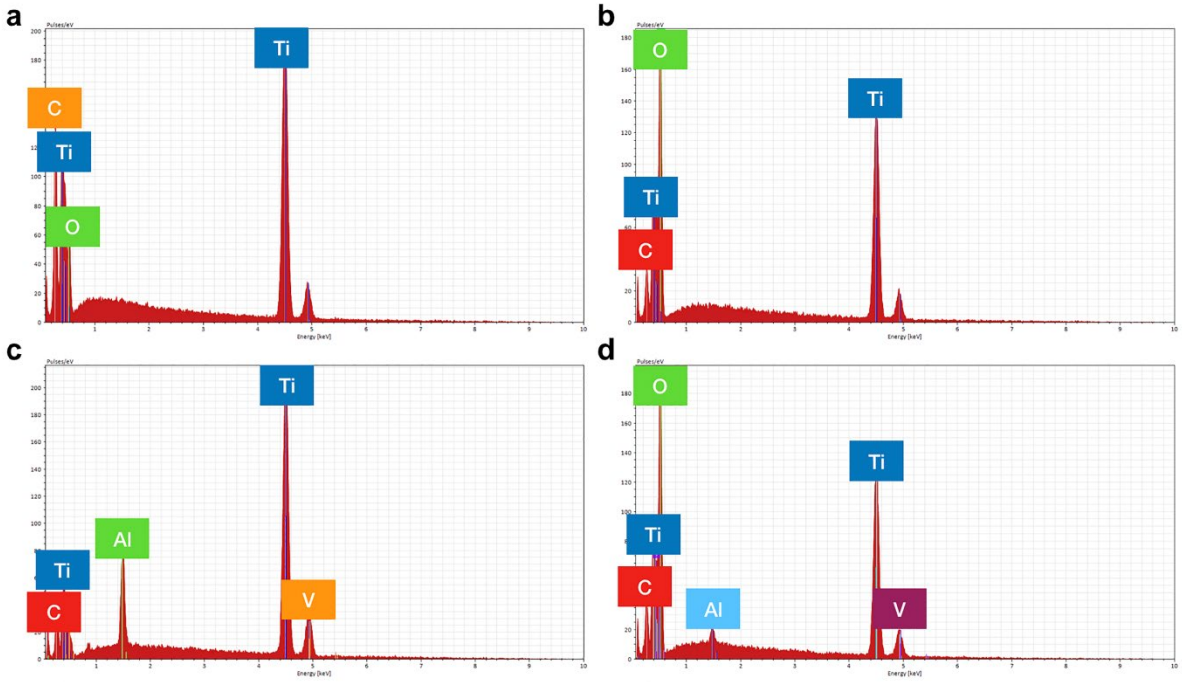

Figure 2 - 3. EDX spectra of particles produced by the mock implantoplasty procedure. a, b Particles from grade 4 commercially pure titanium implant, a angular microparticles and b small spheres. c, d particles from grade 5 titanium alloy, c angular microparticles and d small spheres.

2.3.3 Inductively coupled plasma optical emission spectroscopy

Elemental concentration in the SBF, immersion of the implant particles in SBF and DMEM was measured using ICP over 3- and 10-day time points and at 3 concentrations 0.75. 1.5 and 3 $mg.ml^{-1}$. There was no Al or Fe release detected from grade 4 or grade 5 particles immersed in SBF for all the time points and all three concentrations (Fig. 2 – 4). Ti release was minimal at day 3 and day 10 for both grade 4 and 5 particles. V release was only detected after 10 days of immersion of grade 5 particles Fig. 2 - 4. The pH of SBF remained at 7.4 throughout the time points and at the different particle concentrations.

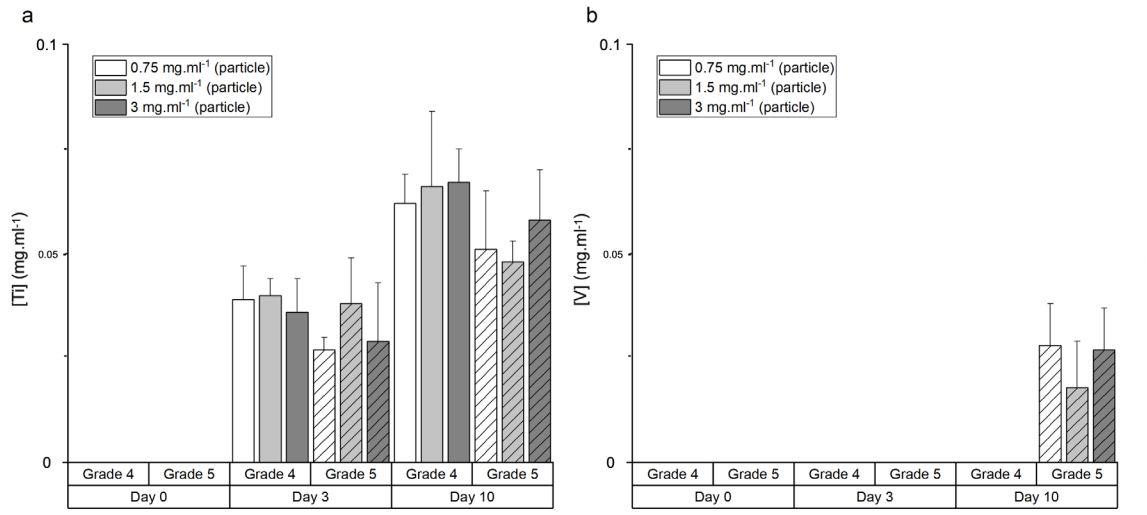

Figure 2 - 4. Titanium (Ti) and vanadium (V) release from the particles in simulated body fluid (SBF). Experimental duration was 10 days. Results presented as mean ± standard deviation, n = 3.

Particles immersed in DMEM released no detectable Fe or Al ions with low levels of Ti ions in both grade 4 and 5 samples. V ions were detected from grade 5 particles at 0.116 $\pm$ 0.023 $mg.ml^{-1}$. The change in concentrations did not have an effect Fig. 2 - 5.

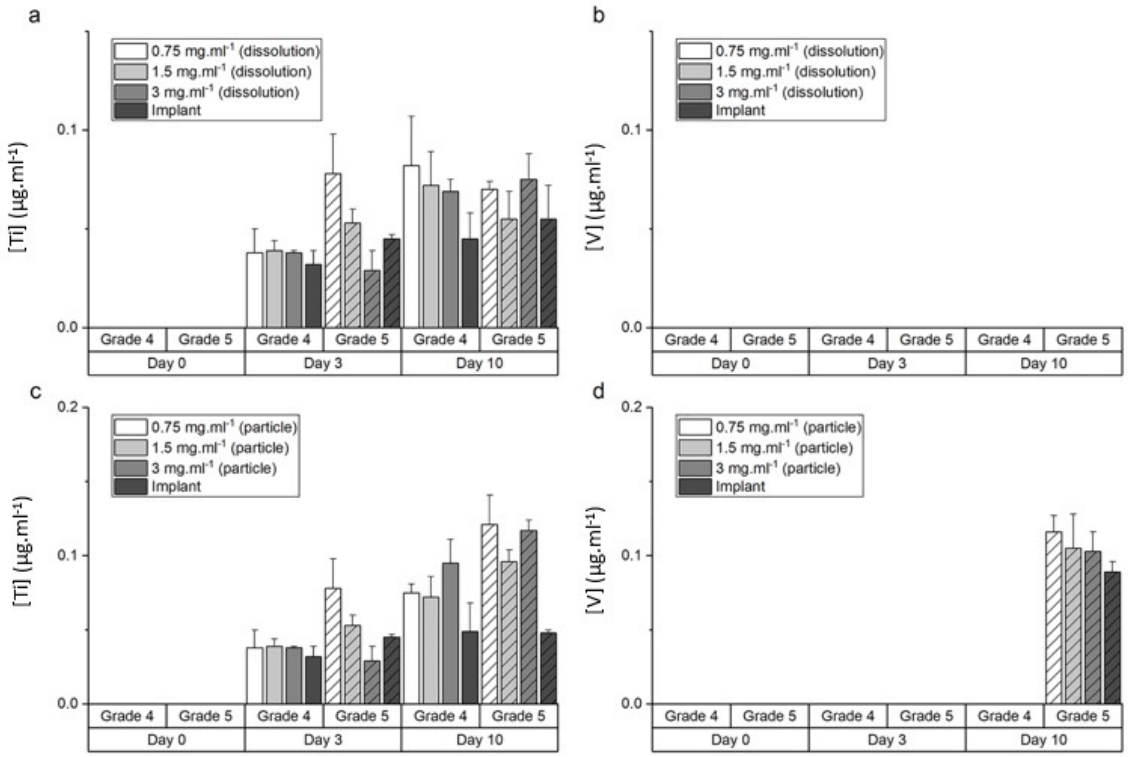

Figure 2 - 5. Titanium (Ti) and vanadium (V) content in Dulbecco's Modified Eagle Medium (DMEM). a, b Dissolution products (media filtered through 0.2 µm PTFE membrane following initial soaking of the particles for 3 days) and c, d DMEM sampled during cell culture studies where cells were cultured with the particles over a period of 10 days (particles removed prior to ICP measurement). Results presented as mean ± standard deviation, n = 3.

2.3.4 Metabolic activity

HFG cells cultured with grade 4 particle dissolution products at all three concentrations had no reduction of metabolic activity at the 3-, 7- and 10-day time points, as assessed with MTT assay. Cells cultured with grade 5 dissolution products had a reduced metabolic activity at the 10 day time point, although this was not statistically significant. The different concentrations of grade 5 particle dissolution products did not have any effect on the results (Fig. 2 – 6a).

HGF cells cultured in the presence of grade 4 particles (without filtering particles from the media) showed no reduction in the metabolic activity at any time point or concentration. However, there was significant reduction in the metabolic activity of cells cultured with grade 5 particles through all the time points. The different

concentrations did not have an effect. There was no reduction in the metabolic activity with cells exposed to the whole implant in either group (Fig. 2 – 6b).

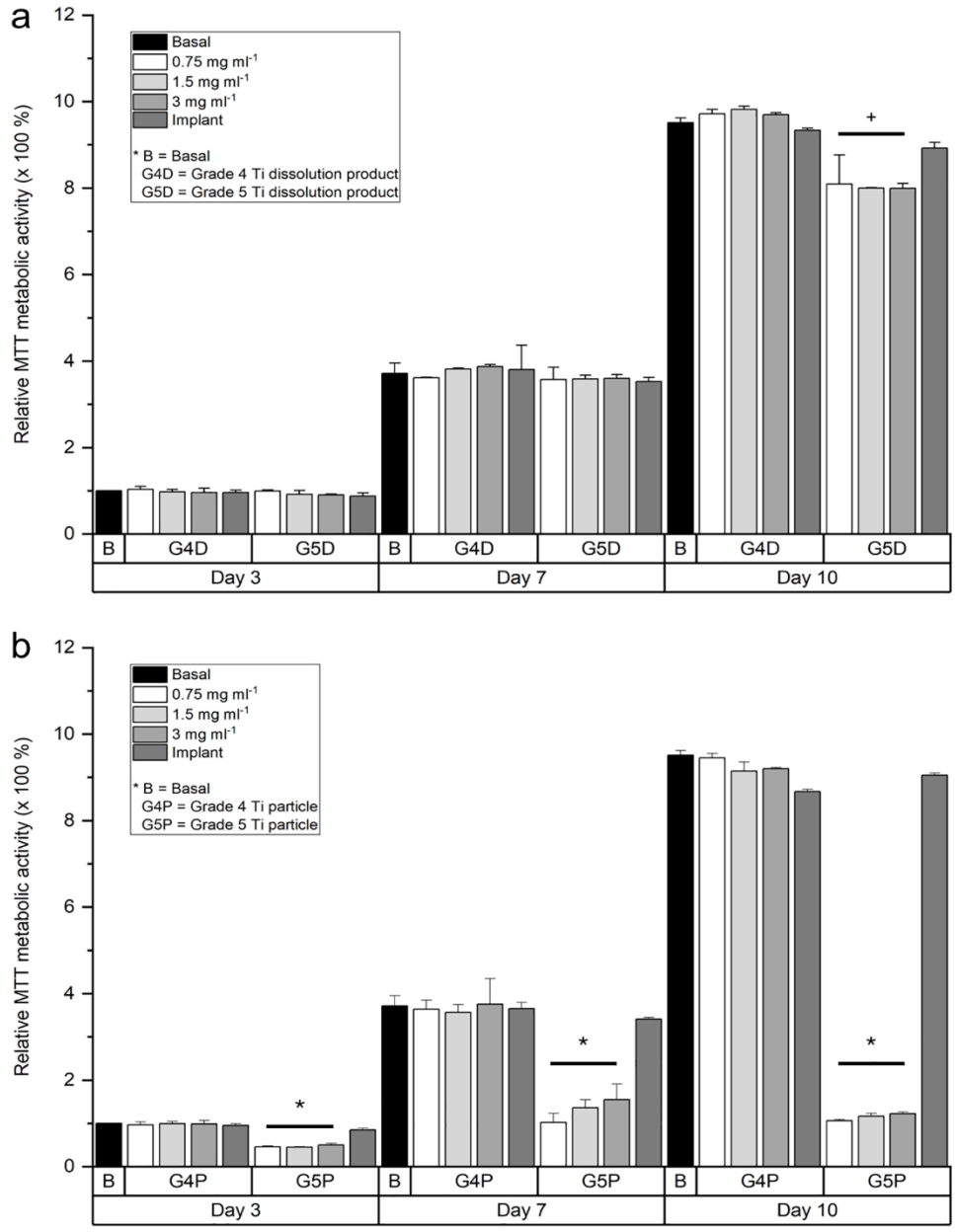

Figure 2 - 6. The effect of different concentrations (0.75, 1.5 or 3 mg.ml^{-1}) of grade 4 and grade 5 implant particles on human gingival fibroblast viability in vitro using an MTT metabolic activity assay. a, cells exposed to a dissolution products (ions and nanoparticles), b, culture medium containing suspended implant particles for the duration of the culture period. Basal medium and basal medium containing unprocessed dental implants were used as controls. All results were normalized against the value of basal medium at day 3. Results presented as mean ± standard deviation, n = 3. The asterisk indicates $p < 0.05$, and + indicates $0.05 < p < 0.1$ when compared to basal medium control at each time point.

2.4 Discussion

Particles produced by performing mock implantoplasty were smaller in the grade 5 implant group than grade 4. This is likely to be due to the higher hardness of grade 5 titanium alloy. G5 hardness of 36 (HRC, Rockwell C) compared to 23 (HRC, Rockwell C) of G4 (82, 83).

The results show no adverse effects on the cell viability when HGF are cultured with grade 4 dissolution products and when exposed to the particles in media for up to 10 days. In contrast, cells cultured with grade 5 particle dissolution products had reduced viability after 10 days, although not statistically significant. The significant difference was seen when the cells were exposed to the grade 5 particles, where the viability was markedly reduced for all time points. There was no change in the pH in any of the groups.

Grade 5 particles' adverse effect on the cell metabolic activity may be as a result of the smaller sized particles, or as a result of the presence of vanadium which has been shown to be toxic (84, 85). The ICP results reflect the presence of vanadium where the cell viability was found to be reduced in MTT assays. This was observed from the first timepoint of 3 days of culturing cells in the presence of grade 5 particles. Other studies support the slow release of V (86, 87) and the increased cytotoxicity of V with increasing concentrations of 1.17–1.53 $\mu g.ml^{-1}$ (85, 88). Although Al was not detected in the ICP analysis, grade 5 alloy contains 6% Al as well as trace elements of Fe. The presence of Al needs to be considered, as it may play a potential role in the reduced cell viability

The V concentration in this study after 10 days in DMEM was approximately 0.1 $\mu g.ml^{-1}$, hence the reduced viability observed in the MTT assay. The grade 4 particle size detected in this study ranged 125.4 ± 10.9 nm–77.4 ± 9.1 µm. For grade 5, the particle size range was 57.74 ± 2.66 nm–48.4 ± 6.4 µm. The smaller particles of grade 5 could be due to the higher hardness of the alloy. This range of nano and fine particles can enter cells through various routes of endocytosis,

which include phagocytosis in specialised cells (macrophages, monocytes and neutrophils) and pinocytosis in other mammalian cells (89, 90). Particle uptake by fibroblasts within the size range in this study has been previously demonstrated (91-93). Once inside the cell, the effects are not fully understood, however, there is potential for damage to the deoxyribonucleic acid (DNA) and other molecular effects (40, 94, 95). The detrimental effects of TiO_2 nano and microparticles were enhanced in the presence of LPS (92). It is important to also consider that even commercially pure titanium has impurities such as iron (Fe) and nickel (Ni), which may also play a role in cellular responses, especially as allergic reactions have been reported in humans (96-100).

2.5 Conclusions

This study shows that grade 5 implant particles reduce HGF cell viability significantly *in vitro*, as early as 3 days in culture. The particle size released from mock implantoplasty ranged from nano to fine particles which can have intracellular consequences that are not yet fully understood, but the reduction in cell metabolic activity is likely to be due to release of V ions, although the presence of Al must also be considered despite the ICP results . The particles may have biological consequences for our patients and although this data is purely from *in vitro* experiments and cannot be extrapolated to the clinical scenario for implant placements where such large amounts of particles are not released, it does raise an important question on the use of the implantoplasty procedure, especially with grade 5 implants.

This page intentionally left blank

3. Particle release from different dental implant systems immediately after placement in an ex-vivo pigs jaw model

3.1 Introduction

Titanium and its alloys have been widely used in orthopaedic and dental implant surgery (101). A major cause of dental implant failure is peri-implantitis, which is characterized by the presence of inflammation in the peri-implant soft tissues and the resultant bone loss (28). The aetiology of peri-implantitis is currently believed to be plaque related (19), however there is some evidence to support aseptic inflammation secondary to particle release from implant surfaces as a contributing factor, if not the primary cause of implant failure (102-104).

Particle release from implants can take place during fixture insertion as a result of shear forces on the micro-roughened surface. Wear from functional loading at the implant-abutment interface and corrosion due to exposure to oral fluids can accelerate the degradation of the surface of the implant resulting in more particle and ion release (103-107). Manufacturers assess the biocompatibility of dental implants using standards such as International Organisation for Standardisation (ISO) 10993 to ensure there is no leaching from the fixture in cell culture. However, the presence of particles in the peri-implant tissues can result in chronic inflammation due to the frustrated phagocytosis of small endocytosed particles (108). Studies have demonstrated a particle size range from nano to micrometer (26, 104, 109) and peri-implant soft tissue biopsies have revealed inflammation around particle aggregates (110, 111). The cellular response to nano sized particles is not fully understood. The higher exposed surface area of small particles can result in a higher rate of ion release. Other studies using orthodontic mini implants have found particles from the implants in lung, liver, spleen and bone tissues (112, 113). Particles released from ultrasonic scaling of grade 5 (titanium alloy consisting of 90% Ti, 6% Al and 4% V) implant surfaces have resulted in the upregulation of inflammatory factors IL1β, IL6 and TNFα, in *in vitro* and animal studies (35).

The aim of this study was to investigate the impact of the dental implant geometric design (tapered or parallel morphology) and material (grade 4, grade 5 and Roxolid®) on the release of particles immediately following ex vivo implant fixture placement in pig mandibles. The uptake of implant particles by HGF and RAW macrophages was also investigated *in vitro*.

3.2 Materials and methods

Dental implants were ordered from Straumann UK for grade 4 commercially pure titanium and Roxolid® (Ti15Zr) with sand blasted large grit acid etched (SLA) surfaces - Straumann Ti-CP4 cylindrical bone level (BL), Straumann Ti-CP4 bone level tapered (BLT-S), Straumann Ti15Zr Bone level tapered Roxolid® (BLT-R). BioHorizons® tapered implants (BH) were ordered for grade 5 alloy (Ti6Al4V) implants.

The Straumann implants had diameters of 3.3 and 4.8 mm, each with 12 mm length and tapered and parallel walled cylindrical implants. BioHorizons® implants were all tapered at 3.4 and 4.6 mm diameters and 12 mm length. Table 3 - 1 summarises the implant variables.

Titanium particles for Ti-CP4 and Ti6Al4V were gifted by Dr Jonathan Jeffers (Imperial College London) and for Roxolid®, discs provided by Straumann (Basel, Switzerland) were used to drill and produce particles. Pig mandibles were purchased from Medical Meat Supplies (Oldham, UK) and the reagents were purchased from Sigma-Aldrich (Dorset, UK) and ThermoFisher Scientific (Paisley, UK).

3.2.1 Implant placement protocol

Implants were placed in the superior aspect of the ramus of pigs' mandibles using the appropriate system's drilling protocol. Each ramus was split in 3 sections, one for implant placement and 2 controls, which consisted of an unprepared section and a section where an osteotomy was drilled but no implant was placed (Fig. 3 -

1). The controls were to assess any particles present in the mandible predrilling or from drilling without implant placement. There were 5 repeats for each implant group.

The bone segments for controls and test sites were then sectioned vertically and the implants removed from test sites. This allowed implant removal without using reverse torque, which could cause further particle release and affect the results of investigating particle release from implant placement alone. Samples collected for SEM and micro-computed tomography (μ-CT) analysis were stored at 4˚C in paraformaldehyde. The samples for ICP were stored at -20˚C for further preparation and analysis.

Table 3 - 1. Summary of implant characteristics with the loss in mass following ex vivo placement. All implants had 12 mm length. Ti-CP4 is commercially pure grade 4 implant; Ti15Zr is the alloyed implant with 85% titanium and 15% zirconium; Ti6Al4V is the grade 5 alloy consisting of 90% titanium, 6% aluminium and 4% vanadium.

Brand	Model no.	Implant type	Material	Surface	Endosteal diameter (mm)	ID in this study	Mass loss after implantation (estimated, μg)
Straumann®	21.2612	Cylindrical	Ti-CP4	SLA®	3.3	BL3	554 ± 15
Straumann®	21.6612	Cylindrical	Ti-CP4	SLA®	4.8	BL4	661 ± 15
Straumann®	21.3412	Tapered	Ti-CP4	SLA®	3.3	BLT-S3	134 ± 13
Straumann®	21.7412	Tapered	Ti-CP4	SLA®	4.8	BLT-S4	519 ± 15
Straumann®	21.3512	Tapered	Roxolid® (Ti15Zr)	SLA®	3.3	BLT-R3	448 ± 35
Straumann®	21.7512	Tapered	Roxolid® (Ti15Zr)	SLA®	4.8	BLT-R4	548 ± 38
BioHorizons®	TLX3412	Tapered	Ti6Al4V	Laser-Lok®/RBT	3.4	BH3	639 ± 54
BioHorizons®	TLX4612	Tapered	Ti6Al4V	Laser-Lok®/RBT	4.6	BH4	691 ± 15

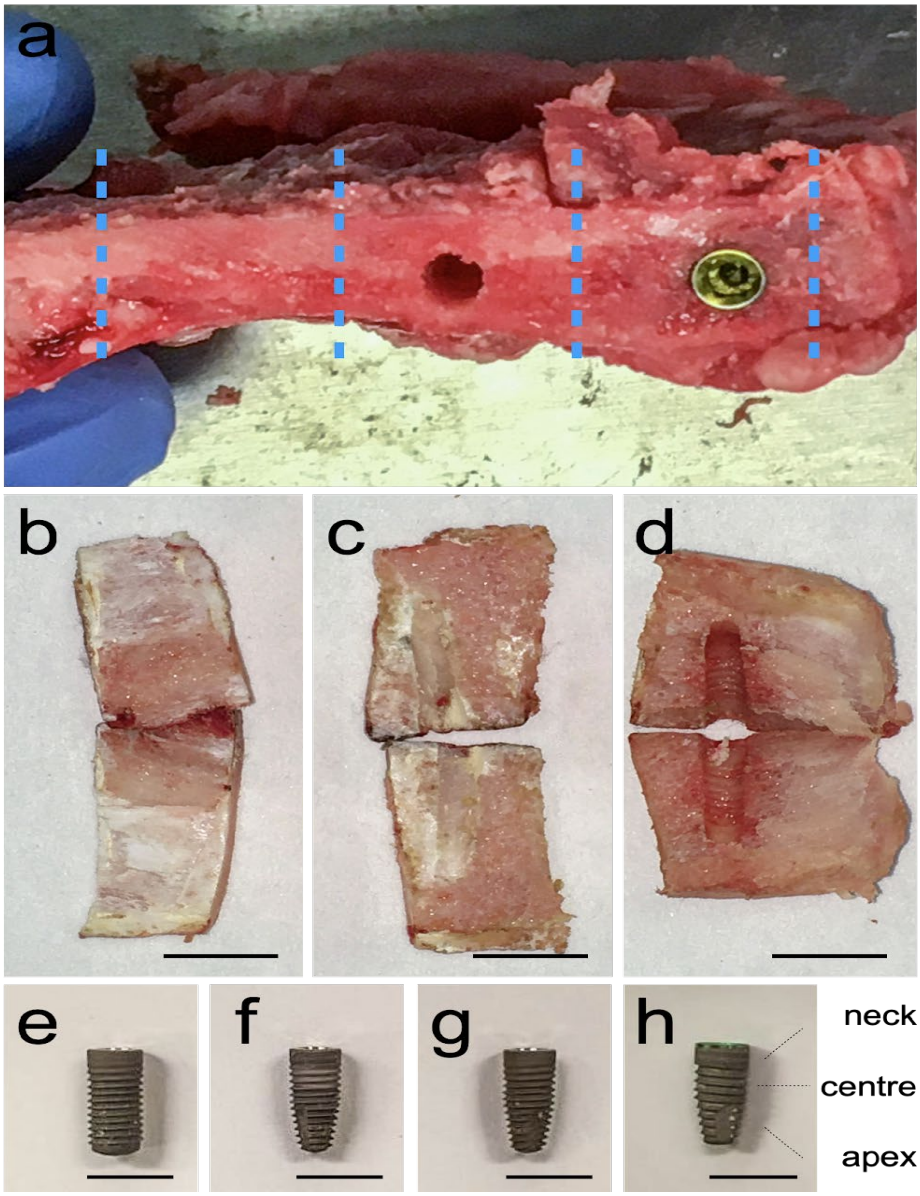

Figure 3 - 1. Image depicting the experimental setup of the pig mandible and the morphology of the different implants. (a) The ramus of the pig mandible was sectioned in 3 compartments: undrilled bone (control), drilled bone without implant placement (control) and implant placement (test). (b) vertical section through the untreated bone, (c) vertical section through the drilled bone without implant placement, (d) vertical section through the bone where implant was placed, after removing the implant. Representative image of implants following placement and removal: (e) Straumann Ti-CP4 cylindrical bone level (BL); (f) Straumann Ti-CP4 bone level tapered SLA surface (BLT-S); (g) Straumann Ti15Zr Bone level tapered Roxolid® (BLT-R) and (h) BioHorizons® Ti6Al4V tapered (BH). Scale bars are 1cm.

3.2.2 Preparation of bone samples

Bone samples were dissolved in acid using 5 ml of 4 parts 65% nitric acid plus 1 part 96% sulfuric acid. Working inside a fume hood, the samples were placed in acid in polypropylene tubes with screw caps pierced to allow fumes to escape. Samples were held in a 40°C bath overnight, the temperature was then increased to 70°C for 2 hours and 95°C for a further hour, as described previously (114). Once the samples cooled down to room temperature, they were centrifuged and the supernatant was collected for analysis. In order to assess the quantity of implant particle released a standard curve was developed by dissolving known amounts (0.75 mg, 1.5 mg and 3.0 mg) of particles of Ti, Ti6Al4V and Ti15Zr in acid using the same method described above.

3.2.3 **Inductively coupled plasma optical emission spectroscopy**

ICP was used to measure the elemental concentration of Ti, V, AL and Fe in the dissolved solutions. Standards for Ti, Al, V and Fe were prepared at 0, 2, 5, 20 and 40 $\mu g.ml^{-1}$ for calibration. Samples were prepared by using 1 ml from the sample in 9 ml of de-ionised water and filtering through the 0.2 µm membrane. The samples were run in triplicates.

3.2.4 Scanning electron microscopy

A representative sample of implants from each group was used for SEM imaging using Zeiss Sigma-300. For each implant 3 images were taken: the neck, body and apex (Fig. 3 – 1h) of each fixture at X125 and X1500 magnifications (Fig. 3 - 6). The implants were prepared for SEM imaging by drying them in 60°C oven overnight and coating with 10 nm gold once secured on an aluminium sample holder by a carbon tape.

3.2.5 Three-dimensional micro-computed tomography

Bone samples were collected for Three-dimensional micro-computed tomography (μ-CT) investigation following implant removal. The samples were stored in polypropylene tubes with 1.5x1.5x1.5 cm dimensions in each tube, wrapped in radiolucent cotton in order to maintain a distance between the samples and prevent overlap during μ-CT scanning. The 3D μ-CT Zeiss Versa 520 X-Ray scanner (Zeiss, Germany) at the Natural History Museum was used for this experiment and the 3-D reconstructed volumes were visualised and analysed using Fiji ImageJ software (version 1.52p, NIH, USA). The settings were 140 kV voltage, 71 μA current (with high efficiency filter), 12.3 μm voxel size, 0.4× optical magnification, 5 s exposure time, 2.5 MHz camera readout, 1 recon binning and 1601 projections. 3D μ-CT images were visualised using Fiji ImageJ software (version 1.52p, NIH, USA). The images were analysed by scrolling through to detect the presence of dense radio-opaque material in the wall of the osteotomies, which would be indicative of titanium particle release.

3.2.6 Cell culture

Particles of grade 4 and grade 5 titanium alloy were functionalised to become fluorescent before culturing with HGF (ATCC, Middlesex, UK) and RAW 264.7 (Sigma-Aldrich, Dorset, UK) cell lines to demonstrate particle uptake by cells.

3.2.7 Particle functionalisation and fluorescent labelling

Particles were placed in absolute ethanol 5 $mg.ml^{-1}$, before gently adding 28% ammonium hydroxide (5%v/v) followed by 3-aminopropyl triethoxysilane (1:5). The solution was placed on an orbital shaker at 200 rpm for 16 hours to complete functionalisation of the particles. Absolute ethanol was used to wash the functionalised particles and fluorescein 5(6)-isothiocyanate (FITC) 1 $mg.ml^{-1}$ dissolved in absolute ethanol was used to label the particles by leaving the solution containing the functionalised particles with a 1:1 weight ration of particle and FITC on an orbital shaker for a further 16 hours at 200 rpm.

The functionalised and FITC labelled particles were prepared for culture by washing with absolute ethanol, deionised water and sterilised with 70% ethanol. For each of the cell lines, HGF and RAW 264.7 three tissue culture µ-dishes (ibidi®, Thistle Scientific Ltd, Glasgow, UK) were seeded with 300 cells/ cm^2 in DMEM supplemented with 1% Penicillin & Streptomycin and 10% FBS and incubated for 24 hours before introducing the FITC labelled particles at a concentration of 250 $\mu g.ml^{-1}$. After 16 hours the cells were fixed with 4% formaldehyde (10 ml 16% vial in 30 ml PBS) to prepare for staining and confocal microscopy.

3.2.8 Preparation of solutions/ reagents for staining

- 1% Bovine serum albumin (BSA) in PBS (0.5 g of BSA in 50 ml PBS) was prepared to block nonspecific binding of antigens and antibodies and to act as carrier for the antibody.
- Permeabilisation buffer was prepared in 50 ml of de-ionised water by adding 5.15 g sucrose, 0.146 g NaCl, 0.03 g $MgCl_2$, 0.238 g HEPES, 0.25 mls of Triton X with pH adjustment to 7.2 (115).
- PBS TWEEN 0.5% was prepared by adding 0.25 ml TWEEN in 50 ml PBS.

3.2.8.1 Staining

Fixative was gently removed from the samples and washed twice with PBS. Permeabilisation buffer solution was added to the surface to be stained and left for 15 minutes before washing with PBS. Blocking BSA solution was then added and left for 10 minutes.

Phalloidin (Alexa Fluor® 568-conjugated phalloidin 1:1000 dilution in labelling buffer) was added, wrapped in foil and kept at 4˚C for 1 hour, washed with Tween for 10 minutes and counter stained with 4',6-diamidino-2-phenylindole (DAPI) (0.1 $\mu g.ml^{-1}$ in PBS) for 10 minutes and kept in dark. The samples were imaged using

Leica SP5 MP laser scanning confocal microscope (Leica Microsystems, Wetzlar, Germany) and soft-Ware Fiji ImageJ software (version 1.52p, NIH, USA) to generate orthogonal views.

3.2.9 Statistical analysis

Results were presented as mean ± standard deviation (S.D.). Statistical analyses including non-parametric t-test (2 groups) and Kruskal-Wallis test with Dunn's post-test (3 or more groups) using Prism 8 (GraphPad Software, US). Results were deemed significant if the probability of occurrence by random chance alone was less than 5% (i.e. $p < 0.05$).

3.4 Results

Titanium particles were detected from all implants tested. Zirconium and vanadium particles were only detected with the alloyed implants, Ti15Zr and Ti6Al4V respectively.

3.4.1 Implant diameter

The increase in diameter of implant resulted in significantly more particle release in the BL and BLT-S groups, both grade 4 commercially pure titanium (Table 3 - 2).

Table 3 - 2. Summary of ICP-OES results for Ti release in the Ti-CP4 group.

Implant diameter and type	**Titanium release detected in bone samples**
3 mm BL	6.0 ± 0.2 mg. ml^{-1} Ti
4 mm BL	8.6 ± 0.2 mg. ml^{-1} Ti
3 mm BLT	1.5 ± 0.1 mg. ml^{-1} Ti
4 mm BLT	5.6 ± 0.2 mg. ml^{-1} Ti

In the BLT-R group (Ti15Zr) and the BH group (Ti6Al4V) the increase in diameter did not result in significantly increased particle release of any of the components.

3.4.2 Morphology and material

The cylindrical implants in the BL group released significantly more particles than the tapered implants of the same diameter and material (Ti-CP4). The BH group (Ti6Al4V, tapered) had significantly more particle release than all the other implant groups for the respective diameters. No particles were detected in either of the two control groups - no drilling, no implant placement and osteotomy drilled but no implant placed (Fig. 3 - 2).

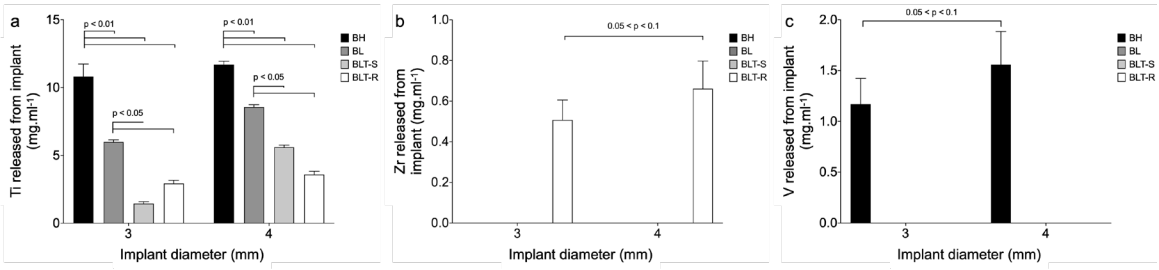

Figure 3 - 2. ICP-OES measurements of (a) Ti, (b) Zr and (c) V detected in dissolved bone samples following implant placement. Results presented as mean ± standard deviation (n=5).

In order to measure the approximate amount of particle lost from the implant surfaces a standard curve was developed using known quantities of particle for ICP analysis. The standard curve was then used to extrapolate approximate particle loss in µg (Fig. 3 - 3).

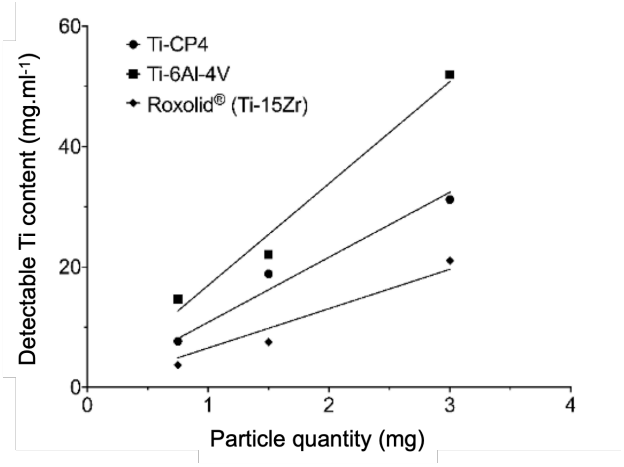

Figure 3 - 3. Standard curve for estimating the quantity of Ti particles detected in bone. This was determined by carrying out ICP-OES analysis of known quantities of implant material.

3.4.3 Three-dimensional micro-computed tomography

The μ-CT scans had a maximum resolution of 12 μm/ voxel and therefore only larger particles were detectable on the images. The presence of particles embedded in the walls of the osteotomy was confirmed in the BH (3 mm and 4 mm diameter), BL (3 mm diameter) and BLT-S (3 mm diameter) groups Fig. 3 - 4.

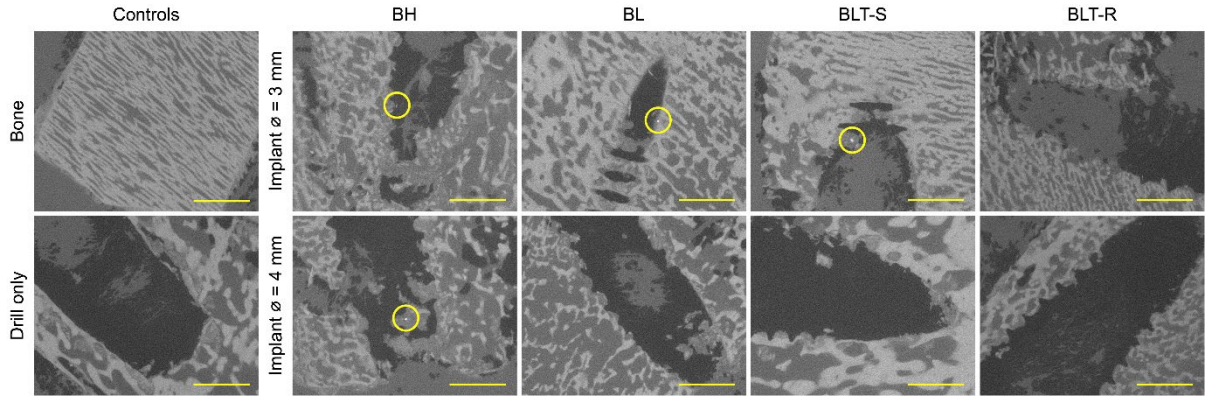

Figure 3 - 4. Representative μ-CT sections of controls and bone samples following implant placement and removal. The yellow circles depict areas of high attenuation (radio-opacity) suggestive of metallic particle. Scale bar for controls is 5 mm and for test group is 2 mm.

3.4.4 Scanning electron microscopy

SEM images were carried out on new, unused titanium implants (Fig. 3 - 5) to compare with the test groups (Fig. 3 - 6). Topographical changes were evident in

the implant type surfaces, in all three regions (apex, centre and neck). Cracks and areas of the surface peeling were more frequent in the alloyed implant surfaces, in particular the Ti6Al4V group.

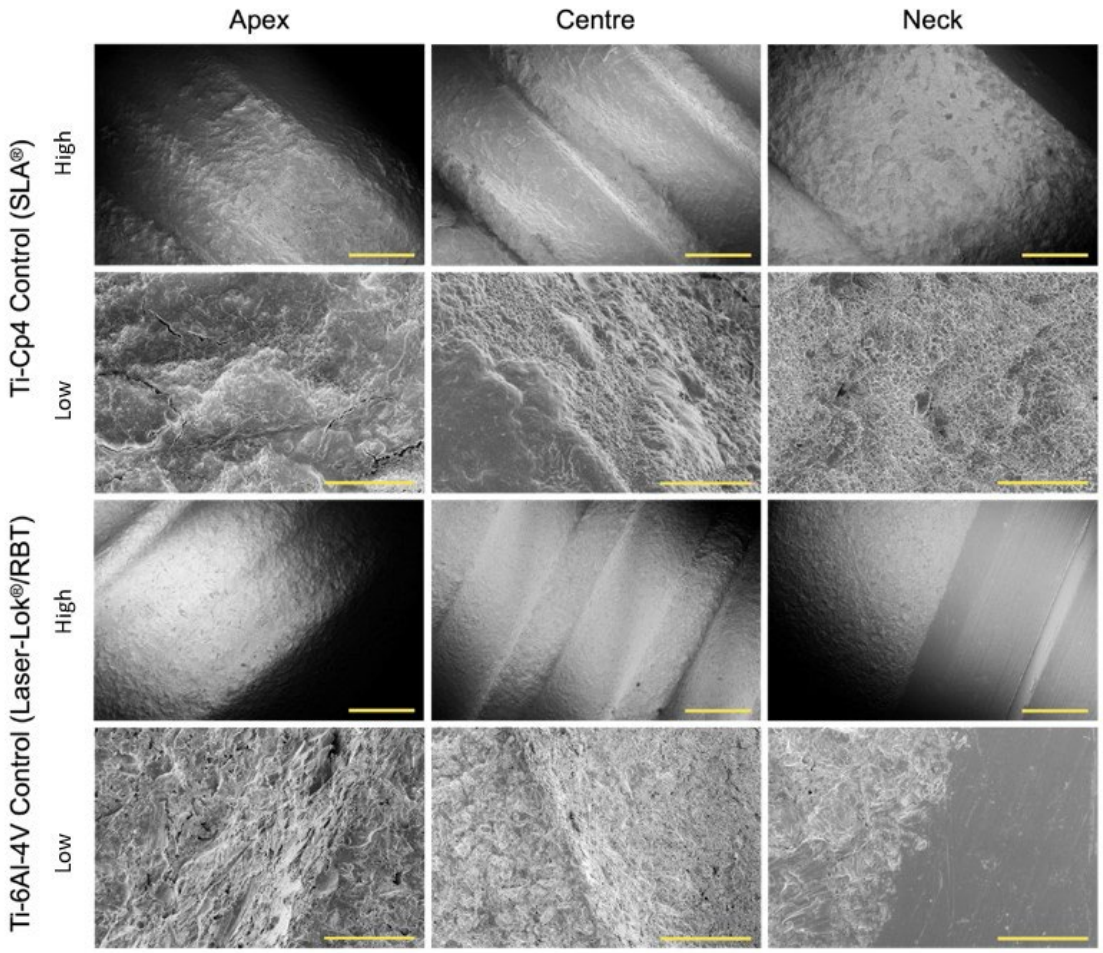

Figure 3 - 5. SEM images of new implants prior to surgical placement. Scale bars for high magnification is 500 µm; scale bars for the low magnification is 50 µm.

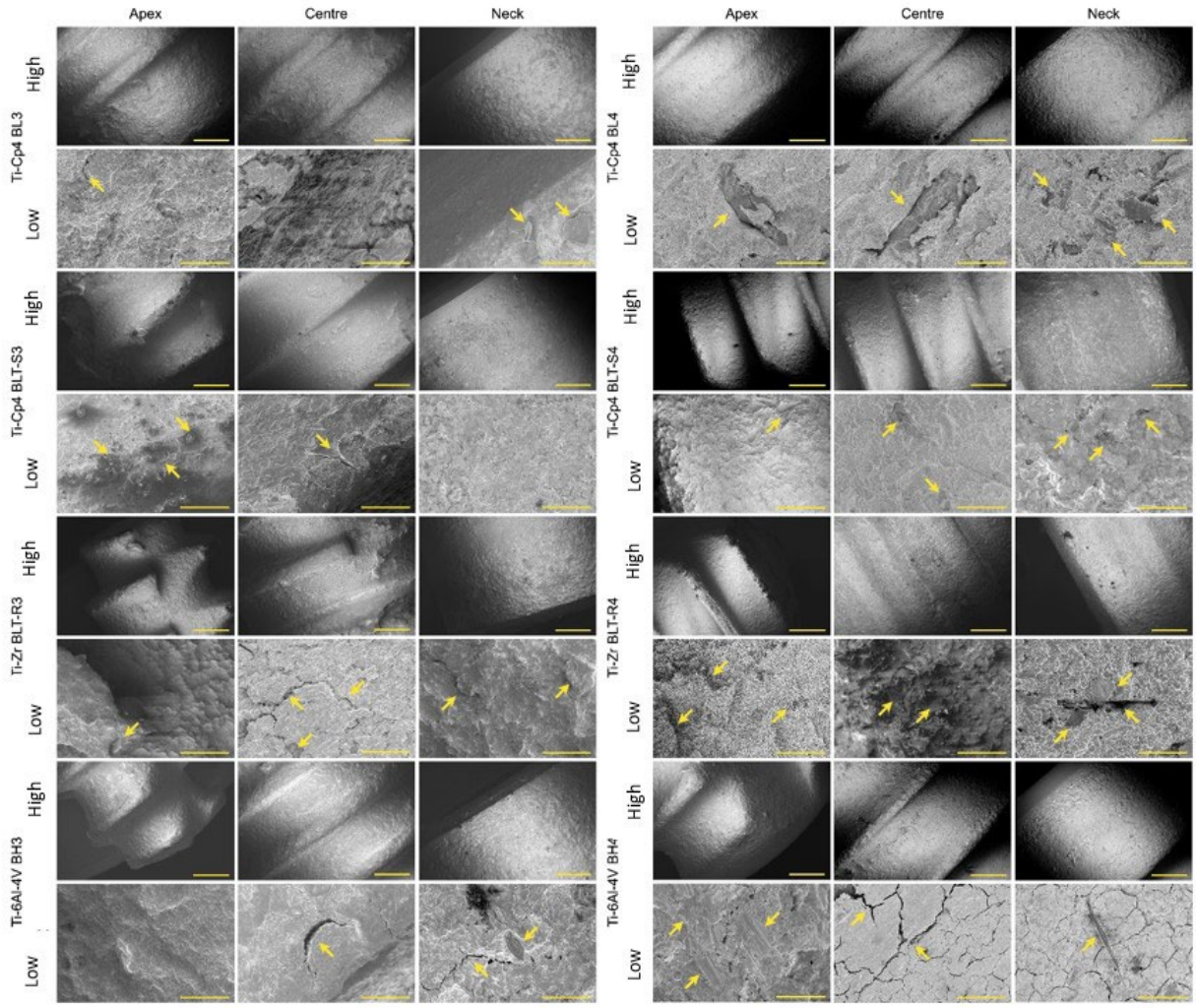

Figure 3 - 6. SEM images of a representative sample of implants following placement and removal. Yellow arrows depict areas of surface damage with visible cracks and peeling. Scale bars for high magnification is 500 µm; scale bars for the low magnification is 50 µm.

Dynamic Light Scattering (DLS) analysis was carried to assess the particle size in the different implant materials, as summarised in table 3 - 3.

Table 3 - 3. Summary of the DLS results for the three implant material groups.

Particle material	**Particle diameter (µm)**	**Nano particle sizes (nm)**
Ti-CP4	34.1 ± 3.8 (D50 = 32.2)	95.4 ± 9.1 (modal number 79.3)
Ti6Al4V	33.3 ± 4.4 (D50 = 30.3)	77.74 ± 10.4 (modal number 70.1)
Ti15Zr	97.8 ± 8.2 (D50 = 85.2)	135.1 ± 11.3 (modal number 86.8)

3.4.5 Confocal microscopy

Particle uptake by the HGF and RAW 264.7 cells was confirmed with confocal microscopy using FITC labelled particles for comparison with controls (Fig. 3 - 7). All particle types were taken up by both cell lines. The orthogonal images developed by z stacking confirmed the presence of the particles mainly within the cytoplasm of the cells.

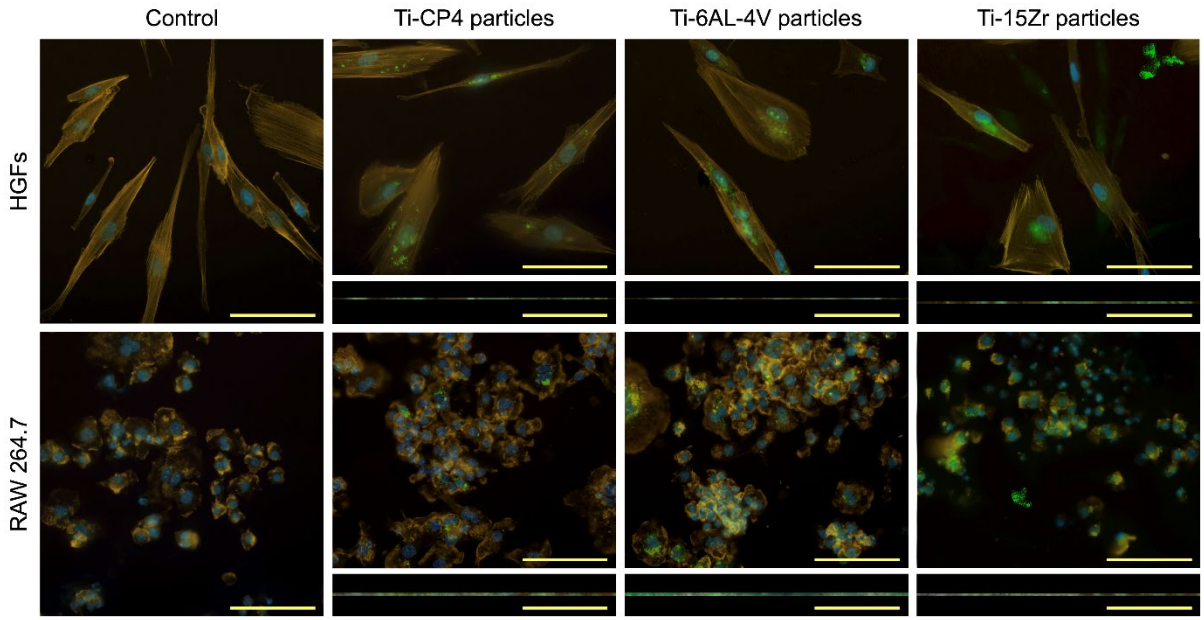

Figure 3 - 7. Confocal images of representative samples of HGF's and RAW 264.7 controls and cells cultured in the presence of functionalised titanium particles. Orthogonal images created using z stacking confirm the presence of the titanium particles within the cells. Yellow staining depicts actin microfilaments, blue depicts the nuclei and green is the FITC functionalised titanium particles. Scale bars are 100 µm.

3.5 Discussion

The aim of this study was to investigate the release of particles from dental implants immediately following placement of the fixtures. Some implant systems have developed narrower implants in order to allow fixture placement in narrower jaw ridges with reduced bone volume. In order to increase the strength of the implants in narrower diameters Ti alloys have been developed (116), the most commonly used ones being Ti6Al4V and Ti15Zr. This study also investigated the

effect of the implant diameter, morphology and material composition on particle release.

Particle release during placement of dental implant fixtures is thought to occur due to placement shear forces as a result of mechanical damage to the micro roughened surfaces, as well as dissolution into surrounding tissues (25, 117). There was no significant difference in the implant placement torques. The particles detected are therefore unlikely to be as a result of the variation in the placement forces.

The wider diameter implants had more Ti release in the Ti-CP4 groups but there was no significant difference in the either of the alloy groups (Ti15Zr and Ti6Al4V). The wider diameter implants have a larger surface area which would explain higher Ti release. The effect of implant morphology was compared using the BL and BLT-S groups as these have identical surfaces and material composition, with the only difference being that BL is cylindrical and BLT-S is tapered. The other implant types (BH, BLT-R) were all tapered. There was significantly more Ti release from the BL cylindrical implants compared to the BLT-S tapered fixtures (Fig. 3 - 2).

The surgical protocol for preparing for the placement of a cylindrical implant varies slightly from the tapered implant in that the osteotomy needs to be tapped to create a thread pattern coincident with the fixture. The reason for this is that the cylindrical implant thread is less aggressive than the tapered one, which is self-tapping. In this study tapping was not performed for any of the implants in order to standardise the procedure. Hence, the results for the higher particle release in the cylindrical implant group needs to be considered with caution as clinically tapping would be indicated. The clinical surgical protocol includes sterile saline irrigation during the drilling process, however, in this study irrigation was not used in order to avoid particles being dislodged from, or pushed into the osteotomy sites.

The SEM images revealed cracks and peeling of the implant surfaces with more damage observed at the neck and apex areas. This may be due to the more

cortical bone quality in the neck region, especially in the mandible model and as the apex of the implant engages the apical bone both of which give the implant the primary stability.

There was significantly more particle release from the Ti6Al4V implants irrespective of the implant diameter ($P<0.01$). There have been reports that Ti alloys have a reduced surface hardness (118, 119) and that Ti6Al4V is also more susceptible to corrosion (120, 121). Ti15Zr has been shown to be more resistant to corrosion than Ti6Al4V (122, 123).

Micro and nano particle release from titanium implants and the presence of particles in intra-operative fluids have been previously reported (104, 124-126). The significance of particle release in the peri-implant tissues has been linked to the aseptic loosening of orthopaedic implants (127, 128). The quantity of particle release has been reported in the range of 0.2 mg – 3 mg with increased osteoclastic activity and implant loosening within 7 days of orthopaedic implant placement (129-131). In this study the amount of particle release from all samples was within this range (0.2 mg – 3 mg), using the standard curve developed to extrapolate the ICP results to measure the quantity of particle released (Fig. 3 - 3).

The effect that the presence of particles has on cells is not fully understood. The cells are unable to spread on small particles which become internalised, as demonstrated with the confocal images in this study (Fig. 3 - 7). The mechanism for internalisation is not clear. This may involve invagination of the cell membrane, possibly with a Trojan Horse effect whereby the particles aggregate with a mixture of tissue proteins, calcium and phosphorous ions (132). In the case of nanoparticles, passive diffusion into the cell may occur with molecular consequences such as DNA methylation and modification of ribonucleic acid (RNA) (109, 124, 133).

The intracellular sequelae form the presence of particles is not understood and may involve inflammatory processes, increase reactive oxygen species, cytotoxicity or carcinogenesis (35, 124, 134). There is evidence for the

mitochondrial and cytotoxicity of vanadium and adverse effects of aluminium, such as neurotoxicity and granulomatosis (135, 136). Zirconium has mainly been shown not to have any adverse effects, however, there have been some reports of zirconium affecting alterations in micro RNA with epigenetic changes (137-139).

3.6 Conclusions

This study confirmed the release of micro and nano particles during implant placement in the ex vivo pig mandible model, which was confirmed with ICP analysis and supported with µCT imaging. The implant morphology and material composition was shown to be relevant. The cylindrical implant released significantly more particles than the tapered one, however, this may be due to omitting tapping of the osteotomy during the surgical protocol and conclusions on this regard need to be guarded.

There was significantly more particle release from the Ti6Al4V implants compared to all the other types. The particles from all implant materials were internalised by both HGF and RAW 264.7 cell lines as demonstrated by confocal microscopy. Further investigations are indicated to understand the effect of the micro and nano particles in the peri-implant tissues and the intracellular pathways involved. This may help our understanding of any potential relationship between particle release and peri-implantitis. In the meantime, the release of vanadium and aluminium containing micro and nano particles, which are then taken up by local cells is a cause for concern as clinicians are using these implants on a global level.

This page intentionally left blank

4. Preparation and characterisation of bioactive glass S53P4

4.1 Introduction

The aim of this study was to prepare S53P4 bioactive glass (BAG), characterise and assess its biocompatibility *in vitro* with a view to investigate its suitability as a potential substrate for application in implant dentistry. S53P4 has been used as a bone substitute with anti-bacterial (70-72) properties.

Bioactive glass in tissue fluid develops a hydroxycarbonate apatite layer, which interacts with the matrix and activates cells enabling the formation of a bond between BAG and the surrounding bone and soft tissues (140). The main aim of this study was to investigate S53P4 bioactive glass preparation methods and properties as a powder and disc and its biocompatibility with HGF. This is with a view to demonstrate HGF attachment and proliferation on bioactive glass surface as a preliminary attempt to mimic the collagen attachment seen in nature between the alveolar bone and cementum on the tooth surface.

4.2 Materials and methods

4.2.1 Materials

Invitrogen (Life Technologies) UK and Sigma-Aldrich UK were used for purchasing the reagents and chemicals needed unless specified otherwise. This includes DMEM (Dulbecco's Modified Eagle Medium Ref: 21885-025), penicillin-streptomycin (P4333), PBS (phosphate buffered saline, tablet, P4417; solution, P5493), trypsin-EDTA (ethylenediaminetetraacetic acid, 10× solution, T4174), L-Ascorbic acid 2- phosphate (A8960), dexamethasone (D4902), citric acid (C2404), DMSO (dimethyl sulfoxide, D2650). Primary gingival fibroblasts (normal, human, LOT# 64440682, PCS-201-018) were purchased from ATCC UK.

Additional chemicals were purchased from Fisher Scientific UK, including ethanol 99.8+% (10437341).

4.2.2 Making and preparing glass

Powder mixture for S53P4 was prepared with the following composition (Table 4 - 1) for a batch of 150 g approximately.

Table 4 - 1. Chemical components of S53P4 bioactive glass expressed in mol% and wt%

Chemical component	mol%	wt%
SiO_2	53.80	52.964
$CaCO_3$	21.80	20.030
Na_2CO_3	22.70	23.052
P_2O_5	1.70	3.954

The furnace was preheated to 1400°C. The powder mixture was thoroughly mixed for 30 minutes on a “roller” prior to being introduced into a platinum crucible Fig. 4 - 1.

Figure 4 - 1. Platinum-4% gold crucible.

The crucible was introduced in the furnace at 1400°C and left for 90 minutes. The molten glass was removed from the furnace and immediately cooled by pouring in room temperature de-ionised water onto a sieve to drain the water. The frit was

then removed from the water and placed in a glass beaker and dried in 120˚C oven for 24 hours. The dry frit was placed in the platinum crucible and introduced to the pre-heated furnace at 1400˚C for 30 minutes to melt. A graphite mould with two cylindrical shapes of 11 mm by 16 mm (Fig. 4 - 2) was placed in a separate adjacent furnace and heated to 520 ˚C.

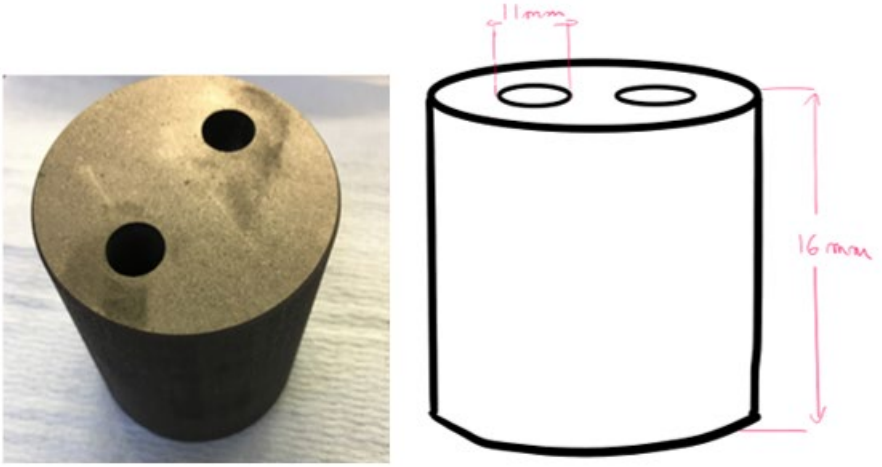

Figure 4 - 2. Graphite mould (left); dimensions for pouring bioactive glass cylinders (right)

The graphite mould was removed from the furnace, the molten frit was poured into it and the mould was re-introduced in the furnace at 520°C for 30 minutes. The furnace temperature was then turned to room temperature and left for 24 hours for furnace cooling before removing it and harvesting the two cylindrical bioactive glass samples Fig. 4 - 3a.

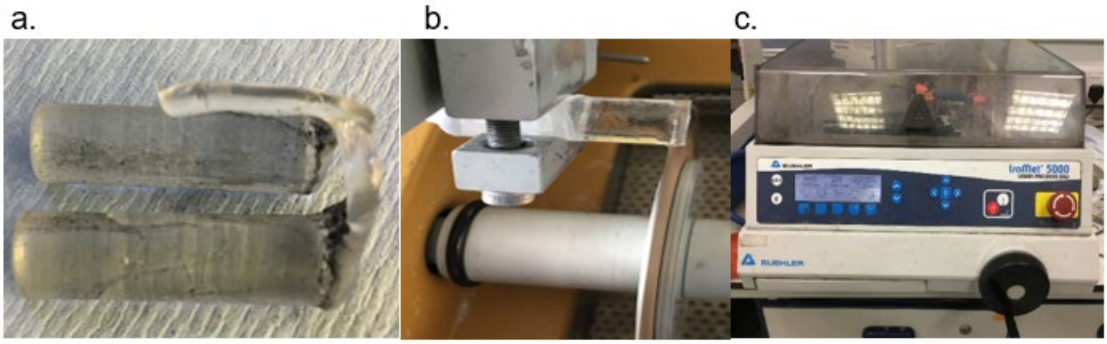

Figure 4 - 3. a. Bioactive glass cylinders removed from mould b. Positioning of bioactive glass cylinder for cutting using diamond disc c. Cutting of bioactive glass cylinders into discs at 2mm intervals Isomet saw.

The bioactive glass cylinders were then sectioned at 2 mm intervals with a 20LC diamond disc (0.8 mm blade) Isomet saw (Buehler) at 4200 rpm at a feed rate of 4.5 mm/ min (Fig. 4 - 3 b and c).

The discs were then polished using 1200P metallographic abrasive paper on Metaserv 250 (grinder polisher) for 2 minutes. This was followed by 3 minutes finer polishing using the Universal polisher with 1 μm polishing discs Fig. 4 - 4.

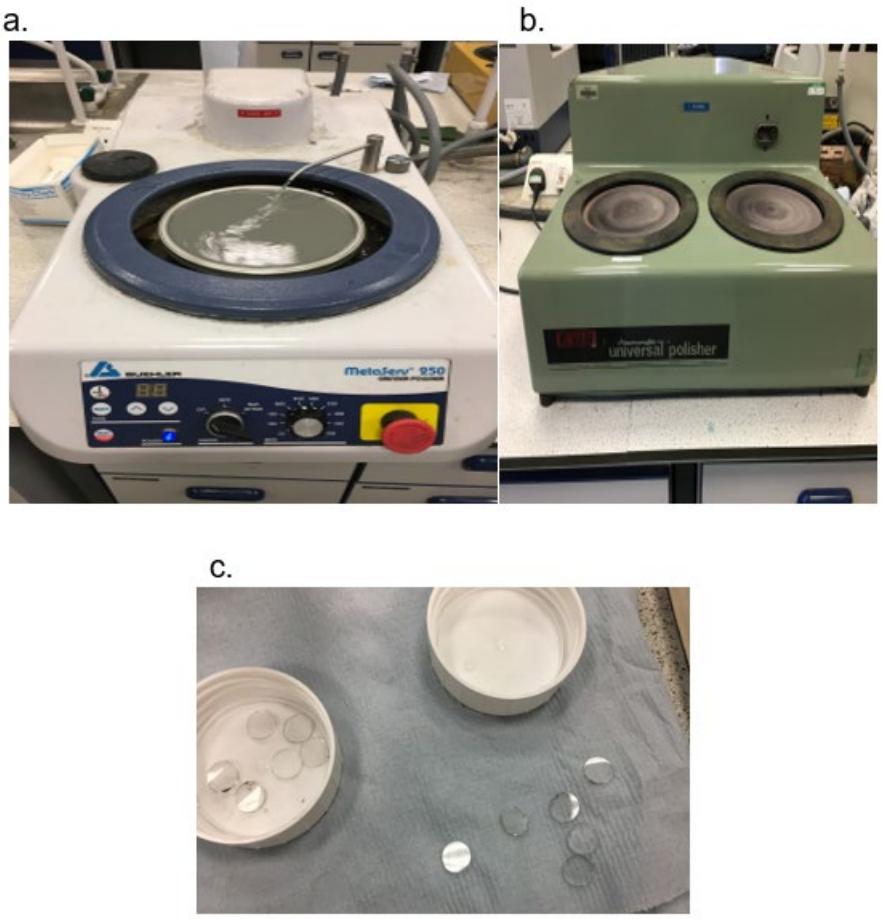

Figure 4 - 4. Polishing instruments: a. Metaserv 250 grinder for coarse polishing; b. Universal polisher for finer polish; c. Polished bioactive glass discs.

Glass powder was prepared by grinding samples using mortar and pestle followed by vibrating micro-mill and sieve shaker for reducing the particle size to 100 μm.

Further BAG powder preparation was carried out using variations in quenching and annealing during the process for analysis using X-Ray diffraction (XRD) in order to assess the influence of the preparation on the crystallinity of the glass. Four preparation groups were used: air cooled in the crucible and unannealed (UA); air cooled in the crucible and annealed (A); water quenched and unannealed; water quenched and annealed. The pH was also measured at multiple timelines for each BAG preparation powder placed in Basal DMEM to assess the dissolution properties of the different preparations.

4.2.3 Preparing culture media

Basal DMEM containing 1% (v/v) penicillin and streptomycin (100 unit.ml^{-1} penicillin and 100 µg.ml^{-1} streptomycin) and 10% (v/v) FBS (Foetal Bovine Serum) was prepared for culture expansion of HGF cell line. Cryopreserved stock HGFs were thawed rapidly in a 37°C water bath. 1 ml of cell suspension was added to 9 ml of basal media and placed in 75 cm^2 flask. Cells were maintained in humidified atmosphere at 37°C, 5% CO_2 and 21% O_2 for 3 days until 70-80% confluence. Culture medium was replaced every 2-3 days.

To passage cells, culture medium was removed and cells were washed with PBS 3 times. 1X TE (1 ml of Trypsin EDTA 0.5% (10X) was added to 9 ml PBS to dilute to 1X TE 0.05%) was added to the culture flask and introduced to the incubator for 1 minute. The flask was removed and cell motility checked under light microscopy to ensure detachment of most cells and basal medium was added to flask to arrest the TE activity. Cell suspension was added to a Falcon tube and centrifuged for 4 minutes at approximately 400G (1200 rpm); the supernatant media was carefully discarded into a separate Falcon tube temporarily. Cells were counted using a haemocytometer and resuspended to achieve the desired concentration.

Haemocytometer cell count in a 2X2 grid was: 3,3,2,2 = Total of 10 cells (or 40 cells in a 4X4) so average of 2.5 cells per single grid square. Therefore, cell density = 2.5 X 4 X 10^4 = 10 X 10^4 = 1 X 10^5 cells.ml^{-1}.

With a cell density of $1X10^5$ ml^{-1}, 0.1 ml will give $1X10^4$. However, 0.1 ml was too much for the 11 mm disc diameter and therefore 0.05 ml was required. In order to keep the same cell number but half the volume, the cells were centrifuged again and placed in 5 ml fresh basal medium, thereby doubling the cell density. So the cell number remained the same but the volume used to cover the discs was now 0.05 ml.

4.2.4 Seeding on discs

The S53P4 glass discs were used for seeding in order to simulate S53P4 surface on dental implants for collagen attachment. The transmucosal component of titanium implants are smooth for soft tissue apposition, hence the S53P4 discs surfaces were polished (using 1200 grit sand paper) to ensure a smooth surface. The discs were marked on the rough surface to ensure the finely polished surface was easily identified when placing them in the wells with the polished surface facing up. Glass discs were sterilised using 70% ethanol for 1 minute and washed 3 times using PBS. Individual discs were placed in each well of a 24-well plate with DMEM medium and placed in the 37°C incubator for 30 minutes. Prior to seeding DMEM was removed, 50 µl of cell suspension (1×10^4 cells/ disc) was placed on the polished disc surface and allowed to settle for 30 minutes in incubator. The cells were visually checked using light microscopy to ensure they have stabilised and 1 ml basal media was added to wells and left in incubator overnight.

The cell number was kept low (1×10^4 cells/ disc) in order to allow better visualisation and confocal imaging of individual cells on the disc surface. However, no cells were seen on the surface during SEM and confocal microscopy. Further attempts were made with careful pipetting during seeding as well as during adding and changing media in order to avoid the loss of cells from the polished S53P4 disc surfaces. New discs were used without polishing the surfaces in order to aid cell attachment and avoid loss of cells due to the high polish. No cells were detected on the surfaces of the discs despite repeating the process while ensuring delicate technique. The process was repeated again with

an increased cell concentration of 2 x 10^5 $ml^{-1}$and the discs were seeded by placing 1ml of cell suspension to cover the entire disc in each well, which resulted in cell attachment as shown in Figs. 4-15 to 4-17. The technique was adjusted to the high cell concentration as this ensured an adequate number of cells to achieve attachment and did not hinder imaging of the cells on the surface of the discs.

4.2.5 Scanning electron microscopy

Representative samples of the S53P4 discs were used to seed with HGF for SEM microscopy and Live-Dead fluorescent staining. For SEM the cells were fixed with 4% formaldehyde (10mls of 16% formaldehyde in 30mls of PBS). Samples were dehydrated with increasing increments of ethanol concentrations (50%, 70%, 90% and 100%) for 10 minutes at each increment and overnight in hexamethyldisilazane (HMDS). The discs were secured using carbon tape on an aluminium sample holder and coated with 10nm gold prior to scanning. A Zeiss Sigma-300 SEM was used to acquire images (EHT = 5 kV, WD = 7 mm).

4.2.6 Live-dead staining

Live-Dead staining was carried out in order to confirm that the cells on the discs are alive and spreading. HGF were seeded on S53P4 discs within 35 mm µ-dishes (ibidi®, Thistle Scientific Ltd, Glasgow, UK) in preparation for staining and fluorescent microscopy. These samples were not fixed. The one step staining solution was prepared according to manufacturer's instructions (Abcam® ad115347 Live and Dead Cell Assay) using 5X dilution of the dye for fluorescent microscopy. Viable cells are permeable to the dye which becomes fluorescent green after intracellular esterases remove ester groups. In contrast dead cells with compromised plasma membranes are stained red following the binding of the dye to DNA with high affinity and the subsequent increase in fluorescence. The samples were imaged using Leica SP5 MP laser scanning confocal microscope (Leica Microsystems, Wetzlar, Germany).

4.2.7 ICP sample preparation

Melt derived S53P4 glass was ground into powder and samples of S53P4 and pure SiO_2 powder (S100) (CAS number 14808-60-7) were collected using a 100 μm sieve. Dissolution products were prepared using 75 mg of powder in 50 ml SBF (68, 81) for both S100 and S53P4 powder. 1 ml samples were removed from each pot at the following time points: 30 minutes, 1 h, 2 h, 4 h, 8 h, 24 h and 1 week. After each time point sample 1 ml of fresh SBF was added back to the pot in order to maintain the 50 ml volume.

In addition, dissolution products of samples were prepared according to ISO standards at 0.2 g. ml^{-1} concentration in DMEM. Dissolution products of samples in disc form were prepared according to ISO standards at 3 $cm^2.ml^{-1}$ concentration in DMEM. 1 ml was collected for each time point: 30 minutes, 1 h, 2 h, 4 h, 8 h, 24 h. Collected samples were filtered through 0.2 μm filter and diluted (1:10 dilution) in nitric acid and stored until all the samples were ready for analysis.

Following sample collection, the powder containing solutions were centrifuged and the supernatant was discarded. The powder and discs were dried in 60℃ oven for 24 hours and used for SEM imaging. ICP standards containing 0, 2, 5, 10, 20 and 40 μg.ml^{-1} Ca, P, Na and Si were prepared. pH measurements were also taken at all the time points used for the ICP.

Standard solution used (μl):	0	50	125	250	500	1000
Concentration (μg. ml^{-1})	0	2	5	10	20	40

Total made up with nitric acid to 25 ml using ICP flasks (2 M nitric acid solution was prepared by adding 127 ml nitric acid to distilled water to make up to 1L).

4.2.8 Metabolic activity assay

Powder and discs of S100 and S53P4 were sterilised using 70% ethanol for 1 minute and washed with PBS three times and powder samples centrifuged to remove the PBS. All samples were placed in DMEM and left for 3 days using ISO concentrations (0.2 $g.ml^{-1}$ for powder and 3 $cm^2.ml^{-1}$ for disks). Samples were collected after 3 days and following another week soaking in DMEM. The resulting dissolution products collected were filtered through membrane with 0.2 µm pores and used for cell culture. Medical grade polyethylene (PE) was used as non-cytotoxic negative control and polyurethane (PU) containing 0.1% (w/w) zinc diethyldithiocarbamate (ZDEC) was used as cytotoxic positive control. Dilution series (25%, 50%, 75% and 100%) were prepared and supplemented with 10% (v/v) FBS prior to use in cell viability assays.

Table 4 - 2 depicts concentrations for each of the dissolution products (S53P4 powder, S53P4 disc, 100S powder, 100S discs, low concentration S53P4 powder and 100S powder) used to seed the plates for the MTT assay.

Table 4 - 2. Dissolution product concentrations for MTT assay (volumes measured in µl).

	Basal medium	**100%**	**75%**	**50%**	**25%**
FBS	50	50	50	50	50
Dissolution Product	0	450	375	250	125
DMEM	450	0	75	200	325

For each of the dissolution product concentrations the total volume was 500 µl (sufficient for 3 repeats of 100 µl each). HGF were seeded on 96-well plate (75 wells were needed with 100 µl per well) at 1×10^4 cells per well and left to grow in basal DMEM for 24 h. The media was then replaced by either fresh basal DMEM or the dissolution products. The plate set up is shown in Table 4 - 3.

Table 4 - 3. MTT assay plate set up.

Basal medium	X3			
S53P4 Powder	100% X 3	75% X 3	50% X 3	25% X 3
SiO_2 Powder	100% X 3	75% X 3	50% X 3	25% X 3
S53P4 Disc	100% X 3	75% X 3	50% X 3	25% X 3
SiO_2 Disc	100% X 3	75% X 3	50% X 3	25% X 3
S53P4 Low Conc.	100% X 3	75% X 3	50% X 3	25% X 3
SiO_2 Low conc.	100% X 3	75% X 3	50% X 3	25% X 3

After 24 h, the dissolution products were removed and replaced with 100 µl MTT (1 $mg.ml^{-1}$ in serum-free medium, freshly prepared) and incubated for 3 h. MTT solution was removed and the formazan derivatives produced by metabolically active cells were then dissolved with 100 µl DMSO and introduced into the plate reader (SpectraMax M5).

Dissolution products of S100 and S53P4 were also prepared using 75 mg in 50 ml concentration (68) and cellular metabolic activity were monitored for 1 week using MTT assay.

4.2.9 X-ray diffraction analysis

XRD analysis was carried out on the S53P4 powder soaked in SBF and DMEM for 2 hours, as well as in SBF for 2 weeks prior to collecting samples by centrifuging at 4000 rpm for 4 minutes, removing supernatant, washing with de-ionised water three times, with centrifuging following each wash and drying in 120°C oven overnight

For the modular powder diffractometer Bruker, Cu Kα radiation at 50 kV and 40 mA was used. 2θ was set between 10 ° and 70 °, 0.0034 increments.

4.3 Results

4.3.1 X-ray diffraction analysis of different preparations of bioactive glass

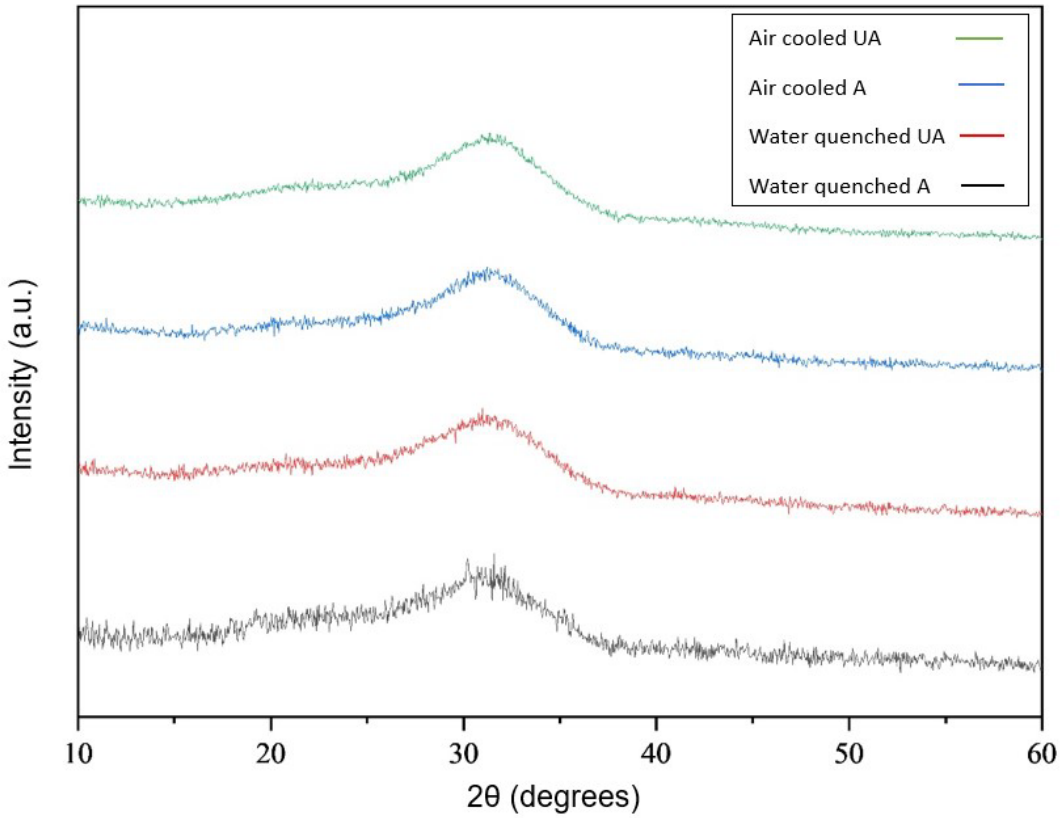

Figure 4 - 5. XRD analysis of the various preparations of BAG powder. Air cooled in crucible, unannealed (UA), green line; air cooled in crucible, annealed (A), blue line; water quenched, unannealed (UA), red line; water quenched and annealed (A), black line.

XRD analysis was carried out (Fig. 4 – 5) to ensure the amorphous structure of the bioactive glass particles prepared with variations in quenching and annealing process. There was no evidence of crystallinity in any of the four samples, with each XRD showing amorphous halos.

Table 4 - 4. Changes in pH for each preparation of the S53P4 BAG powder in DMEM at multiple time points.

Time point (minutes)	**Dissolution pH value of the different S53P4 preparations**			
	Water quenched Annealed	**Water quenched Unannealed**	**Air cooled Annealed**	**Air cooled Unannealed**
0	7.73 ± 0.01	7.64 ± 0.005	7.70 ± 0.005	7.50 ± 0.01
15	7.56 ± 0.01	7.39 ± 0.01	7.41 ± 0.005	7.40 ± 0.005
30	7.77± 0.005	7.51 ± 0.01	7.49 ± 0.01	7.51 ± 0.005
45	7.87 ± 0.005	7.71 ± 0.01	7.71 ± 0.01	7. 70± 0.005
60	8.07 ± 0.005	7.93 ± 0.005	7.86 ± 0.01	7.84 ± 0.005
120	7.77 ± 0.01	7.50 ± 0.005	7.45 ± 0.01	7.45 ± 0.005
240	7.73 ± 0.01	7.51 ± 0.005	7.43 ± 0.005	7.46 ± 0.005

The highest pH recorded for each of the BAG preparation groups was in the 60-minute time point, following which it dropped to near baseline levels in all preparations (Table 4 – 4).

4.3.2 Inductively coupled plasma spectrometry and pH analysis of S53P4 and S100 discs and powder

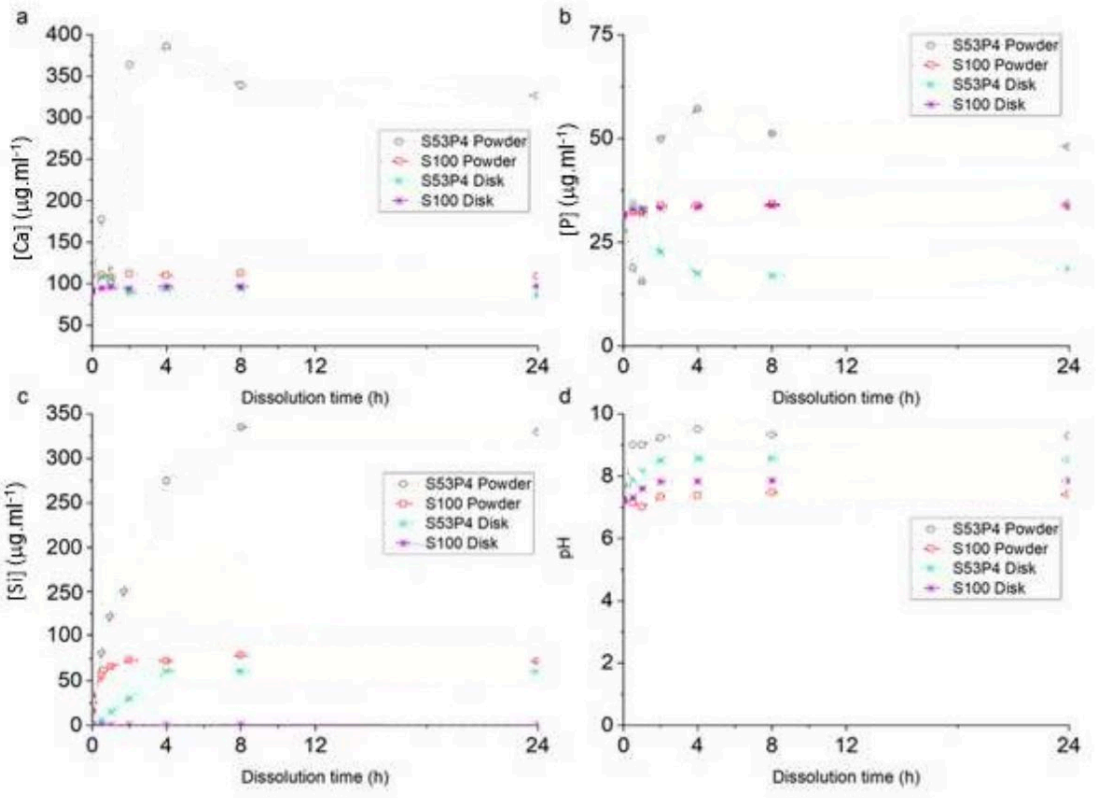

Figure 4 - 6. Elemental concentration of media following immersion of S53P4 and S100 powder and discs in DMEM as measured by ICP-OES: a) Ca b) P c) Si d) pH value. Error bars representing ICP error (n=3).

ICP results from S53P4 powder samples in DMEM showed a sharp rise in Ca levels up to 2 hours and then the levels plateau (Fig. 4 – 6). The P levels with S53P4 powder rose sharply in the second hour to reach a plateau in 4 hours. Si levels rose in both the glass powder groups; with S53P4 the rise was much higher reaching a plateau at 8 hours. There was a rise in Si levels from the S53P4 discs, but none from the S100 disc group. A rise in pH was observed in the S53P4 group, with a more marked rise in the powder group within the first hour (powder pH 9-9.5, disc pH 8-8.5).

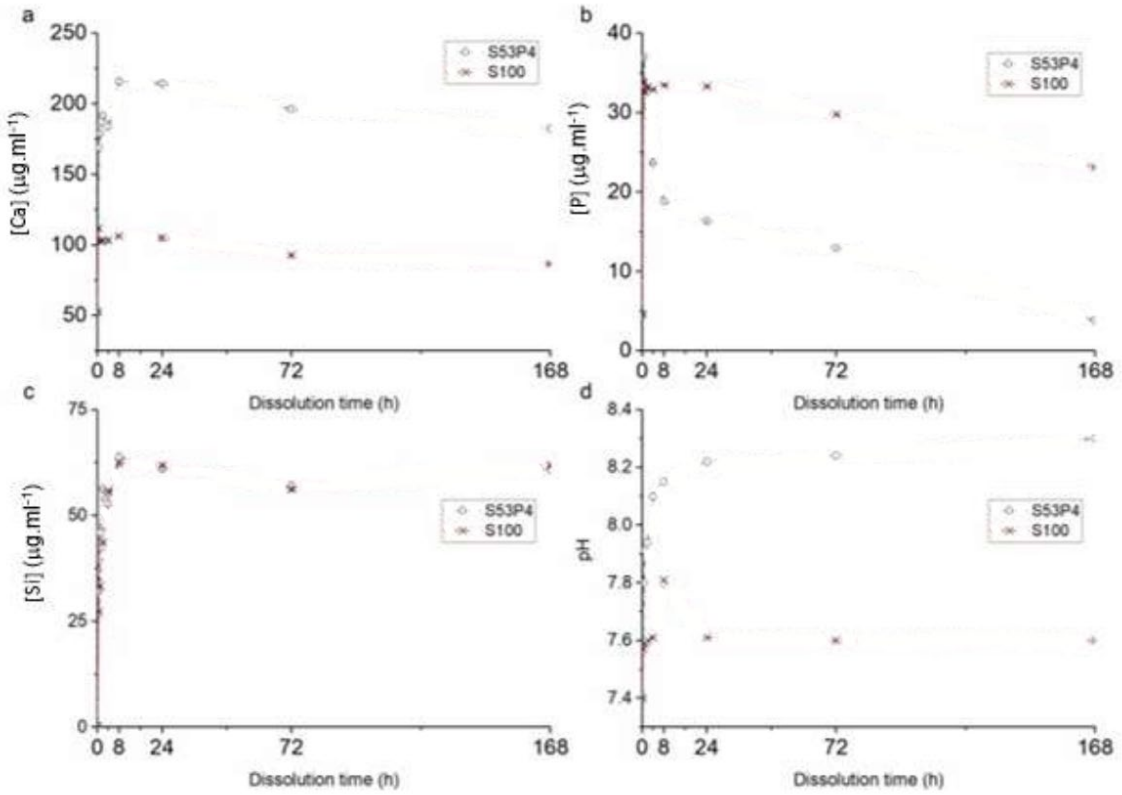

Figure 4 - 7. I Elemental concentration of media following immersion of S53P4 and S100 powder in SBF as measured by ICP-OES: a) Ca b) P c) Si d) pH value. Error bars representing ICP error (n=3).

ICP results from SBF samples revealed a steep rise in the amount of Ca release from S53P4 powder within the first few hours followed by a plateau for the rest of the week (Fig. 4 – 7a). P levels with S53P4 powder drops sharply in the first 24 hours and then more steadily thereafter (Fig. 4 -7b). Si levels rise steadily, in parallel and stay high through all the measurements up to 1 week (Fig. 4 – 7c). In SBF the pH for S53P4 rises steadily from 7.8 to 8.2 over the week, whereas S100 powder stays at 7.6 throughout except for one measurement of 7.8 at 8 hours (Fig. 4 – 7d).

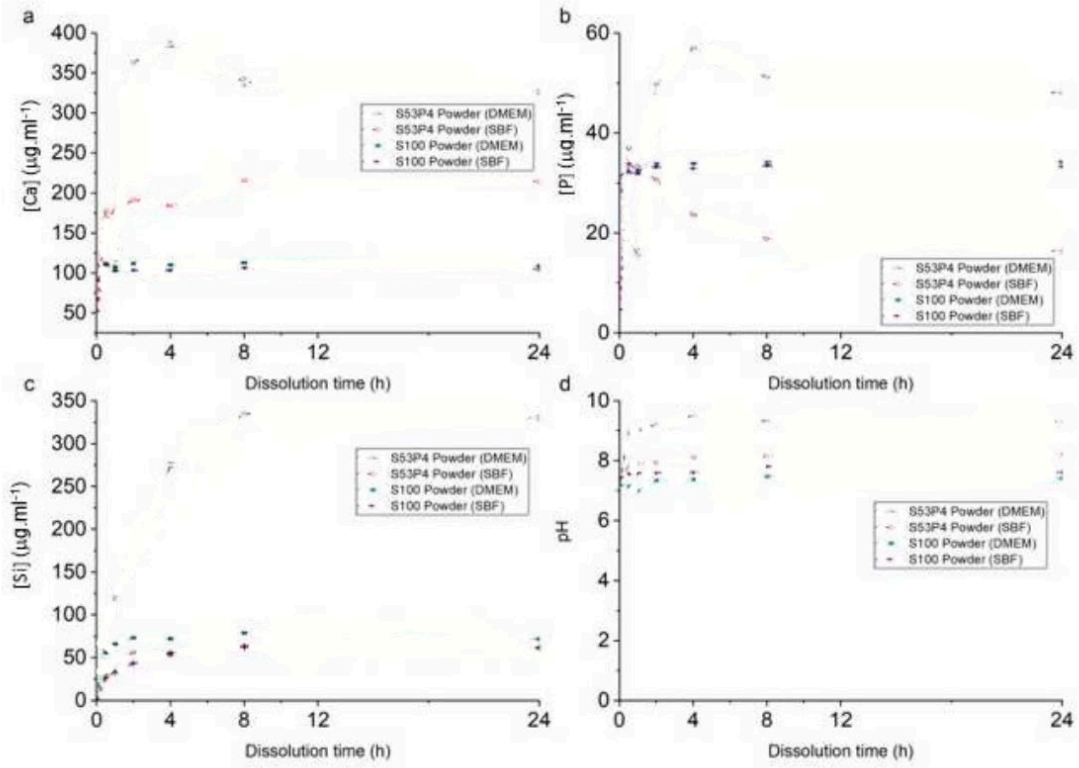

Figure 4 - 8. Elemental concentration of media following immersion of S53P4 and S100 powder in DMEM and SBF over the first 24 h, as measured by ICP-OES: a) Ca b) P c) Si d) pH value. Error bars representing ICP error (n=3).

Fig. 4 – 8 demonstrates the way S53P4 powder behaves in a very different manner in DMEM compared to SBF within the initial 24 hours. Ca, P and Si levels as well the pH is considerably higher in DMEM than in SBF.

4.3.3 Metabolic activity assay

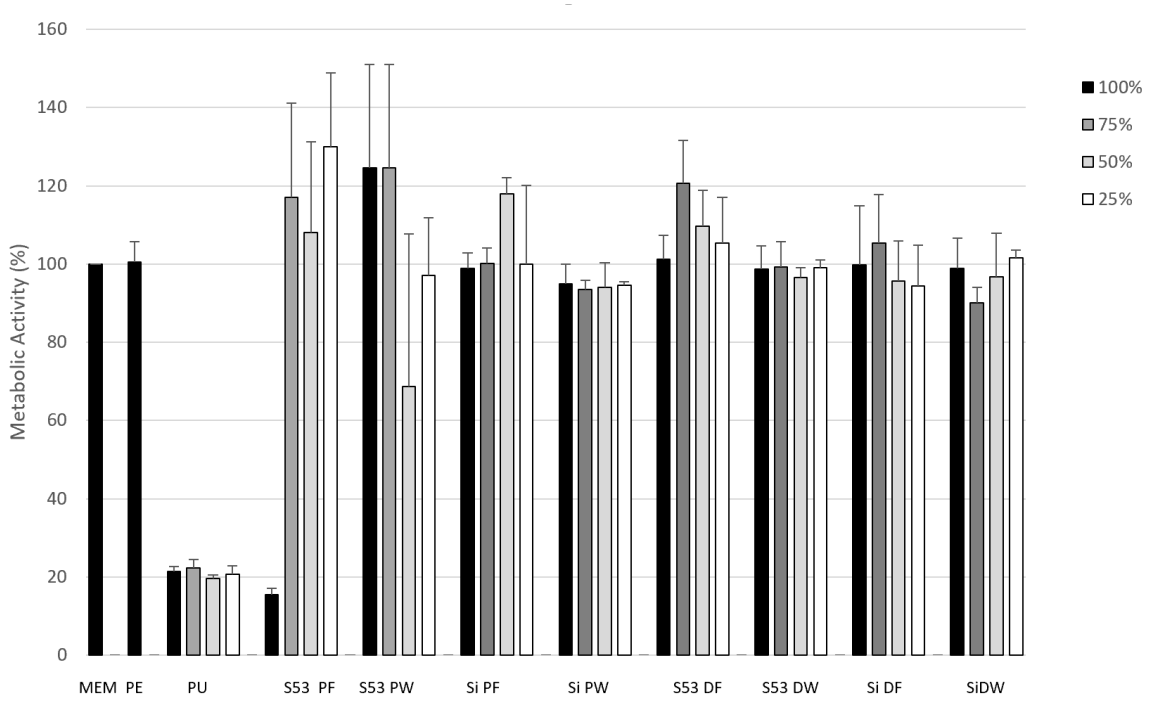

Figure 4 - 9, MTT assay results from dissolution product extracts of S53P4 and S100 powder and disc samples cultured with Human Gingival Fibroblasts. Minimum Essential Medium (MEM) & PE = negative controls, PU = positive control, S53 = S53P4, PF = powder fresh sample, PW = powder 1-week sample, DF = Disc fresh sample, DW = Disc 1-week sample. In this chart Si = S100

The MTT assay (Fig. 4 -9) revealed a very low viability of the HGF in samples of 100% dissolution product from fresh S53P4 powder (S53 PF) (0.2 $g.ml^{-1}$, ISO-10993-12), which was not seen in the 1-week powder samples (S53 PW). There was a smaller drop in vitality in the 50% S53P4 dissolution product at 1 week (S53 PW). All the other results with the discs showed good viability throughout, comparable to the culture medium and medical grade non-toxic controls.

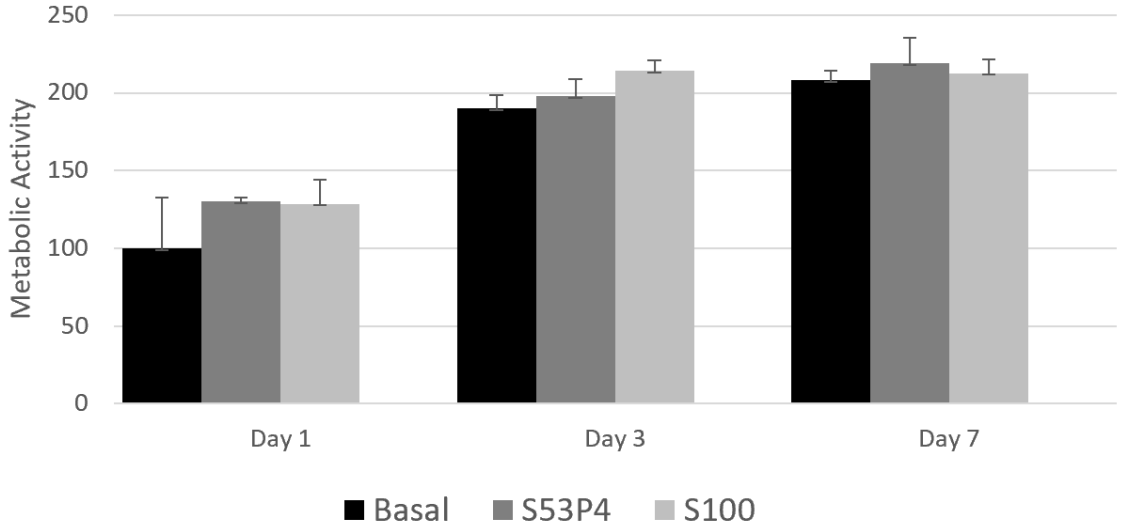

Figure 4 - 10. MTT assay results after 1, 3 and 7 days using basal medium as control, low concentration S53P4 bioactive glass powder and inert S100 glass powder cultured with Human Gingival Fibroblasts.

Human gingival fibroblast cells cultured in dissolution products from 75 mg in 50 ml S53P4 in medium showed good viability, comparable to the culture medium controls (Fig. 4 – 10). Inert S100 glass did not affect cell viability.

4.3.4 Scanning electron and confocal microscopy

SEM images of samples in DMEM (Fig. 4 – 11) and SBF (Fig. 4 -12) without cells revealed nodular structures from the first time point of 30 minutes on S53P4 powder and discs but none on the S100 samples or controls (controls were glass samples not placed in media).

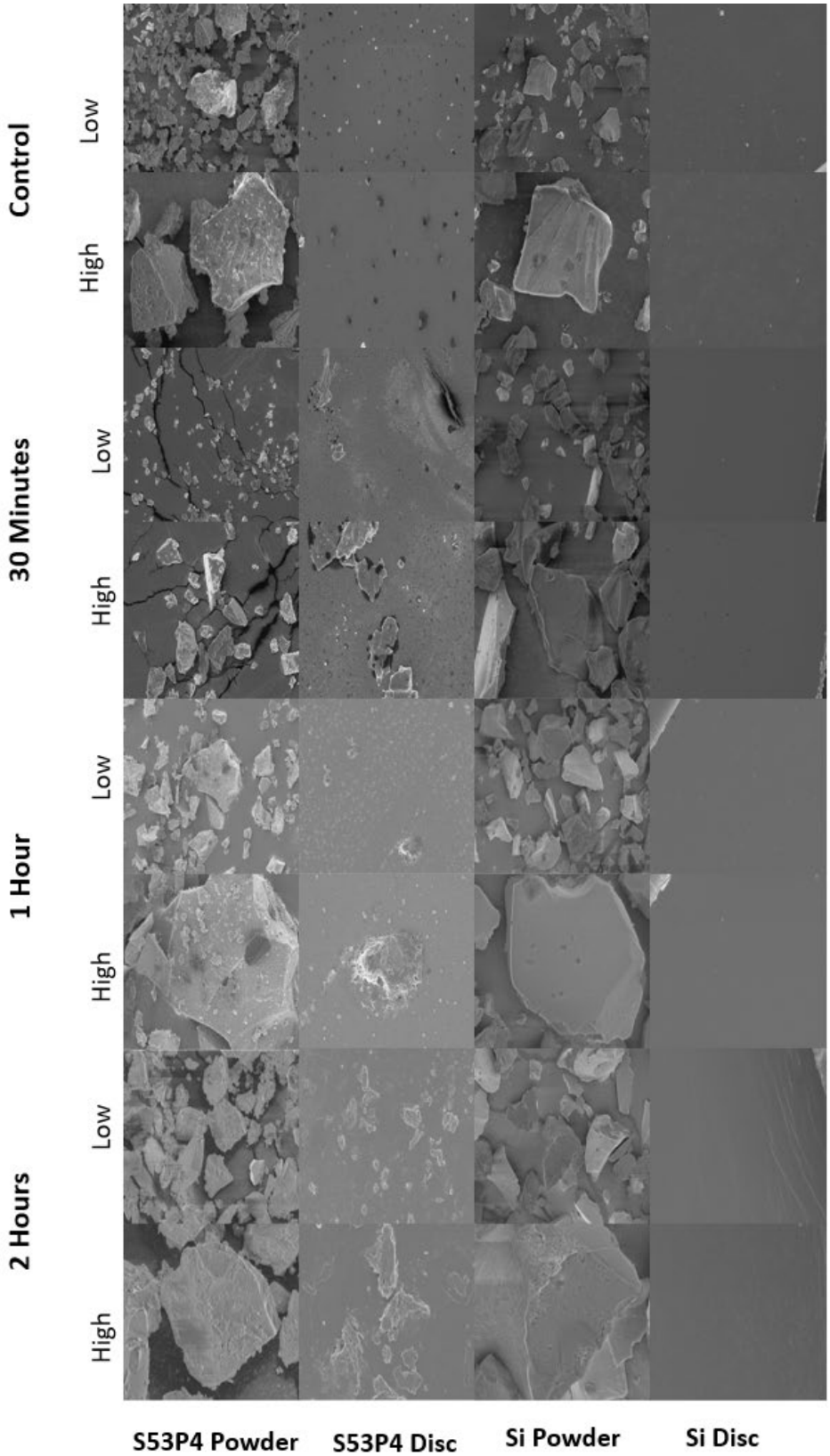

Figure 4 - 11. SEM of S53P4 and S100 powder and disc in DMEM. EHT = 5 kV, WD = 7 mm. Scale bars for low magnification = 15 µm, for high magnification = 10 µm

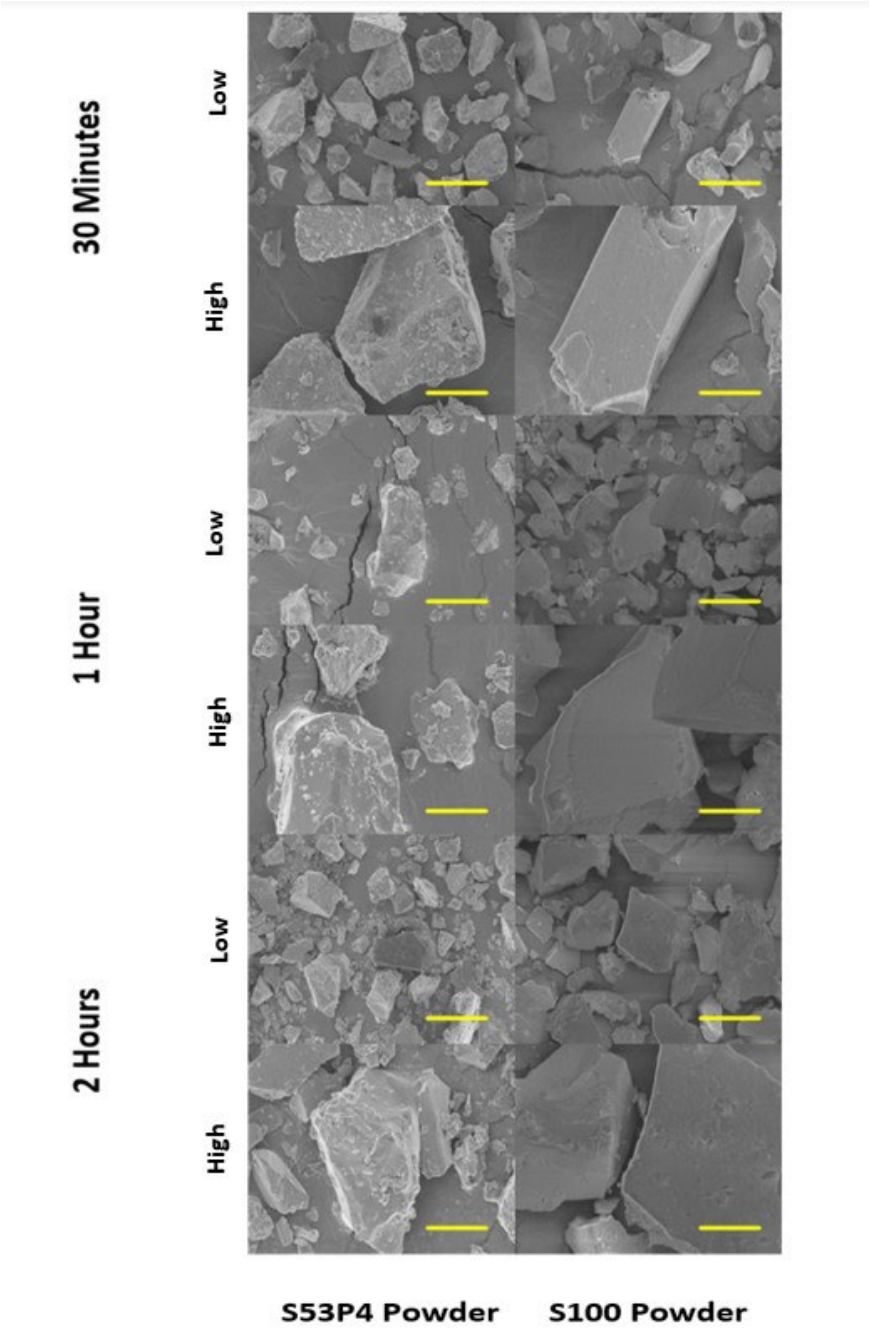

Figure 4 - 12. SEM of S53P4 and S100 powder in SBF. EHT = 5 kV, WD = 7 mm. Scale bars for low magnification = 15 µm, for high magnification = 10 µm

XRD analysis was carried out on the S53P4 powder soaked in SBF and DMEM for 2 hours to confirm the presence of HA/ HCA crystals on the particle surfaces which would explain the nodular appearance on SEM images (Fig. 4-13). However, there were no HA/ HCA peaks for DMEM or SBF after 2 hours of soaking the powders. The peaks in Fig. 14-13 represent calcite deposition. In

order to achieve measurable results for HA on XRD the powder was allowed to soak in SBF for 2 weeks prior to carrying out XRD analysis which resulted in HA peaks as seen in Fig. 4-14 (141, 142).

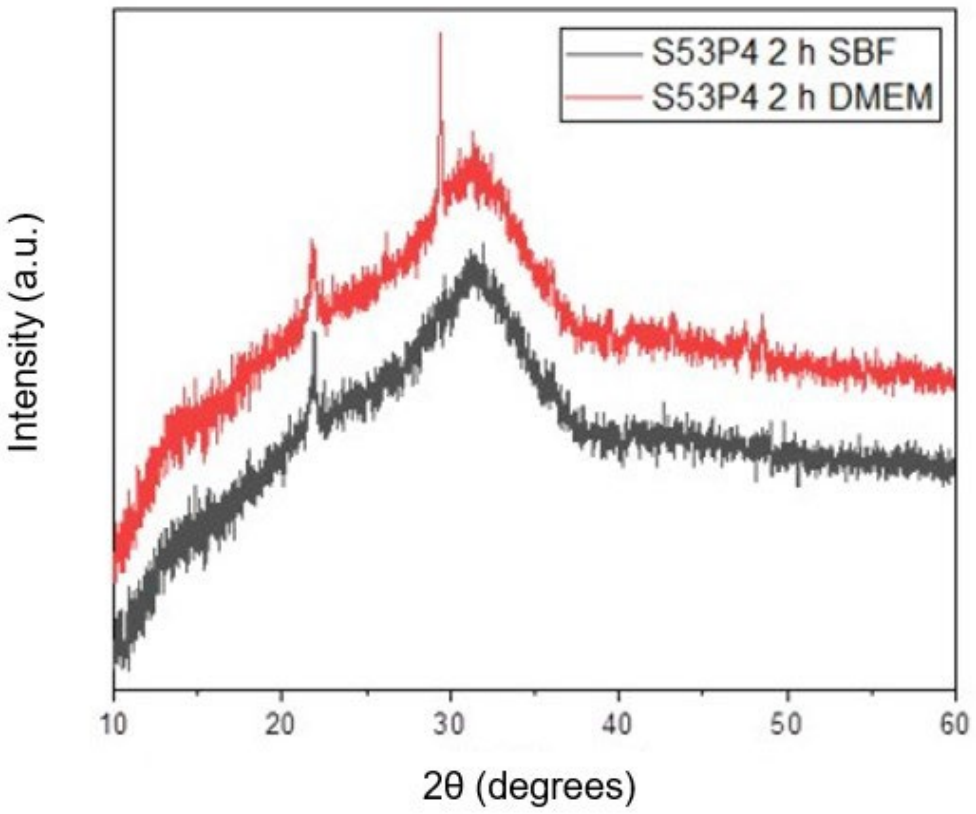

Figure 4 - 13. XRD analysis showing amorphous halos for the melt derived S53P4 powders after 2-hour soaking in SBF (black line) and DMEM (red line). The peak indicates the presence of calcite.

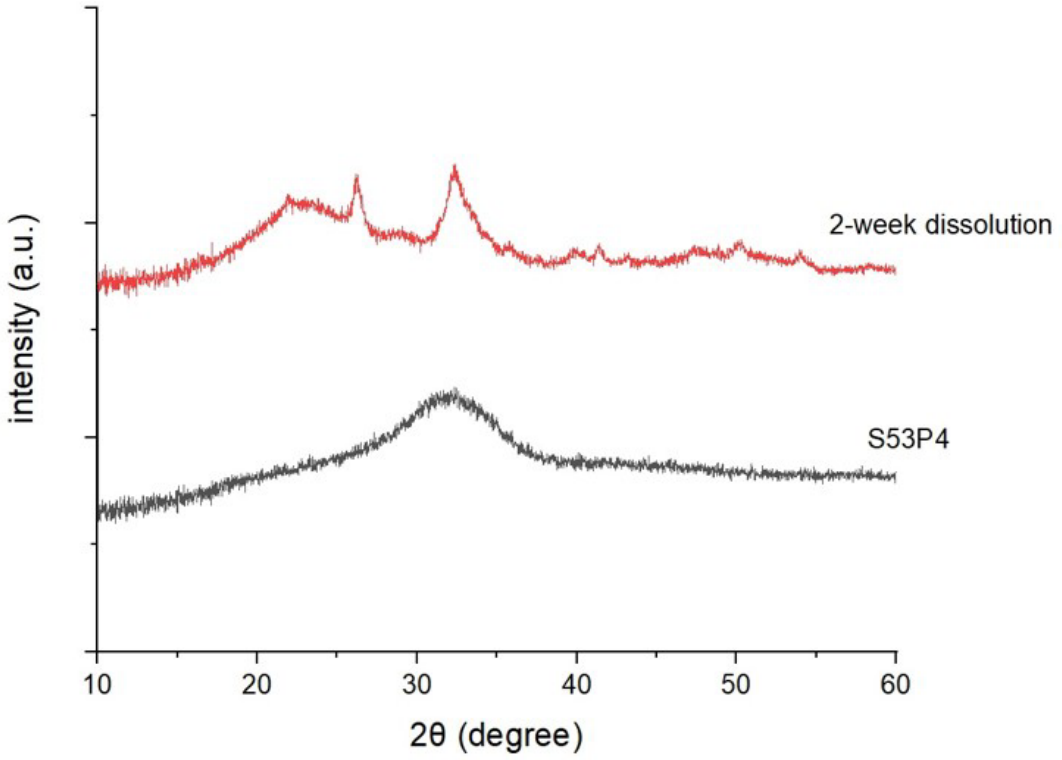

Figure 4 - 14. XRD analysis showing the amorphous halo for the melt derived S53P4 (S53P4, black line), and HCA/ HA crystals peaks after 2-week soaking in SBF (2-week dissolution, red line). hydroxyapatite ($Ca_{10}(PO_4)_6(OH)_2$, ICCD reference code: 9-432 (141, 142).

HGF attachment on S53P4 discs was demonstrated on SEM by the spindle like features of the cells spreading on the disc surface with apparent filopodia (Fig. 4 – 15). The morphology of unviable cells that do not attach would remain round. Confocal microscopy also revealed cell spreading and the green Live/ Dead staining indicating live cells, in the absence of any red staining. (Fig. 4 -16). The FIB-SEM cut sectional images (Fig. 4 - 17) show close approximation of the HGF to the S53P4 disc surface morphology, but with no apparent cellular projections beyond the surface

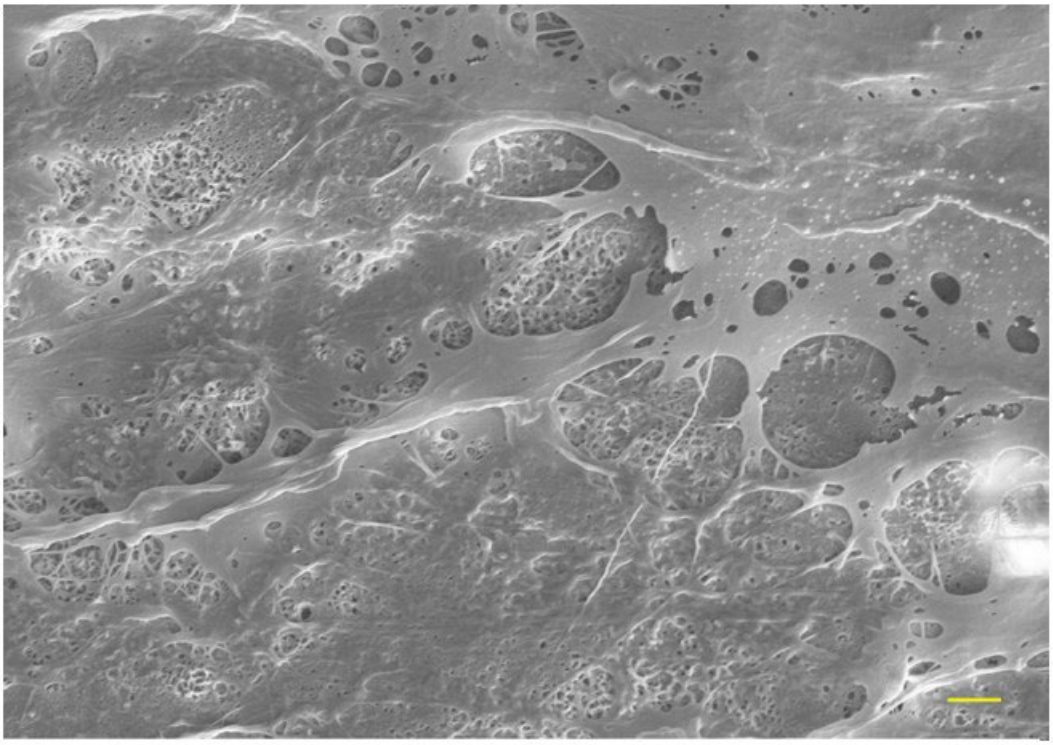

Figure 4 - 15. SEM image of HGF attachment on S53P4 disc surface. WD = 11.5 mm, EHT = 5 kV. 10 K X magnification. Scale bar = 1 µm.

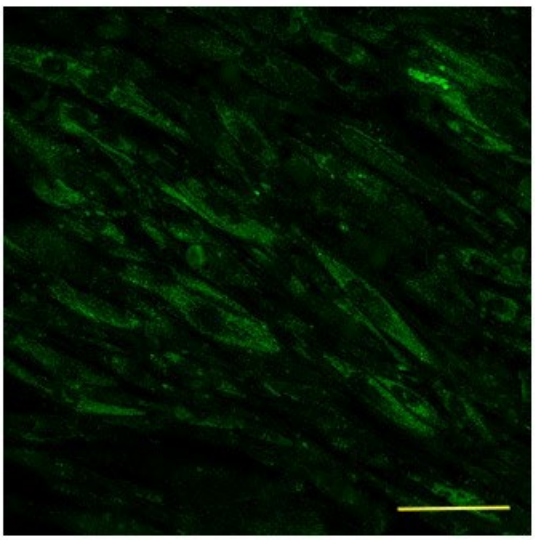

Figure 4 - 16. Confocal image of Live/ Dead staining of HGF on S53P4 discs. The green stain and spreading of the cells indicate live cells. Scale bar = 100 µm.

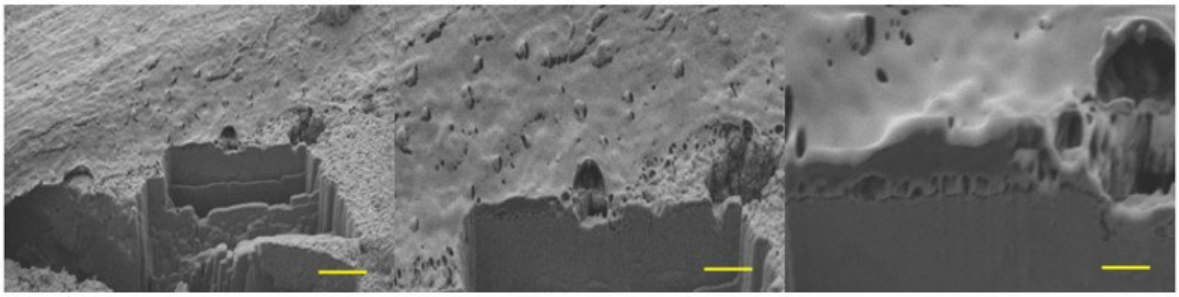

Figure 4 - 17. FIB SEM images showing cut section of HGF attached on S53P4 disc surface at increasing magnifications. (Left)10.5 k X magnification, scale bar = 1 µm. (Middle) 20 k X magnification, scale bar = 450 nm. (Right) 63 k X magnification, scale bar = 140 nm. WD = 5 mm, EHT = 1.49 kV, FIB probe = 20 kV: 50 pA, tilt angle = 54°.

4.4 Discussion

The aim of this study was to investigate the properties of S53P4 as a potential substrate for application in dental implant surgery. The key areas of interest were to confirm the amorphous structure of the glass and investigate the dissolution characteristics and biocompatibility of S53P4.

There was no increase in crystallisation detected from XRD analysis in air cooled samples, where the S53P4 bioactive melt was allowed to cool to room temperature in the crucible, compared with water quenched samples (Fig. 4 - 5). This could be because the air cooling from 1400°C to room temperature is fast enough to supercool the melt to a glass. Currently there are no detailed time-temperature-transformation (TTT) diagrams for S53P4 to show the critical cooling rate to avoid crystallisation (143). The rapid drop in the temperature of the sample to below the transition temperature (Tg) does not provide enough time for crystal formation. This suggests that air cooling in the crucible may be just as effective as water quenching for super cooling for glass formation. Further studies to develop a TTT diagram for S53P4 would allow a more detailed understanding of the time and temperature related behaviour of the material.

pH changes were analysed to assess any potential changes in dissolution behaviour in DMEM for the various BAG preparation methods (Table 4- 4). The pH increased in the first hour and dropped back to near baseline levels with all four preparations. The rise in pH could be due to the release of Na^+ and Ca^{2+} and uptake of H^+ from the media by the BAG glass surface. The subsequent drop in pH back to near baseline levels may be as a result of a precipitation on the glass surface. The presence of HCA precipitation was investigated with XRD analysis Fig. 4-13 and 4-14. Following 2 hours of soaking in SBF and DMEM the XRD revealed amorphous halos with a peak for calcite formation, but no HA/ HCA crystals were detected. However, following a period of soaking for 2 weeks the XRD analysis revealed HA/ HCA peaks indicating the possible need for longer soaking time required for measurable HA or HCA crystal levels to be formed (141, 142).

The ICP results from samples in DMEM revealed Ca level fluctuations with bioactive glass, which is expected due to the dissolution and precipitation at the surface which eventually stabilises (Fig. 4 - 6a). Previous studies using bioactive glass, albeit different glass composition (included Li and K cation substitutions) reported initial rise in P levels followed by a small drop to a plateau level (144). However, with the S53P4 powder the phosphorus levels increased to a plateau (Fig. 4 - 6b). The precipitation seen in Fig. 4-13 XRD analysis is likely to be as a result of calcite deposition. HA/ HCA crystal formation may be enhanced with increased surface area and/ or increased soaking time of the powder (145). The latter was demonstrated with HA/ HCA crystal formation after 2 weeks' soaking of the S53P4 powder in SBF for 2 weeks (Fig. 4-14),

The SEM images (Fig. 4 - 11 & 12) revealed nodular deposits on the surface of S53P4 disc samples, suggestive of precipitation on the disc surfaces. The nodular appearance of precipitation is also found on S53P4 powder, compared to the SiO_2 samples which don't show precipitation on neither powder nor discs due to the more stable and less reactive surface. Si levels rise as expected with a larger rise in S53P4 powder than S100 powder and for both the discs due to higher specific surface area of the particles exposed to the media and higher reactivity of S53P4 (Fig. 4 - 6c). Bioactive glasses with modifier cations (Na in the

case of S53P4 bioactive glass) allow interaction with water where Na is replaced by a proton from water, thus increasing the pH of the solution and allowing for surface interactions resulting in dissolution and subsequent precipitation (144). The pH increase (Fig. 4 - 6d) reflects the loss of H^+ from the media during cation exchange and dissolution of the bioactive glass surface, with DMEM values of pH 9-9.5 for S53P4 powder and pH 8-8.5 for S53P4 discs. The larger increase in pH with the powder S53P4 is due to the larger surface area compared to the disc.

ICP analysis was carried out on powdered S53P4 and S100 in DMEM but also in SBF with a view to assess the BAG behaviour in conditions more representative of the physiological conditions than in DMEM. ICP results from samples in SBF revealed an early sharp rise in Ca release with S53P4, reflecting the high reactivity of S53P4 surfaces. The sharp drop in P level within the first 24 hours followed by a more steady drop in SBF with S53P4 powder is likely to be due to precipitation (Fig. 4 - 7b). Si levels stabilise after an initial rise for both S53P4 and S100 (Fig. 4 - 7c), which can be expected if the suggested precipitation does not involve Si. The pH rise in S53P4 was as expected and for S100 there was a single measure of 7.8 at 8 hours which is likely to be an error, as the rest of the readings were consistent with no change in pH after the initial small rise (Fig. 4 - 7d).

ICP values of powder S53P4 and S100 within the first 24 hours were plotted in Fig. 4 - 8 to demonstrate the marked differences in dissolution behaviour in SBF compared to DMEM. This emphasises that the conclusions drawn from the DMEM dissolution ICP results may not be transferable to the *in vivo* physiological scenario. When these results are compared to studies assessing the *in vitro* dissolution product profile of melt derived 45S5 Bioglass (146), there are some similarities in that the dissolution products behaved differently in culture medium and in SBF. With 45S5 the trend of ion release in culture medium was slower than in SBF, but the final levels were higher in culture medium. This was particularly marked with Si. The pH rise was also higher in culture medium than in SBF, as was the case in this study. S53P4 powder in SBF shows a sharp, short lived spike of P levels in the first hour followed by a gradual drop, which is similar

to the trend seen in the study with 45S5. The early spike in P in SBF may be due to dissolution followed by precipitation.

The higher reactivity of S53P4 powder is reflected in the ICP and pH results. The high pH values found is of importance as it can affect cell viability, which was investigated with the MTT assay. The MTT assay results for the 100% dissolution product from fresh S53P4 powder (0.2 $g.ml^{-1}$ ISO-10993-12) showed a significant drop in cell viability; as stated by ISO-10993-12, if cellular viability is below 70% when in contact with dissolution products, the material cannot be considered biocompatible. The powder S53P4 may therefore not be suitable for fibroblast attachment based on the MTT assay results. This may be due to the large surface area to volume ratio of the powder, resulting in more rapid leaching and dissolution accompanied by the rapid rise in pH. S53P4 powder dissolution products (0.2 $g.ml^{-1}$) were left for 1 week and used to repeat the same MTT assay in accordance to ISO10993 standards. A drop in viability with the 100% samples of S53P4 powders was not observed in the 1 week assay. This may be due to pH buffering having taken place over the one week period. A linear relationship between Na_2O content of glass and rise in pH due to the ionic exchange at the glass surface has been previously shown. The higher Na_2O content also had higher cytotoxicity, which was not seen when the glass was subjected to 'pre-wash' (147). These results are similar to the findings of the current study in that the cytotoxicity from the fresh powder was not found in the 1 week samples which have effectively gone through a 'pre-wash'. The leaching of Na^+ from the high surface area of the glass powder and exchange with H^+ is the likely reason for the raised pH and the resultant cytotoxicity, and it is reversed by the 1 week conditioning which allows for a buffering effect.

There was a low viability result at 1 week only for the 50% concentration, which is likely to be an error as all the other concentrations showed good viability (Fig. 4 - 9, S53PW). The MTT assay showed a gradual improvement in viability from 1 day to 7 days (Fig. 4 - 10), which may be due to the buffering effect taking place and reducing the pH back to physiologic range after the initial sharp rise described above. The sharp rise in Ca levels, and the subsequent rise in pH, may also result in reduced cell viability. All the other results with the discs showed

good viability throughout, comparable to the culture medium and medical grade non-toxic controls.

SEM images (Fig. 4 - 15) showed spreading and cell attachment of HGF on S53P4 discs. The viability of the cells was confirmed with Live-Dead staining and fluorescent microscopy (Fig. 4 - 16), which confirmed live cells with esterase activity rendering the stain fluorescent green, in the absence of red staining which would indicate dead cells. Further imaging using FIB-SEM demonstrated the HGF cells following the rugged contour of the bioactive glass surface (Fig. 4 - 17). Although the SEM and confocal images of the Live-Dead staining confirmed viable HGF spreading on the S53P4 discs, this does not give a measure of the strength of cell attachment. The FIB SEM images show good apposition of the cells against the disc surface. TEM was considered as a means of visualising the cell and disc surface relationship in more detail, however, based on the current FIB-SEM findings this was deemed unlikely to add value. Further studies are required to allow a quantitative measure of the strength of the cellular attachment. This could be carried out using techniques such as atomic force microscopy (AFM) micro and nano mechanical test (148, 149), wash techniques or nano scratch methods (150).The method for seeding was shown to be more effective by ‘flooding’ the discs in wells with high concentrations of HGFs in comparison to the staged addition of low density of cells on the discs, allowing the cells to attach and then adding media to fully cover the discs. The lack of cell attachment observed with the latter approach for seeding may have been due to the polished disc surfaces and the washing off of the cells during the addition of media. The procedure was repeated three times with unpolished disc surfaces and applying very delicate technique for adding and changing media, neither of which improved cell attachment. The lack of cell attachment is unlikely to be due to the pH rise or rapid release of calcium from the disc surface, as the pH measurement Fig. 4-6 did not reveal a significant rise and the MTT assay in Fig. 4-9 demonstrated good viability of HGF in the presence of discs. The lack of HA/ HCA deposition at the early stages of soaking, as demonstrated by the XRD analysis (Fig. 4-13) may have also contributed to the lack of cell attachment as the cells were only cultured with the discs for 24 hours. Longer periods of culture may have allowed adequate HCA precipitation, as demonstrated by the XRD

analysis in Fig. 4-14 with the discs in SBF for 2 weeks, and result in improved cell attachment with even lower density of cells.
There is also some evidence that cell to cell contact plays an important role in the initial cell viability and ability to attach to substrate. The interaction of cells with the ECM and surrounding cells is seen in the majority of the living tissues. The intercellular distance has an influence on the intercellular signalling, cell adhesion and cell activation (151, 152). The improved cell attachment to the S53P4 disc surfaces when the higher cell density was used may have been as a result of the improved cell-cell contact thereby improving viability and ability to attach.

4.5 Conclusions

The S53P4 preparation methods described involving air cooled and melt-derived bioactive glass both result in amorphous structures, as confirmed by XRD analysis. S53P4 powder gives rise to a sharp increase in pH and Ca levels, both of which may affect cell viability at high concentrations. This effect is reduced following a one-week period of buffering. The S53P4 discs do not appear to have the same detrimental effect to viability. HA/ HCA crystal formation was only observed after 2 weeks of soaking the S53P4 powder in SBF. HGF were successfully seeded on S53P4 discs when soaked in media using a high density of cells. FIB-SEM and Live-Dead staining confirmed the spreading and attachment of HGF on the S53P4 disc surface. Therefore, the S53P4 discs appear not to be cytotoxic to HGF and potentially safe for clinical use. S53P4 powder may need to be pre-conditioned prior to clinical use. Further studies to investigate the potential application of the S53P4 bioactive glass in conjunction with dental implant surfaces are planned to assess the ability to attain a robust collagen attachment, as the current study did not demonstrate the strength of attachment beyond surface apposition and spreading of living cells.

This page intentionally left blank

5. Investigation of the influence of bioactive glass S53P4 on inflammatory markers

5.1 Introduction

A common complication in implant dentistry is peri-implantitis, a condition characterised by inflammation in tissues surrounding the implant resulting in the loss of supporting bone (19, 105, 153). Although the consensus opinion states that peri-implantitis is plaque induced (19), there is evidence to suggest that particle release from implant fixtures can cause inflammation and that vanadium (V) containing alloys can cause a rise in inflammatory markers such as IL6, IL1β, TNFα (35, 38, 104, 109, 125). TNFα, IL6 and IL1β are pro-inflammatory cytokines which cause vasodilation and increased permeability by acting on vascular endothelial cells thus enabling the local accumulation of neutrophils and monocytes in response to a foreign body invasion. The upregulation of these cytokines would therefore be an indication of a pro-inflammatory response. The aim of this study was to investigate the potential anti-inflammatory properties of S53P4 BAG by assessing its influence on macrophage polarisation and inflammatory marker release, particularly TNFα, IL6 and IL1β, from three cell lines, HGF, SaOs-2 osteoblasts, human bone marrow derived stromal cells (HBMSC) in the presence of titanium particles from Ti-CP4, Ti15Zr, Ti6Al4V and Zr.

5.2 Materials and methods

Titanium particles for Ti-CP4 and Ti6Al4V (Carpenter Additive, Widnes, UK) were gifted by Professor Jonathan Jeffers, and for Ti15Zr and Zr provided by Straumann® (Basel, Switzerland). Reagents were purchased from Merck Life Science (Dorset UK) and ThermoFisher Scientific (Paisley, UK).

5.2.1 Bioactive glass preparation

Powder mixture for S53P4 was prepared using the composition described in chapter 4.

The mixture was thoroughly mixed on a roller for 30 minutes prior to placing in a platinum crucible to introduce to 1400°C furnace for 90 minutes. The melt was then quenched in de-ionised water at room temperature in a sieve to drain the water from the frit immediately. The frit was placed in a 120°C oven for 24 hours to dry.

Glass powder of 32 μm diameter was prepared by ball milling and sieving the frit. S53P4 dissolution product was prepared by using 75 mg BAG powder in 50 ml of culture media appropriate for each cell line and placed on an orbital roller at 37°C for 72 hours. ICP-OES was used to determine the concentrations of calcium, silicon and phosphorus.

5.2.2 Cell culture

The culture media used for human gingival fibroblasts (HGF PCS-201-018™, ATCC, UK) and SaOs-2 human osteoblastic cell line (HTB-85™, ATCC, UK) was DMEM with 10% (v/v) FBS, 1penicillin (100 unit.ml^{-1}) and streptomycin (100 μg.ml^{-1}) (1% P-S). For human bone marrow derived stromal cells (HBMSC, 2M-392, Lonza, UK) MEM with 10% FBS and 1% P-S was used and for THP-1 human monocytic cell line (88081201, Merck Life Science, UK) the Roswell Park Memorial Institute medium (RPMI-1640) with 10% non-heat activated FBS and 50 pM β-mercaptoethanol (BME) was used.

Differentiation of THP-1 into macrophages was carried out using 24-hour incubation with 150 nM phorbol 12-myristate 13-acetate (PMA) followed by 24 hour incubation with RPMI.

Each cell line (HGF, SaOs-2, HBMSC, THP-1) was cultured in the appropriate media and in S53P4 dissolution products in the presence of the particles (Ti-CP4,

Ti6Al4V, Ti15Zr, Zr) at a concentration of 1.5 mg.ml^{-1}. The particles were sterilised with absolute ethanol and washed with PBS prior to introducing the media. The S53P4 dissolution products were filter sterilised with 2 µm filters prior to adding to cells.

5.2.3 Staining THP-1 cells

THP-1 cells were seeded on 35 mm ibdi® microscopy µ-dish (Thistle Scientific, Glasgow, UK). Samples of 2.5 x 10^4 cells were differentiated by incubating in 150 nM PMA for 24 hours followed by 24 hour incubation in RPMI. Control samples were prepared by centrifuging the undifferentiated cells which do not adhere. Undifferentiated THP-1 cells were fixated on microscopy µ-Dish by drying 100 µL PBS containing 2.5 × 10^4 cells. The cells were fixed with 4% Formaldehyde, which was replaced by 100 µL PBS and allowed to dry in 37°C oven overnight. Following wash and blocking with 1 % (w/v) BSA in PBS, samples were incubated at 4°C overnight with following primary antisera from ThermoFisher Scientific (Paisley, UK): CD14 (MA5-35200, 1:100 dilution), CD36 (PA1-16813, 1:100 dilution) and CD68 (PA5-32330, 1:100 dilution). This was followed by hour-long incubation with Alexa Fluor® 488-conjugated secondary antibody (1:1000 dilution). All samples were counter-stained with 0.1 µg.ml-1 DAPI and imaged under Leica SP5 confocal microscope.

5.2.4 Enzyme-linked immunosorbent assay

Cytokine expressions were measured using enzyme-linked immunosorbent assay (ELISA) kits (Enzo Life Sciences, UK).
for TNFα (ADI-902-099), IL1β (ADI-900-130), IL6 (ENZ-KIT178-0001) and mannose receptor (MMR/CD206, ThermoFisher Scientific, Paisley, UK) following the manufacturers' instructions. Protein standards of known concentration were first prepared in accordance with the instruction of each kit. Blank controls, standards and sample supernatants were incubated in coated 96-well plates at manufacturers' specified duration and temperature, followed by washing and incubation with detection antibody. Wash buffer (Tris buffered saline containing proteins and detergents) was prepared by dilution in distilled water from

manufacturers' supplied stock. Plates were subsequently incubated with protein specific Streptavidin-Horseradish peroxidase conjugated, followed by incubation in 3,3',5,5' tetramethylbenzidine (TMB) and hydrogen peroxide. Reactions were stopped with stop solution (1M solution of hydrochloric acid in water) and optical densities (OD) were measured at specified wavelength using a microplate reader. Average net OD bound for each standard and sample were calculated by subtracting the average blank OD from the average OD for each standard and sample (Average Net OD = Average OD - Average Blank OD). A standard curve was plotted for each of the tested protein and the concentration of the protein of interest in the collected sample supernatants were determined by interpolation.

5.2.5 Statistical analysis

Results were presented as mean ± S.D (n = 3). Non-parametric test with Kruskal-Wallis test (for multiple groups) were performed using GraphPad Prism. Results were deemed significant if the probability of occurrence by random chance alone was less than 5% (i.e. $p < 0.05$).

5.3 Results

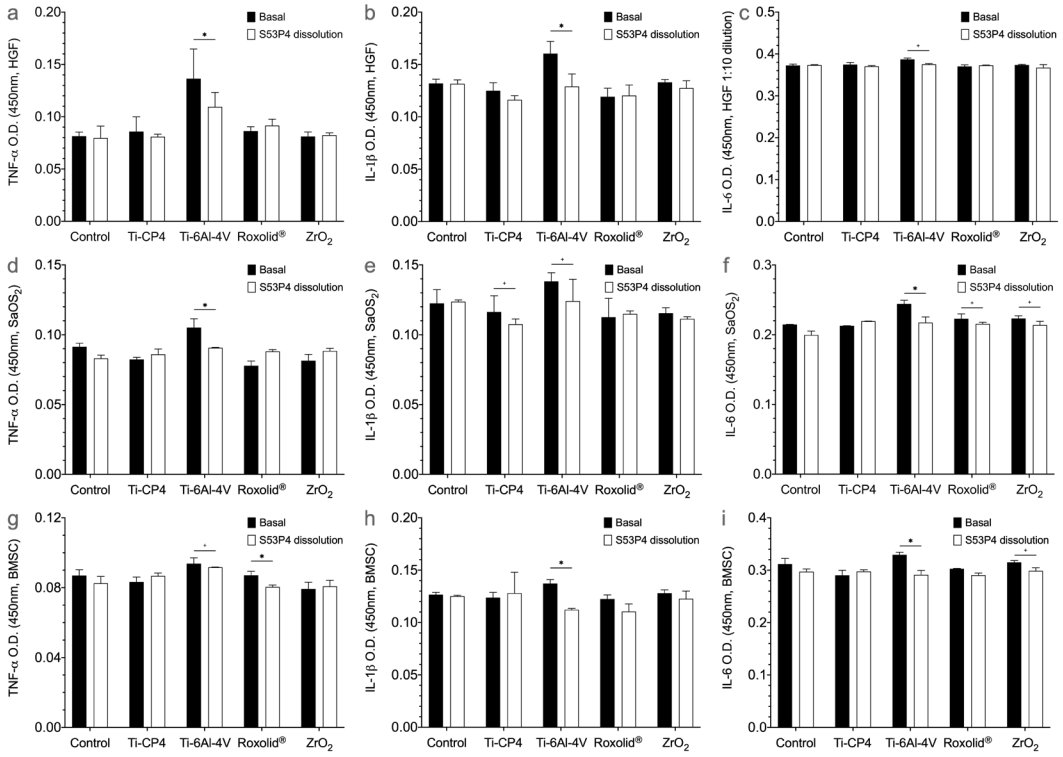

*Figure 5 - 1. ELISA results showing expressions of TNFα, IL1β and IL6 cytokines by HGF (a, b, c respectively), SaOS-2 osteoblastic cells (d, e, f respectively) and BMSC (g, h, I respectively) in response to culturing with various implant material particles. * $p < 0.05$ and $^{+}$ $0.05 < p < 0.1$.*

Of the four implant material particles tested Ti6Al4V was the outlier with significantly higher expression of TNFα and IL1β from HGF, TNFα and IL6 from SaOS-2 osteoblastic cells and IL1β and IL6 from HBMSC (Fig. 5 - 1). There was no statistically significant difference between the other materials and basal controls.

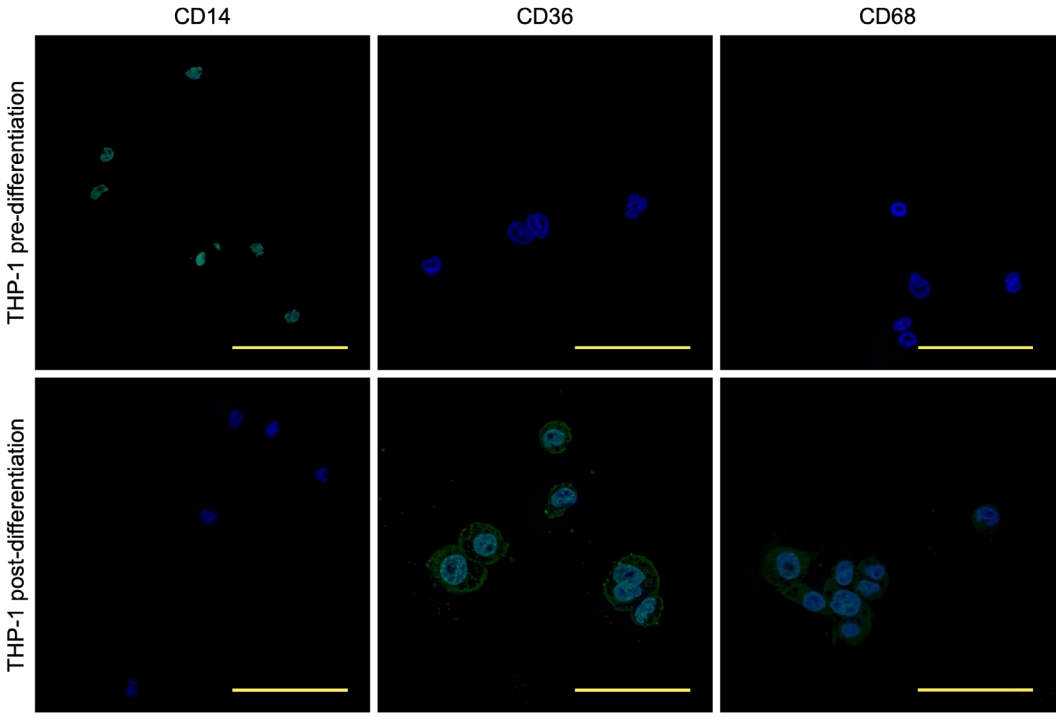

Figure 5 - 2. Confocal images showing THP-1 cells pre and post differentiation. CD14, CD36 and CD68 markers were stained (green) using immunohistochemical labelling and counterstained with DAPI (blue). Scale bar = 50 µm.

The confocal images (Fig. 5 - 2) show the higher intensity green staining of CD14 markers (marker for monocytes) in pre-differentiated THP-1 cells while in differentiated cells the CD36 and CD68 (markers for macrophages) were more intensely stained with the green immunohistochemical labelling confirming the differentiation of the monocytes into macrophages.

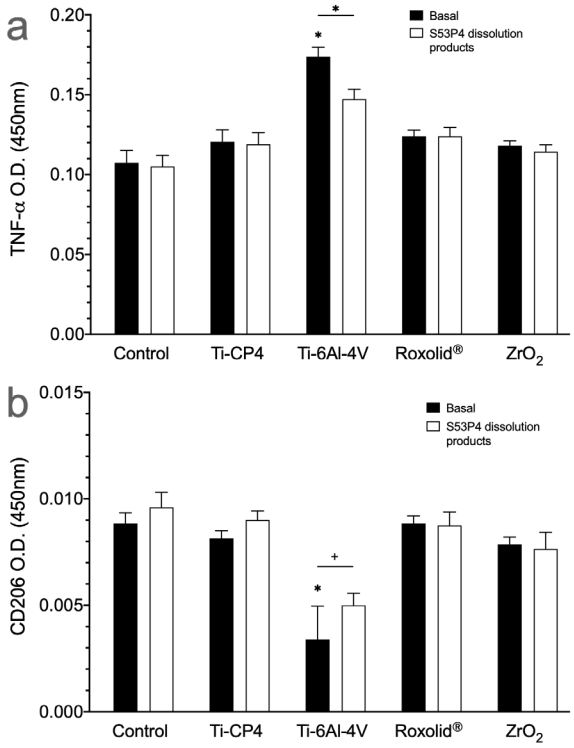

*Figure 5 - 3. THP-1 M1/M2 polarisation. ELISA results from THP-1 cells cultured with four types of implant particles showing the expression of a) TNFα as an M1 marker and b) CD206 as an M2 marker. * $p < 0.05$ and $^{+}$ $0.05 < p < 0.1$.*

The expression of TNFα from THP-1 cells was significantly higher in the presence of Ti6Al4V particles with cells cultured in basal media, while S53P4 dissolution products reduced the TNFα expression in the presence of Ti6Al4V particles (Fig. 5 - 3a). The expression of CD206 markers, representative of M2 polarisation, was significantly reduced from THP-1 cells cultured in basal media with Ti6Al4V. Cells cultured in S53P4 dissolution products did not show a significant reduction in the CD206 markers (Fig. 5 - 3b).

5.4 Discussion

Environmental factors can have an influence on cellular activity including cytokine release and the polarisation of macrophages, pro-inflammatory M1, or anti-inflammatory (reparative) M2 gradient within which the cells are functioning (154, 155). There have been various reports of the ability of dental implant particles causing inflammation (35, 104, 109, 125), which may play a role in peri-implantitis

(38, 109, 125). The aim of this study was to investigate the influence of S53P4 BAG on polarisation of macrophages and on the inflammatory cytokine release in the presence of Ti-CP4, Ti6Al4V, Ti15Zr and Zr implant particles. THP-1 cell line was used for investigating the macrophage polarisation and the HGF, SaOS-2 osteoblastic cells and HBMSC lines were used as relevant cell lines to represent the peri-implant tissues.

The inflammatory markers expression (Fig. 5 - 1) were significantly higher with Ti6Al4V, which agrees with previous reports (35, 109, 125). Cells cultured with the other materials did not show a significant difference in cytokine release compared to cells cultured in basal medium controls with no particles. The influence of S53P4 was to significantly reduce the inflammatory marker expression from cells cultured with Ti6Al4V in all the cell lines.

To assess the macrophage polarisation ELISA was used to measure the expression of TNFα as a marker for M1, pro-inflammatory activity and CD206 as a marker for M2, anti-inflammatory activity of differentiated THP-1 cells. Confocal microscopy of the immunohistochemical labelling (Fig. 5 - 2) confirmed the successful differentiation of THP-1 cells from monocytes to macrophages as evidenced with the green staining of CD36 and CD68, both markers for macrophages. In contrast, the CD14 is a marker for monocytes which is visible in pre-differentiated cells.

The results showed a significant increase in M1 markers with cells cultured in the presence of Ti6Al4V, which was reversed when the same cells were cultured with S53P4 dissolution products (Fig. 5 - 3). Similarly, there was a significant suppression of the M2 markers with cells cultured in the presence of Ti6Al4V, which was reversed when the cells were cultured in S53P4 dissolution products. Although this study looked at a very limited number of markers, there is a suggestion that S53P4 may have anti-inflammatory properties which is likely to be due to the silicate ions found in the S53P4 dissolution products. This effect of reducing inflammatory markers such as TNFα and IL6 has been previously reported with silicate-based glasses when compared to zinc phosphate glasses

(156). Si ions have also been reported to enhance osteoblastic activity (157, 158).

These findings suggest S53P4 is a potentially promising material for application in implant dentistry with the anti-bacterial, regenerative and possible anti-inflammatory properties. Further investigations are warranted to have a better understanding of the inflammatory pathways involving titanium particles, the role of BAG's in modulating these and the clinical application of S53P4 on dental implant surfaces.

This page intentionally left blank

6. Final discussion

The aim of this PhD was to investigate the role of biomaterials in peri-implantitis. Although the consensus opinion on the aetiology of peri-implantitis is bacterial infection, there is evidence that particles released from implants are able to instigate inflammatory responses *in vitro* (108, 159). Particles from implants are also found to migrate to remote sites with unconfirmed consequences (160, 161). The vast majority of dental implant systems use either Ti-CP4 or Ti6Al4V, which have been the focus of this thesis. However, some attention was also given to Ti15Zr (Roxolid®) and Zr as relatively more recent materials used in implantology.

Figs. 16 and 17 summarise how the inflammatory process can be escalated, beginning from the surgical placement of an implant (Fig. 16) to the effects of titanium particles released from the implants which can potentially result in chronic inflammation and formation of FBGC (Fig. 17).

In chapter 2 the release of nano and micro particles from implantoplasty procedures was confirmed, which were shown to be toxic to HGF for Ti6Al4V implants. The particles for Ti6Al4V implants were smaller than Ti-CP4 which may be the reason for the toxicity. However, the reduced cell viability from the MTT assay coincided with the presence of V as measured from ICP, which suggests the toxic effect of vanadium as supported by other studies (85, 88, 160, 161). However, the presence of Al in Ti6Al4V and other trace elements such as Fe must also be taken into consideration as these may play a potential role in the reduced viability of the HGF. The large number of particles produced by this experiment do not relate to the simple implant placement, but rather to the implantoplasty procedure.

In chapter 3 the release of titanium particles from the implant surfaces during their placement was demonstrated in the ex-vivo model with a higher amount of particle release from Ti6Al4V implants. Implant surface damage following placement was observed on SEM as cracks and delamination. Surface damage resulting in pits and crevices can provide ‘protected’ sites for macrophages and

bacteria to adhere undisturbed, releasing ROS, RNS and proteinases which result in increased acidity in the surrounding area with further tissue destruction, corrosion of titanium, which causes further surface damage, particle release and propagation of the inflammatory process. Considering the salivary pH of 6.3-7.0 and that the presence of acidic drinks can drop it to pH 3.5 (46) the oral cavity is potentially an environment in which corrosion is aided. The loss of the passive Ti layer (protective TiO2) can occur at pH 6 exposing the alloying elements, V and Al in grade 5 implants (162). The leaching of ions can cause a failure of osseointegration (47).

The study in chapter 3 also demonstrated the uptake of particles from the different implant materials by both of the cell lines used (RAW 264.7 murine macrophages and HGF). There was no apparent difference in the rate of uptake between different materials, although this was not a quantitative analysis. In chapter 5 the inflammatory response of various cell lines to titanium particles was demonstrated with a significantly higher IL1β, IL6 and TNFα release as well as polarization of macrophages to the pro-inflammatory M1 gradient with Ti6Al4V particles compared to Ti-CP4, Ti15Zr and Zr.

V is known to be toxic (38, 163) and its presence in the grade 5 implants is the likely reason for the reduced cellular viability (Chapter 2) and the increased inflammatory reaction (chapter 5), keeping in mind the presence and potential role of Al. Implant safety should be considered with their constituent elements in mind and not just as a whole unit, because particle release and corrosion of the surface will expose the constituent elements and the subsequent ionic leaching can elicit responses in the local cells (25, 40, 76, 77, 84, 85). The results from the particle studies consistently show that the safety of Ti6Al4V as an implant material needs to be reconsidered due to the V and possibly Al content.

Clinically the tissues could also react to the materials used in the crown components, such as non-precious metals (Nickle, Chromium, Cobalt) used for their reduced price (164, 165). Galvanic currents can be generated between different metals causing corrosion and potentially affecting local cell function (162).

Leached ions can bind to proteins in the ECM forming aggregates which can enter cells through a 'Trojan Horse' mechanism (Fig. 18), or act as haptens eliciting a hypersensitivity reaction which can be T cell or B cell mediated (162). Metals can cross link cell surface molecules directly, or by binding to non-antigenic tissue proteins, to bring about T cell receptor activation without APC presentation (88).

Consideration should be given to the possibility of a hypersensitivity reaction to implant materials as the reason for the inflammatory responses observed in Chapters 2 and 5. There have been reports of suspected Ti delayed hypersensitivity (162). The chronic accumulation of particles in the surrounding tissues as a result of wear, or corrosion could reach a threshold for FBGC or hypersensitivity reaction resulting in clinical bone loss and implant failure. This would fit the clinical picture of peri-implantitis occurring only in some individuals, including those with no known risk factors often several years after fixture placement.

Consideration needs to be given to the purity of titanium dental implants and the potential for toxic, or allogenic contaminants within the fixtures. Dental implant manufacturing standards are set by the ISO standard 5832 and the American Society for Testing and Materials (ASTM) standard F67-13. The standards list the required composition of the elements in implants with ASTM grades 1-5 (commercially pure grades 1-4 and Ti6Al4V alloy grade 5).

The most commonly used grade of titanium in dental implants is grade 4, for which the standardised elemental composition is listed below with the maximum mass% values for each element with titanium as the balance: Nitrogen: maximum of 0.05 mass%, Carbon: maximum of 0.08 mass%, Hydrogen: maximum of 0.0125 mass%, Iron: maximum of 0.5 mass%, Oxygen: maximum of 0.4 mass%.

Despite the ISO and ASTM standards for grades 1-5 titanium implants, impurities have been found which included chromium (Cr), copper (Cu), nickel (Ni), lead (Pb), arsenic (As) and in zirconia implants thorium (Th-232) and uranium (U –

238) radionuclides (166). . There has therefore not been enough attention paid to metal contaminants, especially those that are known to have allogenic properties. Contaminants may be introduced during surface treatments such as abrasion, etching and anodisation. As the various implant systems use different techniques for surface topography treatment, the level and type of contaminants will vary between different implant systems.

The relationship between tissue reaction to different implant systems and their potential contaminants is difficult to ascertain, especially as this may differ not only between systems but also between different batches of the same system. The majority of the clinical data looking at the hypersensitivity reactions to implants have been case reports (166), which limits the data and the conclusions that can be drawn. There is therefore a clinical challenge not only in determining the cause of peri-implant inflammation between bacterial invasion, foreign body reaction, or hypersensitivity reaction but also in the case of the latter, whether it was instigated by one of the standardised component elements or by a contaminant.

6.1 Strategies for the use of biomaterials in the prevention of peri-implantitis

6.1.1 Antibacterial surfaces

Various methods have been used to modify the surface of the intra-osseous aspect of titanium prostheses with antibacterial properties. These include titanium nanotube (TNT) surfaces containing silver, hydrogel and sol-gel surfaces containing antibiotics. Although the latter have been shown to be effective antibacterial agents there are still questions about the long-term toxicity of TNT containing silver and hydrogels tend to be less strong than sol-gel and are lost more easily from implant surfaces (167). There is also potential for the use of multiple agents and patient specific antimicrobial agents. These surface modification techniques are useful and effective as relatively short lived anti-bacterial cover for the surgical aspect of orthopaedic joint replacement implants, as the active anti-microbial agents last for short periods of time (hours to days) to

cover the initial healing period. However, long term bacterial resistance is more important for dental implants as these are exposed to the oral cavity with a potential weak point at the transmucosal aspect as explained in chapter 1. In the absence of a physical barrier of collagen attachment at the transmucosal aspect of current dental implants, effective anti-bacterial surface coatings are the next line of defence. Nicol et al (167) proposed a surface coating with a hybrid sol-gel process onto HA coated titanium implants to allow multi drug delivery with control over physical properties. Future work into the use of this technology to adapt it for use with S53P4 bioactive glass with its antibacterial, anti-inflammatory and potential collagen attachment properties is indicated.

6.2 The potential role of bioactive glass

As part of the scope of this PhD the potential use of a substrate on the dental implant (or the implant abutment) surface to reduce the risk of peri-implantitis was considered. The work started in this PhD is very preliminary in assessing the response of local tissue cell lines to S53P4 as a material as well as the ability of HGF to adhere to its surface. The long-term focus is on the potential for soft tissue attachment rather than bone integration, with a view to achieving a method for stronger connective tissue attachment at the transmucosal junction where bacterial invasion can take place. The desirable characteristics of such a substrate would include the ability to mimic the tooth cementum in allowing collagen attachment, as well as anti-bacterial and anti-inflammatory properties to counteract the potential pro-inflammatory influence of titanium particles. Ideally, the material would also have approval for clinical applications. A coating with such a substrate could also reduce the risk of corrosion of the implant surface in body fluids and leaching of ions into the tissues (168).

S53P4 Bioactive glass has been shown to from an HCA surface layer in tissues (68, 81) which may have the potential for surface collagen attachment as seen from the preliminary results in chapter 4 demonstrating HGF attachment on S53P4 disc surface. S53P4 also has anti-bacterial properties (70-72). In chapter 5 the potential anti-inflammatory property was demonstrated (169). These are

very preliminary *in vitro* results and further work is needed as suggested below (see Future work section) to assess the possibility of clinical application.

6.2.1 Application of bioactive glass on titanium implant surfaces

For a bioactive glass coating to be effective in its proposed function of promoting collagen attachment it needs to be strong enough to withstand physiological and functional stresses, form a strong bond to the implant surface, and have a thermal expansion coefficient (TEC) similar to the implant material to remain attached while maintaining bioactivity. The composition of the BAG can be altered in order to control the TEC, crystallisation potential and bioactivity.

Si is a BAG network former and its content has a key role in determining the network connectivity and hence its properties. Increasing the Si content will reduce the risk of crystallisation and make the TEC of the BAG closer to that of Ti6Al4V. However, increasing the Si content also increases the network connectivity (NC) which reduces the bioactivity of the glass as there will be less ionic leaching required for the precipitation and HCA formation, as well as pH changes deemed to have the antibacterial effects. SiO2 content of 56 to 68 wt% matches the TEC of TiV4Al6, while keeping Tg below Titanium's α to β phase transformation temperature. For Ti6Al4V this temperature of phase transformation is 995-1010 (170). However, BAG compositions with Si content of more than 60 mol% are not bioactive (171). Conversely, if the Si content is too low ionic exchanges can happen more readily from the implant surface which can inhibit the bioactivity of the substrate, and BAG with SiO2 content of less than 53wt% fracture more readily (170).

Network modifiers (Na, K, Ca, Mg) influence the properties and stability of BAG. A higher network modifier content reduces the NC, reduces Tg and increases the ease of crystal formation during heating or cooling of the melt. The charge to size ratio (Field strength) of the network modifiers can also influence the stability of the network, as for example Ca will form a stronger ionic bond with NBO, than Na due to having a similar radius but stronger charge. Therefore, a higher Ca

content will increase network stability, increase Tg and reduce crystallisation tendency. The converse will apply if the Na ratio is increased (172).

Apart from the BAG composition, the method of applying it onto the implant surface can affect its properties. Currently there is no Time-Temperature-Transformation chart for S53P4 to measure the critical cooling rate, in order to help avoid crystallisation. Using data from differential scanning calorimeter onset temperature of crystallisation (Tx) has been shown to be 600-800 and Tg to be 500-600 for S53P4, based on the absence of the exothermic peak from the heat of crystallisation. The sintering window for S53P4 (Tx-Tg) is 130°C which although narrow, it is wider than that for 45S5 (173).

The methods for coating implant surfaces with BAG become relevant when considering the various techniques used. *In vitro* studies have shown promising results with enamelling BAG onto metal implant surfaces, while maintaining a strong bond and bioactivity (168, 170, 171, 174).

6.2.2 Enamelling bioactive glass

BAG compositions with partial substitution of Na_2O with K_2O and CaO with MgO have been shown to lower the TEC to one similar to Ti6Al4V and Ti and have been successfully applied to implant surfaces by enamelling (174).
A surface reaction takes place between titanium and BAG producing titanium silicide and oxygen, as shown in the following equation:
$Ti + 3SiO_2$ (glass) ----- $Ti5Si_3 + 3O_2$ (gas)

Overheating the surface, or heating for too long can result in more brittle glass with air bubbles which compromise the adhesion to the implant surface (174). The surface coating of 50 μm was achieved as a protective layer; the Si content of these compositions were higher (6P57, 6P61 and 6P68) and only 6P57 allowed precipitation to take place, which indicates the other compositions were not bioactive due to a Si content of more than 60 mol%. A second, more bioactive layer was applied using a sol-gel solution (171). There is a potential application

for the use of high silica content BAG to coat the implant surface with a lower silica content outer layer for bioactivity (168, 171).
In summary, the challenges involved in coating implant surfaces with BAG include the loss of compositional control due to crystallisation, transport of unwanted ions from substrate into glass which can inhibit bioactivity, matching of thermal expansion coefficient of BAG and metals to avoid delamination (175).

6.3 Porous gyroid surface

For achieving an effective collagen attachment to the implant surface, akin to the attachment of periodontal ligament Sharpey's fibers onto the root cementum, further work is needed to demonstrate the strength, stability and longevity of attachment that can be achieved with S53P4 BAG. There may be an advantage to having a porous implant surface with interconnecting pores to allow entanglement of the collagen fibers to create a strong attachment for the desired transmucosal barrier to bacterial invasion. One technique that was briefly considered during this PhD was the use of gyroid (176-178) for developing an implant with an interconnecting porous section at the transmucosal part of the implant. This was developed by another PhD student (Dr Yu-Chien Lin) in the same group (Fig. 6 - 1).

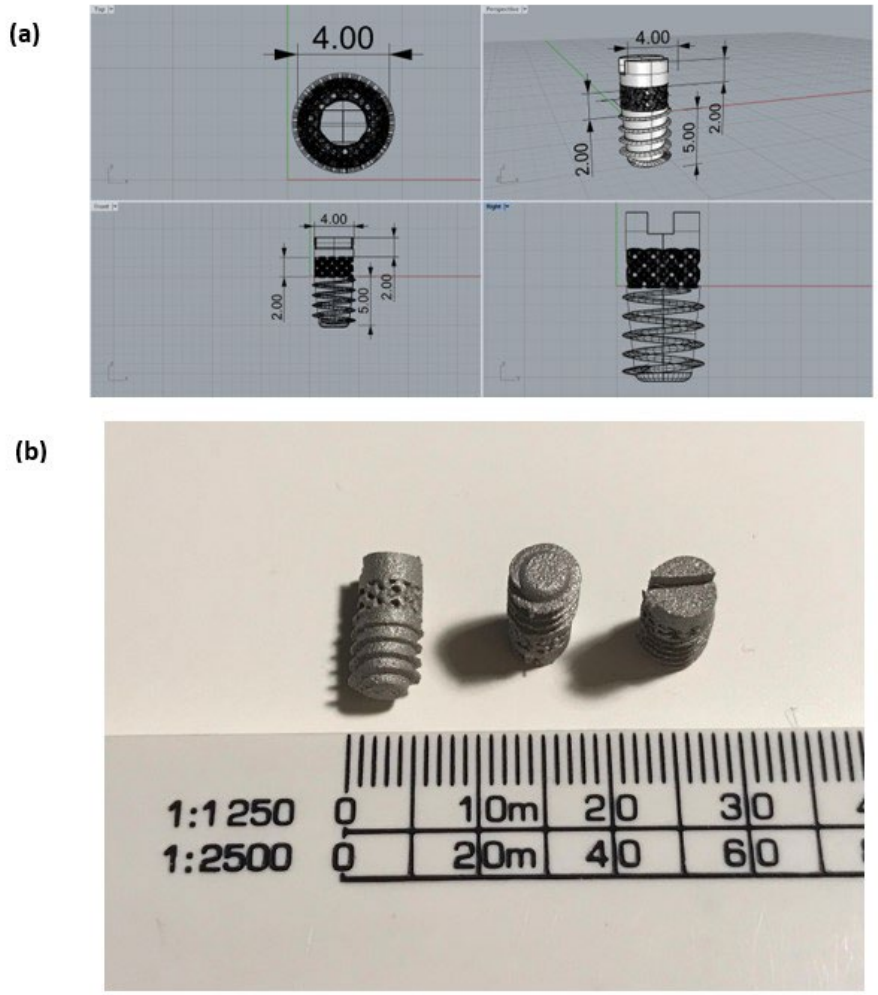

Figure 6 - 1. (a) Schematic design of gyroid implant prototype. (b) Gyroid implant prototypes c/o Dr Yu-Chien Lin.

The use of gyroid with or without the use of S53P4 BAG coating may be a potential solution for achieving the desired protective transmucosal barrier. There are several challenges with the application of the BAG onto an implant surface, which is more complicated when considering a porous structure. Also, the porous structure may become counterproductive if bacterial invasion does occur as a result of exposure to the oral environment following gum recession.
The part that actually emerges from the bone level through the mucosa, which is where connective tissue attachment is desired, is within the implant abutment. One possible solution would be to use the porous component and BAG coating on the implant abutment component, rather than the implant fixture for bone level implants. The abutment can be changed if it becomes contaminated with bacteria

as a result of recession, and placing a new abutment with freshening of the gum margins can create new connective tissue attachment.

Other methods may allow the combination of S53P4 bioactive glass in a porous structure which can be applied to the transmucosal aspect of the dental implants. There have been studies using various electrospinning techniques to combine bioactive glass in a membrane scaffold including strontium borosilicate bioactive glass and poly L lactic acid (179), strontium substituted bioactive glass and polycaprolactone (180) and silver doped nano hydroxyapatite with polycaprolactone (181). These studies demonstrated the effectiveness of combining bioactive glass and HA in the membrane scaffolds to use as a barrier membrane in GBR for bone regeneration. However, the application of the methods described may prove effective for achieving collagen attachment if the scaffold can be non-resorbable and combined with bioactive glass with or without antibacterial agents. Such a technique may allow for the construction of a ring made of electrospun material combined with S53P4, which can be applied to any implant transmucosal component, and ideally this would be replaceable allowing the application of a new ring in case of contamination.

6.4 Other methods for prevention of peri-implantitis

6.4.1 Biomimetics

The use of biomimetics technology in the application of small chain peptides on implant surfaces can involve various methods, including silanisation and carbodiimide cross linking. Silanisation involves surfaces with hydroxyl groups which can be functionalised for peptide conjugation. Bioactive glass is such a surface where silanisation can be used (63). Carbodiimide cross linking involves amide bonds and has been shown to allow covalent bonding of collagen to a substrate. These techniques, although primarily used for bone regeneration, may have a potential application for the desired connective tissue attachment at the transmucosal component of a dental implant simulating the natural tooth’s biologic width.

The application can be via the use bioactive glass surface, a scaffold combined with bioactive glass, or via direct application onto the implant surface which can be smooth or porous such as the gyroid design. One challenge to overcome is the stability and strength of the connective tissue attachment, especially when dealing with the smooth surface of the transmucosal titanium implant or implant abutment.

Some studies have demonstrated a multilayer peptide method to mimic the healing sequence in bone, starting with KRSR outer layer to promote adhesion, BMP mimetic peptide layer to promote differentiation and the final FHRRIKA layer to promote mineralisation (182). Although current studies have focused on osteogenesis, further work on using this degree of influence of cellular activity is needed to investigate the use of multi layered peptides for achieving strong collagen attachment and a controlled layer of mineralisation on implant surfaces in order to mimic the dental root cementum.

This page intentionally left blank

7. Conclusions

The main reason for the late failure of dental implants after they have successfully osseointegrated is Peri-implantitis, which is currently believed to be related to invading bacterial colonies from dental plaque biofilms (19). The treatment of peri-implantitis is complex with unpredictable outcomes (16), which may reflect the lack full understanding of its pathophysiology. Various competing theories to the bacterial aetiology have been provided. The focus of this PhD project has been on gaining a better understanding of the role implant particles, as one of the competing theories in the aetiology of per-implantitis, and also on a potential strategy to prevent its occurrence through a stronger transmucosal attachment barrier.

The following are areas of knowledge that this PhD project has added to:

1. Implant particles are released and surface damage takes place during the implant placement procedure. The amount of particle release is significantly higher from grade 5 tapered dental implants which are titanium alloys containing 6% Al and 4% V, compared to grade 4 commercially pure or Ti15Zr alloyed implants – See chapter 3 (Published) (125).

2. Grade 5 titanium alloy implant particles, were shown to be cytotoxic to HGF cell lines when compared to grade 4 implant particles in a simulated implantoplasty model. However, the undisturbed whole grade 5 implant did not demonstrate cytotoxicity – See chapter 2 (Published) (109).

3. Grade 5 titanium alloy particles were shown to elicit significant inflammatory responses (IL1β, IL6, TNFα) in four different cell lines and influence the polarity of macrophages to an M1 pro-inflammatory state when compared to grade 4, Ti15Zr alloy and Zr implant particles. This inflammatory response was reversed in the presence of S53P4 bioactive glass dissolution products – See chapter 5 (Published) (169).

4. Although the actual mechanism of cytotoxicity of grade 5 implant particles has not been established in this project, it was demonstrated that the particles were toxic only when present in the media (the dissolution products were not toxic) and that the particles are taken up and internalised by cell lines. This suggests that the cytotoxicity is related to the uptake of particles by cells (chapter 2 and 3).

S53P4 bioactive glass has potential anti-inflammatory properties (chapter 5) and allows fibroblast spreading on its surface which needs further investigation into the strength of the cell attachment (chapter 4).

Although all of the research in this PhD has been *in vitro* and therefore, cannot be directly related to the clinical scenario, the above findings have potential clinical implications for dental implant companies, dental surgeons, and for researchers. Dental implant manufacturers currently test the implant fixtures for toxicity as a whole unit. There is enough evidence in the literature, including this project, to suggest that testing of tissue response to particles should be considered as part of the standard manufacturing procedure to ensure patient safety, especially as new material are being developed. The Dental surgeons' decision on which material to use needs to be based on evidence and consideration needs to be given to the possible adverse effects from particles released from their choice of implant such as grade 5 implants. Clinical research carried out in peri-implantitis needs to take into account the materials used in the implants and include this data in their results for a better understanding of the role of materials; this is currently often missing and may therefore mask any influence on the onset or peri-implantitis.

In conclusion, more *in vitro* evidence has been provided for the possible role of implant particles as a competing theory in the aetiology of peri-implantitis and the demonstrated anti-inflammatory property and potential for collagen attachment of S53P4 bioactive glass indicates the need for further research in its use as a substrate on dental implant surfaces.

This page intentionally left

8. Future work

Mechanism of inflammatory reaction to implant particles

Further investigation is required to understand the interaction between ions leached from dental implant materials and the local bone and mucosa matrix proteins.

c. Identifying the proteins involved in the formation of aggregates could help in recognizing the relevant cellular pathways involved in the inflammatory responses, as well as the possible mechanism for internalization of the particles. Different metal implant constituents may influence different cellular pathways with the different downstream outcomes, such as seen with the pro-inflammatory effects of V compared to Ti and Zr in the previous chapters.

d. Investigating the ability of the metal ions to act directly on T Helper cell receptors, bypassing the antigen presenting cell MHCII interactions, would help in understanding whether the inflammatory reactions to particles are as a result of a delayed type 4 hypersensitivity reaction.

Confirming collagen attachment potential of S53P4 bioactive glass

Although this research showed cell spreading and surface apposition of HGF on S53P4 bioactive glass surface, further investigation is required in the degree and strength of collagen attachment using quantitative methods such as AFM mechanical tests, nano scratch methods and wash techniques. A means of attaining a robust collagen attachment at the transmucosal aspect of dental implants is desirable as a potential barrier to microbial invasion, similar to the natural tooth.

Application of glass to implant surfaces

Following on from previous work on graded enameling of BAG onto metal implant surfaces (168, 170, 171, 174), further investigation into achieving enameling of S53P4 as an outer surface is indicated for its desired antibacterial and possible anti-inflammatory properties as well as its collagen attachment potential.

Sol-gel derived S53P4 application to implant surfaces

Investigating methods for applying sol-gel derived S53P4 to titanium implant surfaces without losing the amorphous structure may provide a solution for the desired surface coating at the transmucosal section.

Use of porous gyroid implant design

Collagen attachment and interconnection through the porous structure of an implant surface may provide the physical collagen barrier desired to reduce the ease of microbial invasion around a dental implant. This work can start by investigating the effectiveness of the gyroid design using various pore sizes in an *in vitro* membrane model followed by histological sections to confirm collagen interconnection within the porous structure.

Biomimetics to achieve collagen attachment

The aim of this work would be to identify and test small peptide chains that are capable of encouraging collagen attachment onto a substrate surface. If successful, the investigation can progress to developing the application of the appropriate peptide chains directly onto titanium implant surfaces, or on their coatings. Multilayer peptide chains can be tested for various desired properties, such as antibacterial.

This page intentionally left blank

References

1. Alrabeah GO, Brett P, Knowles JC, Petridis H. The effect of metal ions released from different dental implant-abutment couples on osteoblast function and secretion of bone resorbing mediators. J Dent. 2017;66:91-101.
2. Mohajerani H, Roozbayani R, Taherian S, Tabrizi R. The Risk Factors in Early Failure of Dental Implants: a Retrospective Study. J Dent (Shiraz). 2017;18(4):298-303.
3. Dean R. The Periodontal Ligament: Development, Anatomy and Function. Journal of Oral Health and Dental Management. 2017;16.
4. Kim Y, Oh TJ, Misch CE, Wang HL. Occlusal considerations in implant therapy: clinical guidelines with biomechanical rationale. Clin Oral Implants Res. 2005;16(1):26-35.
5. Pearson CH. The Ground Substance of the Periodontal Ligament. In: Berkovitz BH, Moxham BJ, Newman HN, editors. The Periodntal Health in Health and Disease. Oxford: Pergamon Press; 1982.
6. Kobayashi K, Rose GG, Mahan CJ. Ultrastructure of the dento-epithelial junction. J Periodontal Res. 1976;11(6):313-30.
7. Abdallah MN, Badran Z, Ciobanu O, Hamdan N, Tamimi F. Strategies for Optimizing the Soft Tissue Seal around Osseointegrated Implants. Adv Healthc Mater. 2017;6(20).
8. Hasan A, Palmer RM. A clinical guide to periodontology: pathology of periodontal disease. Br Dent J. 2014;216(8):457-61.
9. Liu D, Xu J, Liu O, Fan Z, Liu Y, Wang F, et al. Mesenchymal stem cells derived from inflamed periodontal ligaments exhibit impaired immunomodulation. J Clin Periodontol. 2012;39(12):1174-82.
10. Salvi GE, Cosgarea R, Sculean A. Prevalence and Mechanisms of Peri-implant Diseases. J Dent Res. 2017;96(1):31-7.
11. Straumann. Annual Report. 2016.
12. Nations U. World Population Prospects: The 2015 Revision. 2015.
13. Feine JS, Carlsson GE, Awad MA, Chehade A, Duncan WJ, Gizani S, et al. The McGill consensus statement on overdentures. Mandibular two-implant overdentures as first choice standard of care for edentulous patients. Gerodontology. 2002;19(1):3-4.
14. Thomason JM, Kelly SA, Bendkowski A, Ellis JS. Two implant retained overdentures--a review of the literature supporting the McGill and York consensus statements. J Dent. 2012;40(1):22-34.
15. Derks J, Schaller D, Hakansson J, Wennstrom JL, Tomasi C, Berglundh T. Peri-implantitis - onset and pattern of progression. J Clin Periodontol. 2016;43(4):383-8.
16. Esposito M, Grusovin MG, Worthington HV. Treatment of peri-implantitis: what interventions are effective? A Cochrane systematic review. Eur J Oral Implantol. 2012;5 Suppl:S21-41.
17. Fretwurst T, Nelson K, Tarnow DP, Wang HL, Giannobile WV. Is Metal Particle Release Associated with Peri-implant Bone Destruction? An Emerging Concept. J Dent Res. 2018;97(3):259-65.
18. Villar CC, Huynh-Ba G, Mills MP, Cochran DL. Wound healing around dental implants. Endodontic Topics. 2011;25(1):44-62.
19. Berglundh T, Armitage G, Araujo MG, Avila-Ortiz G, Blanco J, Camargo PM, et al. Peri-implant diseases and conditions: Consensus report of workgroup 4 of the 2017 World Workshop on the Classification of Periodontal and Peri-Implant Diseases and Conditions. J Periodontol. 2018;89 Suppl 1:S313-S8.
20. Shariff JA, Gurpegui Abud D, Bhave MB, Tarnow DP. Selective Serotonin Reuptake Inhibitors (SSRI) and Dental Implant Failure: A Systematic Review and Meta-Analysis. J Oral Implantol. 2023.

21. Berglundh T, Lindhe J, Ericsson I, Marinello CP, Liljenberg B, Thomsen P. The soft tissue barrier at implants and teeth. Clin Oral Implants Res. 1991;2(2):81-90.
22. Fransson C, Tomasi C, Pikner SS, Grondahl K, Wennstrom JL, Leyland AH, et al. Severity and pattern of peri-implantitis-associated bone loss. J Clin Periodontol. 2010;37(5):442-8.
23. Lindhe J, Berglundh T, Ericsson I, Liljenberg B, Marinello C. Experimental breakdown of peri-implant and periodontal tissues. A study in the beagle dog. Clin Oral Implants Res. 1992;3(1):9-16.
24. Albrektsson T, Canullo L, Cochran D, De Bruyn H. "Peri-Implantitis": A Complication of a Foreign Body or a Man-Made "Disease". Facts and Fiction. Clin Implant Dent Relat Res. 2016;18(4):840-9.
25. Delgado-Ruiz R, Romanos G. Potential Causes of Titanium Particle and Ion Release in Implant Dentistry: A Systematic Review. Int J Mol Sci. 2018;19(11).
26. Mombelli A, Hashim D, Cionca N. What is the impact of titanium particles and biocorrosion on implant survival and complications? A critical review. Clinical Oral Implants Research. 2018;29:37-53.
27. Steinemann SG. Titanium--the material of choice? Periodontol 2000. 1998;17:7-21.
28. Moraschini V, Poubel LA, Ferreira VF, Barboza Edos S. Evaluation of survival and success rates of dental implants reported in longitudinal studies with a follow-up period of at least 10 years: a systematic review. Int J Oral Maxillofac Surg. 2015;44(3):377-88.
29. Sikora CL, Alfaro MF, Yuan JCC, Barao VA, Sukotjo C, Mathew MT. Wear and corrosion interactions at the titanium/zirconia interface: dental implant application. Journal of Prosthodontics. 2018;27(9):842-52.
30. Medvedev AE, Molotnikov A, Lapovok R, Zeller R, Berner S, Habersetzer P, et al. Microstructure and mechanical properties of Ti–15Zr alloy used as dental implant material. journal of the mechanical behavior of biomedical materials. 2016;62:384-98.
31. Osman RB, Swain MV. A Critical Review of Dental Implant Materials with an Emphasis on Titanium versus Zirconia. Materials (Basel). 2015;8(3):932-58.
32. Bahadirli G, Yilmaz S, Jones T, Sen D. Influences of Implant and Framework Materials on Stress Distribution: A Three-Dimensional Finite Element Analysis Study. Int J Oral Maxillofac Implants. 2018;33(5):e117-e26.
33. Straumann. MATERIAL INFORMATION: Straumann.com; 2014 [Available from: https://www.straumann.com/content/dam/media-center/straumann/en/documents/brochure/technical-information/490.019-en_low.pdf.
34. Obando-Pereda GA, Fischer L, Stach-Machado DR. Titanium and zirconia particle-induced pro-inflammatory gene expression in cultured macrophages and osteolysis, inflammatory hyperalgesia and edema in vivo. Life Sci. 2014;97(2):96-106.
35. Eger M, Sterer N, Liron T, Kohavi D, Gabet Y. Scaling of titanium implants entrains inflammation-induced osteolysis. Sci Rep. 2017;7:39612.
36. Pettersson M, Pettersson J, Molin Thoren M, Johansson A. Release of titanium after insertion of dental implants with different surface characteristics - an ex vivo animal study. Acta Biomater Odontol Scand. 2017;3(1):63-73.
37. Anderson JM, Rodriguez A, Chang DT, editors. Foreign body reaction to biomaterials. Seminars in immunology; 2008: Elsevier.
38. Willis J, Li S, Crean SJ, Barrak FN. Is titanium alloy Ti-6Al-4 V cytotoxic to gingival fibroblasts—A systematic review. Clinical and experimental dental research. 2021;7(6):1037-44.
39. Purdue PE, Koulouvaris P, Potter HG, Nestor BJ, Sculco TP. The cellular and molecular biology of periprosthetic osteolysis. Clinical Orthopaedics and Related Research®. 2007;454:251-61.
40. Yao JJ, Lewallen EA, Trousdale WH, Xu W, Thaler R, Salib CG, et al. Local cellular responses to titanium dioxide from orthopedic implants. BioResearch open access. 2017;6(1):94-103.

41. Trindade R, Albrektsson T, Tengvall P, Wennerberg A. Foreign body reaction to biomaterials: on mechanisms for buildup and breakdown of osseointegration. Clinical implant dentistry and related research. 2016;18(1):192-203.
42. Medzhitov R. Origin and physiological roles of inflammation. Nature. 2008;454(7203):428-35.
43. Florencio-Silva R, Sasso GRdS, Sasso-Cerri E, Simões MJ, Cerri PS. Biology of bone tissue: structure, function, and factors that influence bone cells. BioMed research international. 2015;2015.
44. Penmetsa SLD, Shah R, Thomas R, Kumar ABT, Gayatri PSD, Mehta DS. Titanium particles in tissues from peri-implant mucositis: An exfoliative cytology-based pilot study. Journal of Indian Society of Periodontology. 2017;21(3):192.
45. Kazazian NH. NLRP3 inflammasome activation by crystal structures. BioSciences Master Reviews. 2014:1-8.
46. Mathew MT, Abbey S, Hallab NJ, Hall DJ, Sukotjo C, Wimmer MA. Influence of pH on the tribocorrosion behavior of CpTi in the oral environment: synergistic interactions of wear and corrosion. Journal of Biomedical Materials Research Part B: Applied Biomaterials. 2012;100(6):1662-71.
47. Rodrigues DC, Valderrama P, Wilson TG, Palmer K, Thomas A, Sridhar S, et al. Titanium corrosion mechanisms in the oral environment: a retrieval study. Materials. 2013;6(11):5258-74.
48. Jämsen E, Pajarinen J, Kouri V-P, Rahikkala A, Goodman SB, Manninen M, et al. Tumor necrosis factor primes and metal particles activate the NLRP3 inflammasome in human primary macrophages. Acta biomaterialia. 2020;108:347-57.
49. Barão VA, Mathew MT, Assunção WG, Yuan JCC, Wimmer MA, Sukotjo C. Stability of cp-Ti and Ti-6 Al-4 V alloy for dental implants as a function of saliva pH–an electrochemical study. Clinical oral implants research. 2012;23(9):1055-62.
50. Raisanen L, Kononen M, Juhanoja J, Varpavaara P, Hautaniemi J, Kivilahti J, et al. Expression of cell adhesion complexes in epithelial cells seeded on biomaterial surfaces. J Biomed Mater Res. 2000;49(1):79-87.
51. Abrahamsson I. The mucosal attachment at different abutments An experimental study in dogs. Journal of Clinical Periodontology. 2005;25(9):721-7.
52. Chevalier J, Gremillard L, Deville S. Low-temperature degradation of Zirconia and implications for biomedical implants. Annu Rev Mater Res. 2007;37:1-32.
53. Pendegrass CJ, Goodship AE, Blunn GW. Development of a soft tissue seal around bone-anchored transcutaneous amputation prostheses. Biomaterials. 2006;27(23):4183-91.
54. Lai Y, Chen J, Zhang T, Gu D, Zhang C, Li Z, et al. Effect of 3D microgroove surface topography on plasma and cellular fibronectin of human gingival fibroblasts. J Dent. 2013;41(11):1109-21.
55. Kim H, Murakami H, Chehroudi B, Textor M, Brunette DM. Effects of surface topography on the connective tissue attachment to subcutaneous implants. Int J Oral Maxillofac Implants. 2006;21(3):354-65.
56. Chehroudi B, Gould TR, Brunette DM. Titanium-coated micromachined grooves of different dimensions affect epithelial and connective-tissue cells differently in vivo. J Biomed Mater Res. 1990;24(9):1203-19.
57. Nevins M, Nevins ML, Camelo M, Boyesen JL, Kim DM. Human histologic evidence of a connective tissue attachment to a dental implant. Int J Periodontics Restorative Dent. 2008;28(2):111-21.
58. Farrell BJ, Prilutsky BI, Ritter JM, Kelley S, Popat K, Pitkin M. Effects of pore size, implantation time, and nano-surface properties on rat skin ingrowth into percutaneous porous titanium implants. J Biomed Mater Res A. 2014;102(5):1305-15.

59. Park JC, Kim HM, Ko J. Effects of extracellular matrix constituents on the attachment of human oral epithelial cells at the titanium surface. Int J Oral Maxillofac Implants. 1998;13(6):826-36.
60. Bates C, Marino V, Fazzalari NL, Bartold PM. Soft tissue attachment to titanium implants coated with growth factors. Clin Implant Dent Relat Res. 2013;15(1):53-63.
61. Pendegrass CJ, Tucker B, Patel S, Dowling R, Blunn GW. The effect of adherens junction components on keratinocyte adhesion in vitro: potential implications for sealing the skin-implant interface of intraosseous transcutaneous amputation prostheses. J Biomed Mater Res A. 2012;100(12):3463-71.
62. Satue M, Gomez-Florit M, Monjo M, Ramis JM. Improved human gingival fibroblast response to titanium implants coated with ultraviolet-irradiated vitamin D precursor and vitamin E. J Periodontal Res. 2016;51(3):342-9.
63. Bullock G, Atkinson J, Gentile P, Hatton P, Miller C. Osteogenic Peptides and Attachment Methods Determine Tissue Regeneration in Modified Bone Graft Substitutes. J Funct Biomater. 2021;12(2).
64. Stähli A, Strauss FJ, Gruber R. The use of platelet-rich plasma to enhance the outcomes of implant therapy: A systematic review. Clin Oral Implants Res. 2018;29 Suppl 18(Suppl Suppl 18):20-36.
65. Reyes CD, Petrie TA, Burns KL, Schwartz Z, Garcia AJ. Biomolecular surface coating to enhance orthopaedic tissue healing and integration. Biomaterials. 2007;28(21):3228-35.
66. Beertsen W, McCulloch CA, Sodek J. The periodontal ligament: a unique, multifunctional connective tissue. Periodontol 2000. 1997;13:20-40.
67. Aguiar HG, P. Serra, J. Bioactive glass structure and solubility. Bioactive glasses. 2nd ed: Wodhead publishing series in biomaterials; 2018. p. 37-61.
68. Jones JR. Reprint of: Review of bioactive glass: From Hench to hybrids. Acta Biomater. 2015;23 Suppl:S53-82.
69. Wilson J, Low SB. Bioactive ceramics for periodontal treatment: comparative studies in the Patus monkey. J Appl Biomater. 1992;3(2):123-9.
70. Lepparanta O, Vaahtio M, Peltola T, Zhang D, Hupa L, Hupa M, et al. Antibacterial effect of bioactive glasses on clinically important anaerobic bacteria in vitro. J Mater Sci Mater Med. 2008;19(2):547-51.
71. Munukka E, Lepparanta O, Korkeamaki M, Vaahtio M, Peltola T, Zhang D, et al. Bactericidal effects of bioactive glasses on clinically important aerobic bacteria. J Mater Sci Mater Med. 2008;19(1):27-32.
72. Gubler M, Brunner TJ, Zehnder M, Waltimo T, Sener B, Stark WJ. Do bioactive glasses convey a disinfecting mechanism beyond a mere increase in pH? International Endodontic Journal. 2008;41(8):670-8.
73. Alrabiah M, Alrahlah A, Al-Hamdan RS, Al-Aali KA, Labban N, Abduljabbar T. Survival of adjacent-dental-implants in prediabetic and systemically healthy subjects at 5-years follow-up. Clin Implant Dent Relat Res. 2019;21(2):232-7.
74. Francetti L, Cavalli N, Taschieri S, Corbella S. Ten years follow-up retrospective study on implant survival rates and prevalence of peri-implantitis in implant-supported full-arch rehabilitations. Clin Oral Implants Res. 2019;30(3):252-60.
75. Longhofer LK, Chong A, Strong NM, Wooley PH, Yang S-Y. Specific material effects of wear-particle-induced inflammation and osteolysis at the bone-implant interface: A rat model. J Orthop Translat. 2016;8:5-11.
76. Rivera MC, Perni S, Sloan A, Prokopovich P. Anti-inflammatory drug-eluting implant model system to prevent wear particle-induced periprosthetic osteolysis. Int J Nanomedicine. 2019;14:1069-84.

77. Barbieri M, Mencio F, Papi P, Rosella D, Di Carlo S, Valente T, et al. Corrosion behavior of dental implants immersed into human saliva: preliminary results of an in vitro study. Eur Rev Med Pharmacol Sci. 2017;21(16):3543-8.
78. Mabilleau G, Bourdon S, Joly-Guillou ML, Filmon R, Basle MF, Chappard D. Influence of fluoride, hydrogen peroxide and lactic acid on the corrosion resistance of commercially pure titanium. Acta Biomater. 2006;2(1):121-9.
79. Siirilä HS, Könönen M. The effect of oral topical fluorides on the surface of commercially pure titanium. Int J Oral Maxillofac Implants. 1991;6(1):50-4.
80. Kokubo T, Kushitani H, Sakka S, Kitsugi T, Yamamuro T. Solutions able to reproduce in vivo surface-structure changes in bioactive glass-ceramic A-W. J Biomed Mater Res. 1990;24(6):721-34.
81. Maçon AL, Kim TB, Valliant EM, Goetschius K, Brow RK, Day DE, et al. A unified in vitro evaluation for apatite-forming ability of bioactive glasses and their variants. J Mater Sci Mater Med. 2015;26(2):115.
82. UK SMCL. Ti-6Al-4V (Grade 5) Technical Datasheet. 2018.
83. UK SMCL. CP Grade 4 Technical Datasheet. 2018.
84. Sargeant A, Goswami T, Swank M. Ion concentrations from hip implants. J Surg Orthop Adv. 2006;15(2):113-4.
85. Costa BC, Tokuhara CK, Rocha LA, Oliveira RC, Lisboa-Filho PN, Costa Pessoa J. Vanadium ionic species from degradation of Ti-6Al-4V metallic implants: In vitro cytotoxicity and speciation evaluation. Mater Sci Eng C Mater Biol Appl. 2019;96:730-9.
86. Zhang Y, Addison O, Yu F, Troconis BCR, Scully JR, Davenport AJ. Time-dependent Enhanced Corrosion of Ti6Al4V in the Presence of H2O2 and Albumin. Sci Rep. 2018;8(1):3185.
87. Rodrigues DC, Urban RM, Jacobs JJ, Gilbert JL. In vivo severe corrosion and hydrogen embrittlement of retrieved modular body titanium alloy hip-implants. J Biomed Mater Res B Appl Biomater. 2009;88(1):206-19.
88. Hallab NJ, Mikecz K, Vermes C, Skipor A, Jacobs JJ. Orthopaedic implant related metal toxicity in terms of human lymphocyte reactivity to metal-protein complexes produced from cobalt-base and titanium-base implant alloy degradation. Mol Cell Biochem. 2001;222(1-2):127-36.
89. Conner SD, Schmid SL. Regulated portals of entry into the cell. Nature. 2003;422(6927):37-44.
90. He X, Hartlieb E, Rothmund L, Waschke J, Wu X, Van Landuyt KL, et al. Intracellular uptake and toxicity of three different Titanium particles. Dent Mater. 2015;31(6):734-44.
91. Caputi S, Diomede F, Lanuti P, Marconi GD, Di Carlo P, Sinjari B, et al. Microplastics Affect the Inflammation Pathway in Human Gingival Fibroblasts: A Study in the Adriatic Sea. Int J Environ Res Public Health. 2022;19(13).
92. Li L, Sun W, Yu J, Lei W, Zeng H, Shi B. Effects of titanium dioxide microparticles and nanoparticles on cytoskeletal organization, cell adhesion, migration, and proliferation in human gingival fibroblasts in the presence of lipopolysaccharide. J Periodontal Res. 2022;57(3):644-59.
93. Sabbioni E, Fortaner S, Farina M, Del Torchio R, Petrarca C, Bernardini G, et al. Interaction with culture medium components, cellular uptake and intracellular distribution of cobalt nanoparticles, microparticles and ions in Balb/3T3 mouse fibroblasts. Nanotoxicology. 2014;8(1):88-99.
94. Haleem-Smith H, Argintar E, Bush C, Hampton D, Postma WF, Chen FH, et al. Biological responses of human mesenchymal stem cells to titanium wear debris particles. J Orthop Res. 2012;30(6):853-63.
95. Okafor CC, Haleem-Smith H, Laqueriere P, Manner PA, Tuan RS. Particulate endocytosis mediates biological responses of human mesenchymal stem cells to titanium wear debris. J Orthop Res. 2006;24(3):461-73.

96. Rosen PS, Qari M, Froum SJ, Dibart S, Chou LL. A Pilot Study on the Efficacy of a Treatment Algorithm to Detoxify Dental Implant Surfaces Affected by Peri-implantitis. Int J Periodontics Restorative Dent. 2018;38(2):261-7.
97. ASM Aerospace Specification Metals Inc - Titanium Grade 4 specification sheet (Web access) [Available from: http://asm.matweb.com/search/SpecificMaterial.asp?bassnum=MTU040.
98. Boyer R, Welsch G, Collings W. Materials Properties Handbook: Titanium Alloys. Ohio: ASM International; 1994.
99. Harloff T, Hönle W, Holzwarth U, Bader R, Yhomas P, Schuh A. Titanium allergy or not? "Impurity" of titanium implant materials. Health. 2010;2(4):306–10.
100. Chaturvedi T. Allergy related to dental implant and its clinical significance. Clin Cosmet Investig Dent. 2013;5:57-61.
101. Diebold U. The surface science of titanium dioxide. Surf Sci Reports. 2003;48(5-8):53-229.
102. Revell PA. The combined role of wear particles, macrophages and lymphocytes in the loosening of total joint prostheses. J R Soc Interface. 2008;5(28):1263-78.
103. Mathew MT, Srinivasa Pai P, Pourzal R, Fischer A, Wimmer MA. Significance of Tribocorrosion in Biomedical Applications: Overview and Current Status. Adv Tribol. 2009;doi: 10.1155/2009/250986:1-12.
104. Matusiewicz H. Potential release of in vivo trace metals from metallic medical implants in the human body: from ions to nanoparticles--a systematic analytical review. Acta Biomater. 2014;10(6):2379-403.
105. Derks J, Tomasi C. Peri-implant health and disease. A systematic review of current epidemiology. J Clin Periodontol. 2015;42 Suppl 16:S158-71.
106. Wawrzinek C, Sommer T, Fischer-Brandies H. Microdamage in cortical bone due to the overtightening of orthodontic microscrews. J Orofac Orthop. 2008;69(2):121-34.
107. Guan H, van Staden RC, Johnson NW, Loo Y-C. Dynamic modelling and simulation of dental implant insertion process - A finiteelement study. Finite Elem Anal Des. 2011;47:886-97.
108. Konttinen YT, Pajarinen J, Takakubo Y, Gallo J, Nich C, Takagi M, et al. Macrophage polarization and activation in response to implant debris: influence by "particle disease" and "ion disease". J Long Term Eff Med Implants. 2014;24(4):267-81.
109. Barrak FN, Li S, Muntane AM, Jones JR. Particle release from implantoplasty of dental implants and impact on cells. Int J Implant Dent. 2020;6(1):50.
110. Schlegel KA, Eppeneder S, Wiltfang J. Soft tissue findings above submerged titanium implants--a histological and spectroscopic study. Biomaterials. 2002;23(14):2939-44.
111. Olmedo DG, Paparella ML, Spielberg M, Brandizzi D, Guglielmotti MB, Cabrini RL. Oral mucosa tissue response to titanium cover screws. J Periodontol. 2012;83(8):973-80.
112. de Morais LS, Serra GG, Albuquerque Palermo EF, Andrade LR, Muller CA, Meyers MA, et al. Systemic levels of metallic ions released from orthodontic mini-implants. Am J Orthod Dentofacial Orthop. 2009;135(4):522-9.
113. Buzea C, Pacheco, II, Robbie K. Nanomaterials and nanoparticles: sources and toxicity. Biointerphases. 2007;2(4):MR17-71.
114. van Ginkel MF, van der Voet GB, de Wolff FA. Improved method of analysis for aluminum in brain tissue. Clin Chem. 1990;36(4):658-61.
115. Nelson M, Li S, Page SJ, Shi X, Lee PD, Stevens MM, et al. 3D printed silica-gelatin hybrid scaffolds of specific channel sizes promote collagen Type II, Sox9 and Aggrecan production from chondrocytes. Mater Sci Eng C Mater Biol Appl. 2021;123:111964.
116. Brizuela-Velasco A, Pérez-Pevida E, Jiménez-Garrudo A, Gil-Mur FJ, Manero JM, Punset-Fuste M, et al. Mechanical Characterisation and Biomechanical and Biological Behaviours of Ti-Zr Binary-Alloy Dental Implants. BioMed Research International. 2017;2017:10.

117. Seki Y, Bessho K, Sugatani T, Kageyama T, Inui M, Tagawa T. Clinicopathological study on titanium miniplates. J Oral Maxillofac Surg. 1994;40:892-6.
118. Frączek T, Olejnik M, Tokarz A. Evaluation of plasma nitriding efficiency of titanium alloys for medical applications. METABK. 2009;48(2):83-6.
119. Textor M, Sittig C, Frauchiger V, Tosatti S, Brunette DM, Tengvall P, et al. Properties and Biological Significance of Natural Oxide Films on Titanium and Its Alloys. The Effect of Hydrogen and Hydrides on the Integrity of Zirconium Alloy Components: Springer Science and Business Media LLC; 2001. p. 171-230.
120. Jorge JR, Barao VA, Delben JA, Faverani LP, Queiroz TP, Assuncao WG. Titanium in dentistry: historical development, state of the art and future perspectives. J Indian Prosthodont Soc. 2013;13(2):71-7.
121. Kuphasuk C, Oshida Y, Andres CJ, Hovijitra ST, Barco MT, Brown DT. Electrochemical corrosion of titanium and titanium-based alloys. J Prosthet Dent. 2001;85(2):195-202.
122. Grandin HM, Berner S, Dard M. A review of titanium zirconium (TiZr) alloys for use in endosseous dental implants. Materials. 2012;5:1348-60.
123. Correa DR, Vicente FB, Donato TA, Arana-Chavez VE, Buzalaf MA, Grandini CR. The effect of the solute on the structure, selected mechanical properties, and biocompatibility of Ti-Zr system alloys for dental applications. Mater Sci Eng C Mater Biol Appl. 2014;34:354-9.
124. Bressan E, Ferroni L, Gardin C, Bellin G, Sbricoli L, Sivolella S, et al. Metal Nanoparticles Released from Dental Implant Surfaces: Potential Contribution to Chronic Inflammation and Peri-Implant Bone Loss. Materials (Basel). 2019;12(12).
125. Barrak F, Li S, Muntane A, Bhatia M, Crossthwaite K, Jones J. Particle release from dental implants immediately after placement - An ex vivo comparison of different implant systems. Dent Mater. 2022.
126. Cundy WJ, Mascarenhas AR, Antoniou G, Freeman BJ, Cundy PJ. Local and systemic metal ion release occurs intraoperatively during correction and instrumented spinal fusion for scoliosis. J Child Orthop. 2015;9(1):39-43.
127. Hallab NJ, Jacobs JJ. Chemokines Associated with Pathologic Responses to Orthopedic Implant Debris. Front Endocrinol (Lausanne). 2017;8:5.
128. Landgraeber S, Jager M, Jacobs JJ, Hallab NJ. The pathology of orthopedic implant failure is mediated by innate immune system cytokines. Mediators Inflamm. 2014;2014:185150.
129. Kaar SG, Ragab AA, Kaye SJ, Kilic BA, Jinno T, Goldberg VM, et al. Rapid repair of titanium particle-induced osteolysis is dramatically reduced in aged mice. J Orthop Res. 2001;19(2):171-8.
130. Shin DK, Kim MH, Lee SH, Kim TH, Kim SY. Inhibitory effects of luteolin on titanium particle-induced osteolysis in a mouse model. Acta Biomater. 2012;8(9):3524-31.
131. Senna P, Antoninha Del Bel Cury A, Kates S, Meirelles L. Surface Damage on Dental Implants with Release of Loose Particles after Insertion into Bone. Clin Implant Dent Relat Res. 2015;17(4):681-92.
132. Ribeiro AR, Gemini-Piperni S, Travassos R, Lemgruber L, Silva RC, Rossi AL, et al. Trojan-Like Internalization of Anatase Titanium Dioxide Nanoparticles by Human Osteoblast Cells. Sci Rep. 2016;6:23615.
133. Sierra MI, Valdes A, Fernandez AF, Torrecillas R, Fraga MF. The effect of exposure to nanoparticles and nanomaterials on the mammalian epigenome. Int J Nanomedicine. 2016;11:6297-306.
134. Geetha M, Singh AK, Asokamani R, Gogia AK. Ti based biomaterials, the ultimate choice for orthopaedic implants – A review. Progress in Materials Science. 2009;54(3):397-425.
135. Khadija G, Saleem A, Akhtar Z, Naqvi Z, Gull M, Masood M, et al. Short term exposure to titanium, aluminum and vanadium (Ti 6Al 4V) alloy powder drastically affects behavior and antioxidant metabolites in vital organs of male albino mice. Toxicol Rep. 2018;5:765-70.
136. Kim KT, Eo MY, Nguyen TTH, Kim SM. General review of titanium toxicity. Int J Implant Dent. 2019;5(1):10.

137. Kohal RJ, Schwindling FS, Bachle M, Spies BC. Peri-implant bone response to retrieved human zirconia oral implants after a 4-year loading period: A histologic and histomorphometric evaluation of 22 cases. J Biomed Mater Res B Appl Biomater. 2016;104(8):1622-31.
138. Cossellu G, Motta V, Dioni L, Angelici L, Vigna L, Farronato G, et al. Titanium and Zirconium Levels Are Associated with Changes in MicroRNAs Expression: Results from a Human Cross-Sectional Study on Obese Population. PLoS One. 2016;11(9):e0161916.
139. Zhang Y, Guo L, Li Y, Feng GH, Teng F, Li W, et al. MicroRNA-494 promotes cancer progression and targets adenomatous polyposis coli in colorectal cancer. Mol Cancer. 2018;17(1):1.
140. Baino F, Novajra G, Miguez-Pacheco V, Boccaccini AR, Vitale-Brovarone C. Bioactive glasses: Special applications outside the skeletal system. Journal of Non-Crystalline Solids. 2016;432:15-30.
141. Guillen-Romero LD, Oropeza-Guzmán MT, López-Maldonado EA, Iglesias AL, Paz-González JA, Ng T, et al. Synthetic hydroxyapatite and its use in bioactive coatings. Journal of Applied Biomaterials & Functional Materials. 2019;17(1):2280800018817463.
142. Mohammad NF, Othman R, Abdullah NA, Yeoh FY. In vitro Evaluation of Mesoporous Carbonated Hydroxyapatite in MC3T3-E1 Osteoblast Cells. Procedia Chemistry. 2016;19:259-66.
143. Fagerlund S, Massera J, Moritz N, Hupa L, Hupa M. Phase composition and in vitro bioactivity of porous implants made of bioactive glass S53P4. Acta Biomaterialia. 2012;8(6):2331-9.
144. Bruckner R, Tylkowski M, Hupa L, Brauer DS. Controlling the ion release from mixed alkali bioactive glasses by varying modifier ionic radii and molar volume. J Mater Chem B. 2016;4(18):3121-34.
145. Shih S-J, Chen C-Y, Lin Y-C, Lee J-C, Chung R-J. Investigation of bioactive and antibacterial effects of graphene oxide-doped bioactive glass. Advanced Powder Technology. 2016;27(3):1013-20.
146. Sepulveda P, Jones JR, Hench LL. In vitro dissolution of melt-derived 45S5 and sol-gel derived 58S bioactive glasses. J Biomed Mater Res. 2002;61(2):301-11.
147. Wallace KE, Hill RG, Pembroke JT, Brown CJ, Hatton PV. Influence of sodium oxide content on bioactive glass properties. J Mater Sci Mater Med. 1999;10(12):697-701.
148. Orefice R, Hench L, Brennan A. Evaluation of the interactions between collagen and the surface of a bioactive glass during in vitro test. J Biomed Mater Res A. 2009;90(1):114-20.
149. Stolz M, Raiteri R, Daniels AU, VanLandingham MR, Baschong W, Aebi U. Dynamic Elastic Modulus of Porcine Articular Cartilage Determined at Two Different Levels of Tissue Organization by Indentation-Type Atomic Force Microscopy. Biophysical Journal. 2004;86(5):3269-83.
150. Weitz-Schmidt G, Chreng S. Cell adhesion assays. Methods Mol Biol. 2012;757:15-30.
151. Buxboim A, Ivanovska IL, Discher DE. Matrix elasticity, cytoskeletal forces and physics of the nucleus: how deeply do cells 'feel' outside and in? J Cell Sci. 2010;123(Pt 3):297-308.
152. Venugopal B, Mogha P, Dhawan J, Majumder A. Cell density overrides the effect of substrate stiffness on human mesenchymal stem cells' morphology and proliferation. Biomater Sci. 2018;6(5):1109-19.
153. Klinge B, Klinge A, Bertl K, Stavropoulos A. Peri-implant diseases. Eur J Oral Sci. 2018;126 Suppl 1:88-94.
154. Witherel CE, Sao K, Brisson BK, Han B, Volk SW, Petrie RJ, et al. Regulation of extracellular matrix assembly and structure by hybrid M1/M2 macrophages. Biomaterials. 2021;269:120667.
155. Miron RJ, Bosshardt DD. OsteoMacs: Key players around bone biomaterials. Biomaterials. 2016;82:1-19.
156. Day RM, Boccaccini AR. Effect of particulate bioactive glasses on human macrophages and monocytes in vitro. J Biomed Mater Res A. 2005;73(1):73-9.

157. Arcos D, Vallet-Regí M. Sol–gel silica-based biomaterials and bone tissue regeneration. Acta Biomaterialia. 2010;6(8):2874-88.
158. Obata A, Iwanaga N, Terada A, Jell G, Kasuga T. Osteoblast-like cell responses to silicate ions released from 45S5-type bioactive glass and siloxane-doped vaterite. Journal of Materials Science. 2017;52(15):8942-56.
159. Zhou Z, Shi Q, Wang J, Chen X, Hao Y, Zhang Y, et al. The unfavorable role of titanium particles released from dental implants. Nanotheranostics. 2021;5(3):321-32.
160. Noronha Oliveira M, Schunemann WVH, Mathew MT, Henriques B, Magini RS, Teughels W, et al. Can degradation products released from dental implants affect peri-implant tissues? J Periodontal Res. 2018;53(1):1-11.
161. Přikrylová J, Procházková J, Podzimek Š. Side Effects of Dental Metal Implants: Impact on Human Health (Metal as a Risk Factor of Implantologic Treatment). BioMed Research International. 2019;2019:2519205.
162. Vijayaraghavan V, Sabane AV, Tejas K. Hypersensitivity to titanium: a less explored area of research. J Indian Prosthodont Soc. 2012;12(4):201-7.
163. Zwolak I. Vanadium carcinogenic, immunotoxic and neurotoxic effects: a review of in vitro studies. Toxicol Mech Methods. 2014;24(1):1-12.
164. Leinfelder KF, Lemons JE. Clinical restorative materials and techniques. Philadelphia: Lea & Febiger; 1988. p. 139-59.
165. Lucas LC, Lemons JE. Biodegradation of restorative metallic systems. Adv Dent Res. 1992;6:32-7.
166. Stricker A, Bergfeldt T, Fretwurst T, Addison O, Schmelzeisen R, Rothweiler R, et al. Impurities in commercial titanium dental implants–A mass and optical emission spectrometry elemental analysis. Dental Materials. 2022;38(8):1395-403.
167. Nichol T, Callaghan J, Townsend R, Stockley I, Hatton PV, Le Maitre C, et al. The antimicrobial activity and biocompatibility of a controlled gentamicin-releasing single-layer sol-gel coating on hydroxyapatite-coated titanium. Bone Joint J. 2021;103-b(3):522-9.
168. Saiz E, Goldman M, Gomez-Vega JM, Tomsia AP, Marshall GW, Marshall SJ. In vitro behavior of silicate glass coatings on Ti6A14V. Biomaterials. 2002;23(17):3749-56.
169. Barrak FN, Li S, Mohammed AA, Myant C, Jones JR. Anti-inflammatory properties of S53P4 bioactive glass implant material. J Dent. 2022;127:104296.
170. Gomez-Vega JM, Saiz E, Tomsia AP. Glass-based coatings for titanium implant alloys. J Biomed Mater Res. 1999;46(4):549-59.
171. Gomez-Vega JM, Hozumi A, Saiz E, Tomsia AP, Sugimura H, Takai O. Bioactive glass-mesoporous silica coatings on Ti6Al4V through enameling and triblock-copolymer-templated sol-gel processing. J Biomed Mater Res. 2001;56(3):382-9.
172. Brauer DS, Möncke D. Introduction to the structure of silicate, phosphate and borate glasses. Bioactive Glasses: Fundamentals, Technology and Applications: Royal Society of Chemistry; 2016. p. P61-88.
173. Fagerlund S, Hupa L. Melt-derived Bioactive Silicate Glasses. Bioactive Glasses: Fundamentals, Technology and Applications: Royal Society of Chemistry; 2016. p. P1-26.
174. Oku T, Suganuma K, Wallenberg LR, Tomsia AP, Gomez-Vega JM, Saiz E. Structural characterization of the metal/glass interface in bioactive glass coatings on Ti-6Al-4V. J Mater Sci Mater Med. 2001;12(5):413-7.
175. Moritz N, Vallittu PK. Introduction to the structure of silicate, phosphate and borate glasses. Bioactive Silicate Glass in Implantable Medical Devices: From Research to Clinical Applications: Royal Society of Chemistry; 2016. p. P442-70.
176. Kelly CN, Francovich J, Julmi S, Safranski D, Guldberg RE, Maier HJ, et al. Fatigue behavior of As-built selective laser melted titanium scaffolds with sheet-based gyroid microarchitecture for bone tissue engineering. Acta Biomaterialia. 2019;94:610-26.

177. Ataee A, Li Y, Brandt M, Wen C. Ultrahigh-strength titanium gyroid scaffolds manufactured by selective laser melting (SLM) for bone implant applications. Acta Materialia. 2018;158:354-68.
178. Yánez A, Cuadrado A, Martel O, Afonso H, Monopoli D. Gyroid porous titanium structures: A versatile solution to be used as scaffolds in bone defect reconstruction. Materials & Design. 2018;140:21-9.
179. Fernandes JS, Gentile P, Martins M, Neves NM, Miller C, Crawford A, et al. Reinforcement of poly-l-lactic acid electrospun membranes with strontium borosilicate bioactive glasses for bone tissue engineering. Acta Biomater. 2016;44:168-77.
180. Santocildes-Romero ME, Goodchild RL, Hatton PV, Crawford A, Reaney IM, Miller CA. Preparation of Composite Electrospun Membranes Containing Strontium-Substituted Bioactive Glasses for Bone Tissue Regeneration. Macromolecular Materials and Engineering. 2016;301(8):972-81.
181. Paterson TE, Shi R, Tian J, Harrison CJ, De Sousa Mendes M, Hatton PV, et al. Electrospun Scaffolds Containing Silver-Doped Hydroxyapatite with Antimicrobial Properties for Applications in Orthopedic and Dental Bone Surgery. J Funct Biomater. 2020;11(3).
182. Gentile P, Ferreira AM, Callaghan JT, Miller CA, Atkinson J, Freeman C, et al. Multilayer Nanoscale Encapsulation of Biofunctional Peptides to Enhance Bone Tissue Regeneration In Vivo. Adv Healthc Mater. 2017;6(8).

1. Alrabeah GO, Brett P, Knowles JC, Petridis H. The effect of metal ions released from different dental implant-abutment couples on osteoblast function and secretion of bone resorbing mediators. J Dent. 2017;66:91-101.
2. Mohajerani H, Roozbayani R, Taherian S, Tabrizi R. The Risk Factors in Early Failure of Dental Implants: a Retrospective Study. J Dent (Shiraz). 2017;18(4):298-303.
3. Dean R. The Periodontal Ligament: Development, Anatomy and Function. Journal of Oral Health and Dental Management. 2017;16.
4. Kim Y, Oh TJ, Misch CE, Wang HL. Occlusal considerations in implant therapy: clinical guidelines with biomechanical rationale. Clin Oral Implants Res. 2005;16(1):26-35.
5. Pearson CH. The Ground Substance of the Periodontal Ligament. In: Berkovitz BH, Moxham BJ, Newman HN, editors. The Periodntal Health in Health and Disease. Oxford: Pergamon Press; 1982.
6. Kobayashi K, Rose GG, Mahan CJ. Ultrastructure of the dento-epithelial junction. J Periodontal Res. 1976;11(6):313-30.
7. Abdallah MN, Badran Z, Ciobanu O, Hamdan N, Tamimi F. Strategies for Optimizing the Soft Tissue Seal around Osseointegrated Implants. Adv Healthc Mater. 2017;6(20).
8. Hasan A, Palmer RM. A clinical guide to periodontology: pathology of periodontal disease. Br Dent J. 2014;216(8):457-61.
9. Liu D, Xu J, Liu O, Fan Z, Liu Y, Wang F, et al. Mesenchymal stem cells derived from inflamed periodontal ligaments exhibit impaired immunomodulation. J Clin Periodontol. 2012;39(12):1174-82.
10. Salvi GE, Cosgarea R, Sculean A. Prevalence and Mechanisms of Peri-implant Diseases. J Dent Res. 2017;96(1):31-7.
11. Straumann. Annual Report. 2016.
12. Nations U. World Population Prospects: The 2015 Revision. 2015.
13. Feine JS, Carlsson GE, Awad MA, Chehade A, Duncan WJ, Gizani S, et al. The McGill consensus statement on overdentures. Mandibular two-implant overdentures as first choice standard of care for edentulous patients. Gerodontology. 2002;19(1):3-4.

14. Thomason JM, Kelly SA, Bendkowski A, Ellis JS. Two implant retained overdentures--a review of the literature supporting the McGill and York consensus statements. J Dent. 2012;40(1):22-34.
15. Derks J, Schaller D, Hakansson J, Wennstrom JL, Tomasi C, Berglundh T. Peri-implantitis - onset and pattern of progression. J Clin Periodontol. 2016;43(4):383-8.
16. Esposito M, Grusovin MG, Worthington HV. Treatment of peri-implantitis: what interventions are effective? A Cochrane systematic review. Eur J Oral Implantol. 2012;5 Suppl:S21-41.
17. Fretwurst T, Nelson K, Tarnow DP, Wang HL, Giannobile WV. Is Metal Particle Release Associated with Peri-implant Bone Destruction? An Emerging Concept. J Dent Res. 2018;97(3):259-65.
18. Villar CC, Huynh-Ba G, Mills MP, Cochran DL. Wound healing around dental implants. Endodontic Topics. 2011;25(1):44-62.
19. Berglundh T, Armitage G, Araujo MG, Avila-Ortiz G, Blanco J, Camargo PM, et al. Peri-implant diseases and conditions: Consensus report of workgroup 4 of the 2017 World Workshop on the Classification of Periodontal and Peri-Implant Diseases and Conditions. J Periodontol. 2018;89 Suppl 1:S313-S8.
20. Shariff JA, Gurpegui Abud D, Bhave MB, Tarnow DP. Selective Serotonin Reuptake Inhibitors (SSRI) and Dental Implant Failure: A Systematic Review and Meta-Analysis. J Oral Implantol. 2023.
21. Berglundh T, Lindhe J, Ericsson I, Marinello CP, Liljenberg B, Thomsen P. The soft tissue barrier at implants and teeth. Clin Oral Implants Res. 1991;2(2):81-90.
22. Fransson C, Tomasi C, Pikner SS, Grondahl K, Wennstrom JL, Leyland AH, et al. Severity and pattern of peri-implantitis-associated bone loss. J Clin Periodontol. 2010;37(5):442-8.
23. Lindhe J, Berglundh T, Ericsson I, Liljenberg B, Marinello C. Experimental breakdown of peri-implant and periodontal tissues. A study in the beagle dog. Clin Oral Implants Res. 1992;3(1):9-16.
24. Albrektsson T, Canullo L, Cochran D, De Bruyn H. "Peri-Implantitis": A Complication of a Foreign Body or a Man-Made "Disease". Facts and Fiction. Clin Implant Dent Relat Res. 2016;18(4):840-9.
25. Delgado-Ruiz R, Romanos G. Potential Causes of Titanium Particle and Ion Release in Implant Dentistry: A Systematic Review. Int J Mol Sci. 2018;19(11).
26. Mombelli A, Hashim D, Cionca N. What is the impact of titanium particles and biocorrosion on implant survival and complications? A critical review. Clinical Oral Implants Research. 2018;29:37-53.
27. Steinemann SG. Titanium--the material of choice? Periodontol 2000. 1998;17:7-21.
28. Moraschini V, Poubel LA, Ferreira VF, Barboza Edos S. Evaluation of survival and success rates of dental implants reported in longitudinal studies with a follow-up period of at least 10 years: a systematic review. Int J Oral Maxillofac Surg. 2015;44(3):377-88.
29. Sikora CL, Alfaro MF, Yuan JCC, Barao VA, Sukotjo C, Mathew MT. Wear and corrosion interactions at the titanium/zirconia interface: dental implant application. Journal of Prosthodontics. 2018;27(9):842-52.
30. Medvedev AE, Molotnikov A, Lapovok R, Zeller R, Berner S, Habersetzer P, et al. Microstructure and mechanical properties of Ti–15Zr alloy used as dental implant material. journal of the mechanical behavior of biomedical materials. 2016;62:384-98.
31. Osman RB, Swain MV. A Critical Review of Dental Implant Materials with an Emphasis on Titanium versus Zirconia. Materials (Basel). 2015;8(3):932-58.
32. Bahadirli G, Yilmaz S, Jones T, Sen D. Influences of Implant and Framework Materials on Stress Distribution: A Three-Dimensional Finite Element Analysis Study. Int J Oral Maxillofac Implants. 2018;33(5):e117-e26.

33. Straumann. MATERIAL INFORMATION: Straumann.com; 2014 [Available from: https://www.straumann.com/content/dam/media-center/straumann/en/documents/brochure/technical-information/490.019-en_low.pdf.
34. Obando-Pereda GA, Fischer L, Stach-Machado DR. Titanium and zirconia particle-induced pro-inflammatory gene expression in cultured macrophages and osteolysis, inflammatory hyperalgesia and edema in vivo. Life Sci. 2014;97(2):96-106.
35. Eger M, Sterer N, Liron T, Kohavi D, Gabet Y. Scaling of titanium implants entrains inflammation-induced osteolysis. Sci Rep. 2017;7:39612.
36. Pettersson M, Pettersson J, Molin Thoren M, Johansson A. Release of titanium after insertion of dental implants with different surface characteristics - an ex vivo animal study. Acta Biomater Odontol Scand. 2017;3(1):63-73.
37. Anderson JM, Rodriguez A, Chang DT, editors. Foreign body reaction to biomaterials. Seminars in immunology; 2008: Elsevier.
38. Willis J, Li S, Crean SJ, Barrak FN. Is titanium alloy Ti-6Al-4 V cytotoxic to gingival fibroblasts—A systematic review. Clinical and experimental dental research. 2021;7(6):1037-44.
39. Purdue PE, Koulouvaris P, Potter HG, Nestor BJ, Sculco TP. The cellular and molecular biology of periprosthetic osteolysis. Clinical Orthopaedics and Related Research®. 2007;454:251-61.
40. Yao JJ, Lewallen EA, Trousdale WH, Xu W, Thaler R, Salib CG, et al. Local cellular responses to titanium dioxide from orthopedic implants. BioResearch open access. 2017;6(1):94-103.
41. Trindade R, Albrektsson T, Tengvall P, Wennerberg A. Foreign body reaction to biomaterials: on mechanisms for buildup and breakdown of osseointegration. Clinical implant dentistry and related research. 2016;18(1):192-203.
42. Medzhitov R. Origin and physiological roles of inflammation. Nature. 2008;454(7203):428-35.
43. Florencio-Silva R, Sasso GRdS, Sasso-Cerri E, Simões MJ, Cerri PS. Biology of bone tissue: structure, function, and factors that influence bone cells. BioMed research international. 2015;2015.
44. Penmetsa SLD, Shah R, Thomas R, Kumar ABT, Gayatri PSD, Mehta DS. Titanium particles in tissues from peri-implant mucositis: An exfoliative cytology-based pilot study. Journal of Indian Society of Periodontology. 2017;21(3):192.
45. Kazazian NH. NLRP3 inflammasome activation by crystal structures. BioSciences Master Reviews. 2014:1-8.
46. Mathew MT, Abbey S, Hallab NJ, Hall DJ, Sukotjo C, Wimmer MA. Influence of pH on the tribocorrosion behavior of CpTi in the oral environment: synergistic interactions of wear and corrosion. Journal of Biomedical Materials Research Part B: Applied Biomaterials. 2012;100(6):1662-71.
47. Rodrigues DC, Valderrama P, Wilson TG, Palmer K, Thomas A, Sridhar S, et al. Titanium corrosion mechanisms in the oral environment: a retrieval study. Materials. 2013;6(11):5258-74.
48. Jämsen E, Pajarinen J, Kouri V-P, Rahikkala A, Goodman SB, Manninen M, et al. Tumor necrosis factor primes and metal particles activate the NLRP3 inflammasome in human primary macrophages. Acta biomaterialia. 2020;108:347-57.
49. Barão VA, Mathew MT, Assunção WG, Yuan JCC, Wimmer MA, Sukotjo C. Stability of cp-Ti and Ti-6 Al-4 V alloy for dental implants as a function of saliva pH–an electrochemical study. Clinical oral implants research. 2012;23(9):1055-62.
50. Raisanen L, Kononen M, Juhanoja J, Varpavaara P, Hautaniemi J, Kivilahti J, et al. Expression of cell adhesion complexes in epithelial cells seeded on biomaterial surfaces. J Biomed Mater Res. 2000;49(1):79-87.
51. Abrahamsson I. The mucosal attachment at different abutments An experimental study in dogs. Journal of Clinical Periodontology. 2005;25(9):721-7.

52. Chevalier J, Gremillard L, Deville S. Low-temperature degradation of Zirconia and implications for biomedical implants. Annu Rev Mater Res. 2007;37:1-32.
53. Pendegrass CJ, Goodship AE, Blunn GW. Development of a soft tissue seal around bone-anchored transcutaneous amputation prostheses. Biomaterials. 2006;27(23):4183-91.
54. Lai Y, Chen J, Zhang T, Gu D, Zhang C, Li Z, et al. Effect of 3D microgroove surface topography on plasma and cellular fibronectin of human gingival fibroblasts. J Dent. 2013;41(11):1109-21.
55. Kim H, Murakami H, Chehroudi B, Textor M, Brunette DM. Effects of surface topography on the connective tissue attachment to subcutaneous implants. Int J Oral Maxillofac Implants. 2006;21(3):354-65.
56. Chehroudi B, Gould TR, Brunette DM. Titanium-coated micromachined grooves of different dimensions affect epithelial and connective-tissue cells differently in vivo. J Biomed Mater Res. 1990;24(9):1203-19.
57. Nevins M, Nevins ML, Camelo M, Boyesen JL, Kim DM. Human histologic evidence of a connective tissue attachment to a dental implant. Int J Periodontics Restorative Dent. 2008;28(2):111-21.
58. Farrell BJ, Prilutsky BI, Ritter JM, Kelley S, Popat K, Pitkin M. Effects of pore size, implantation time, and nano-surface properties on rat skin ingrowth into percutaneous porous titanium implants. J Biomed Mater Res A. 2014;102(5):1305-15.
59. Park JC, Kim HM, Ko J. Effects of extracellular matrix constituents on the attachment of human oral epithelial cells at the titanium surface. Int J Oral Maxillofac Implants. 1998;13(6):826-36.
60. Bates C, Marino V, Fazzalari NL, Bartold PM. Soft tissue attachment to titanium implants coated with growth factors. Clin Implant Dent Relat Res. 2013;15(1):53-63.
61. Pendegrass CJ, Tucker B, Patel S, Dowling R, Blunn GW. The effect of adherens junction components on keratinocyte adhesion in vitro: potential implications for sealing the skin-implant interface of intraosseous transcutaneous amputation prostheses. J Biomed Mater Res A. 2012;100(12):3463-71.
62. Satue M, Gomez-Florit M, Monjo M, Ramis JM. Improved human gingival fibroblast response to titanium implants coated with ultraviolet-irradiated vitamin D precursor and vitamin E. J Periodontal Res. 2016;51(3):342-9.
63. Bullock G, Atkinson J, Gentile P, Hatton P, Miller C. Osteogenic Peptides and Attachment Methods Determine Tissue Regeneration in Modified Bone Graft Substitutes. J Funct Biomater. 2021;12(2).
64. Stähli A, Strauss FJ, Gruber R. The use of platelet-rich plasma to enhance the outcomes of implant therapy: A systematic review. Clin Oral Implants Res. 2018;29 Suppl 18(Suppl Suppl 18):20-36.
65. Reyes CD, Petrie TA, Burns KL, Schwartz Z, Garcia AJ. Biomolecular surface coating to enhance orthopaedic tissue healing and integration. Biomaterials. 2007;28(21):3228-35.
66. Beertsen W, McCulloch CA, Sodek J. The periodontal ligament: a unique, multifunctional connective tissue. Periodontol 2000. 1997;13:20-40.
67. Aguiar HG, P. Serra, J. Bioactive glass structure and solubility. Bioactive glasses. 2nd ed: Wodhead publishing series in biomaterials; 2018. p. 37-61.
68. Jones JR. Reprint of: Review of bioactive glass: From Hench to hybrids. Acta Biomater. 2015;23 Suppl:S53-82.
69. Wilson J, Low SB. Bioactive ceramics for periodontal treatment: comparative studies in the Patus monkey. J Appl Biomater. 1992;3(2):123-9.
70. Lepparanta O, Vaahtio M, Peltola T, Zhang D, Hupa L, Hupa M, et al. Antibacterial effect of bioactive glasses on clinically important anaerobic bacteria in vitro. J Mater Sci Mater Med. 2008;19(2):547-51.

71. Munukka E, Lepparanta O, Korkeamaki M, Vaahtio M, Peltola T, Zhang D, et al. Bactericidal effects of bioactive glasses on clinically important aerobic bacteria. J Mater Sci Mater Med. 2008;19(1):27-32.
72. Gubler M, Brunner TJ, Zehnder M, Waltimo T, Sener B, Stark WJ. Do bioactive glasses convey a disinfecting mechanism beyond a mere increase in pH? International Endodontic Journal. 2008;41(8):670-8.
73. Alrabiah M, Alrahlah A, Al-Hamdan RS, Al-Aali KA, Labban N, Abduljabbar T. Survival of adjacent-dental-implants in prediabetic and systemically healthy subjects at 5-years follow-up. Clin Implant Dent Relat Res. 2019;21(2):232-7.
74. Francetti L, Cavalli N, Taschieri S, Corbella S. Ten years follow-up retrospective study on implant survival rates and prevalence of peri-implantitis in implant-supported full-arch rehabilitations. Clin Oral Implants Res. 2019;30(3):252-60.
75. Longhofer LK, Chong A, Strong NM, Wooley PH, Yang S-Y. Specific material effects of wear-particle-induced inflammation and osteolysis at the bone-implant interface: A rat model. J Orthop Translat. 2016;8:5-11.
76. Rivera MC, Perni S, Sloan A, Prokopovich P. Anti-inflammatory drug-eluting implant model system to prevent wear particle-induced periprosthetic osteolysis. Int J Nanomedicine. 2019;14:1069-84.
77. Barbieri M, Mencio F, Papi P, Rosella D, Di Carlo S, Valente T, et al. Corrosion behavior of dental implants immersed into human saliva: preliminary results of an in vitro study. Eur Rev Med Pharmacol Sci. 2017;21(16):3543-8.
78. Mabilleau G, Bourdon S, Joly-Guillou ML, Filmon R, Basle MF, Chappard D. Influence of fluoride, hydrogen peroxide and lactic acid on the corrosion resistance of commercially pure titanium. Acta Biomater. 2006;2(1):121-9.
79. Siirilä HS, Könönen M. The effect of oral topical fluorides on the surface of commercially pure titanium. Int J Oral Maxillofac Implants. 1991;6(1):50-4.
80. Kokubo T, Kushitani H, Sakka S, Kitsugi T, Yamamuro T. Solutions able to reproduce in vivo surface-structure changes in bioactive glass-ceramic A-W. J Biomed Mater Res. 1990;24(6):721-34.
81. Maçon AL, Kim TB, Valliant EM, Goetschius K, Brow RK, Day DE, et al. A unified in vitro evaluation for apatite-forming ability of bioactive glasses and their variants. J Mater Sci Mater Med. 2015;26(2):115.
82. UK SMCL. Ti-6Al-4V (Grade 5) Technical Datasheet. 2018.
83. UK SMCL. CP Grade 4 Technical Datasheet. 2018.
84. Sargeant A, Goswami T, Swank M. Ion concentrations from hip implants. J Surg Orthop Adv. 2006;15(2):113-4.
85. Costa BC, Tokuhara CK, Rocha LA, Oliveira RC, Lisboa-Filho PN, Costa Pessoa J. Vanadium ionic species from degradation of Ti-6Al-4V metallic implants: In vitro cytotoxicity and speciation evaluation. Mater Sci Eng C Mater Biol Appl. 2019;96:730-9.
86. Zhang Y, Addison O, Yu F, Troconis BCR, Scully JR, Davenport AJ. Time-dependent Enhanced Corrosion of Ti6Al4V in the Presence of H2O2 and Albumin. Sci Rep. 2018;8(1):3185.
87. Rodrigues DC, Urban RM, Jacobs JJ, Gilbert JL. In vivo severe corrosion and hydrogen embrittlement of retrieved modular body titanium alloy hip-implants. J Biomed Mater Res B Appl Biomater. 2009;88(1):206-19.
88. Hallab NJ, Mikecz K, Vermes C, Skipor A, Jacobs JJ. Orthopaedic implant related metal toxicity in terms of human lymphocyte reactivity to metal-protein complexes produced from cobalt-base and titanium-base implant alloy degradation. Mol Cell Biochem. 2001;222(1-2):127-36.
89. Conner SD, Schmid SL. Regulated portals of entry into the cell. Nature. 2003;422(6927):37-44.

90. He X, Hartlieb E, Rothmund L, Waschke J, Wu X, Van Landuyt KL, et al. Intracellular uptake and toxicity of three different Titanium particles. Dent Mater. 2015;31(6):734-44.
91. Caputi S, Diomede F, Lanuti P, Marconi GD, Di Carlo P, Sinjari B, et al. Microplastics Affect the Inflammation Pathway in Human Gingival Fibroblasts: A Study in the Adriatic Sea. Int J Environ Res Public Health. 2022;19(13).
92. Li L, Sun W, Yu J, Lei W, Zeng H, Shi B. Effects of titanium dioxide microparticles and nanoparticles on cytoskeletal organization, cell adhesion, migration, and proliferation in human gingival fibroblasts in the presence of lipopolysaccharide. J Periodontal Res. 2022;57(3):644-59.
93. Sabbioni E, Fortaner S, Farina M, Del Torchio R, Petrarca C, Bernardini G, et al. Interaction with culture medium components, cellular uptake and intracellular distribution of cobalt nanoparticles, microparticles and ions in Balb/3T3 mouse fibroblasts. Nanotoxicology. 2014;8(1):88-99.
94. Haleem-Smith H, Argintar E, Bush C, Hampton D, Postma WF, Chen FH, et al. Biological responses of human mesenchymal stem cells to titanium wear debris particles. J Orthop Res. 2012;30(6):853-63.
95. Okafor CC, Haleem-Smith H, Laqueriere P, Manner PA, Tuan RS. Particulate endocytosis mediates biological responses of human mesenchymal stem cells to titanium wear debris. J Orthop Res. 2006;24(3):461-73.
96. Rosen PS, Qari M, Froum SJ, Dibart S, Chou LL. A Pilot Study on the Efficacy of a Treatment Algorithm to Detoxify Dental Implant Surfaces Affected by Peri-implantitis. Int J Periodontics Restorative Dent. 2018;38(2):261-7.
97. ASM Aerospace Specification Metals Inc - Titanium Grade 4 specification sheet (Web access) [Available from: http://asm.matweb.com/search/SpecificMaterial.asp?bassnum=MTU040.
98. Boyer R, Welsch G, Collings W. Materials Properties Handbook: Titanium Alloys. Ohio: ASM International; 1994.
99. Harloff T, Hönle W, Holzwarth U, Bader R, Yhomas P, Schuh A. Titanium allergy or not? “Impurity” of titanium implant materials. Health. 2010;2(4):306–10.
100. Chaturvedi T. Allergy related to dental implant and its clinical significance. Clin Cosmet Investig Dent. 2013;5:57-61.
101. Diebold U. The surface science of titanium dioxide. Surf Sci Reports. 2003;48(5-8):53-229.
102. Revell PA. The combined role of wear particles, macrophages and lymphocytes in the loosening of total joint prostheses. J R Soc Interface. 2008;5(28):1263-78.
103. Mathew MT, Srinivasa Pai P, Pourzal R, Fischer A, Wimmer MA. Significance of Tribocorrosion in Biomedical Applications: Overview and Current Status. Adv Tribol. 2009;doi: 10.1155/2009/250986:1-12.
104. Matusiewicz H. Potential release of in vivo trace metals from metallic medical implants in the human body: from ions to nanoparticles--a systematic analytical review. Acta Biomater. 2014;10(6):2379-403.
105. Derks J, Tomasi C. Peri-implant health and disease. A systematic review of current epidemiology. J Clin Periodontol. 2015;42 Suppl 16:S158-71.
106. Wawrzinek C, Sommer T, Fischer-Brandies H. Microdamage in cortical bone due to the overtightening of orthodontic microscrews. J Orofac Orthop. 2008;69(2):121-34.
107. Guan H, van Staden RC, Johnson NW, Loo Y-C. Dynamic modelling and simulation of dental implant insertion process - A finiteelement study. Finite Elem Anal Des. 2011;47:886-97.
108. Konttinen YT, Pajarinen J, Takakubo Y, Gallo J, Nich C, Takagi M, et al. Macrophage polarization and activation in response to implant debris: influence by "particle disease" and "ion disease". J Long Term Eff Med Implants. 2014;24(4):267-81.
109. Barrak FN, Li S, Muntane AM, Jones JR. Particle release from implantoplasty of dental implants and impact on cells. Int J Implant Dent. 2020;6(1):50.

110. Schlegel KA, Eppeneder S, Wiltfang J. Soft tissue findings above submerged titanium implants--a histological and spectroscopic study. Biomaterials. 2002;23(14):2939-44.
111. Olmedo DG, Paparella ML, Spielberg M, Brandizzi D, Guglielmotti MB, Cabrini RL. Oral mucosa tissue response to titanium cover screws. J Periodontol. 2012;83(8):973-80.
112. de Morais LS, Serra GG, Albuquerque Palermo EF, Andrade LR, Muller CA, Meyers MA, et al. Systemic levels of metallic ions released from orthodontic mini-implants. Am J Orthod Dentofacial Orthop. 2009;135(4):522-9.
113. Buzea C, Pacheco, II, Robbie K. Nanomaterials and nanoparticles: sources and toxicity. Biointerphases. 2007;2(4):MR17-71.
114. van Ginkel MF, van der Voet GB, de Wolff FA. Improved method of analysis for aluminum in brain tissue. Clin Chem. 1990;36(4):658-61.
115. Nelson M, Li S, Page SJ, Shi X, Lee PD, Stevens MM, et al. 3D printed silica-gelatin hybrid scaffolds of specific channel sizes promote collagen Type II, Sox9 and Aggrecan production from chondrocytes. Mater Sci Eng C Mater Biol Appl. 2021;123:111964.
116. Brizuela-Velasco A, Pérez-Pevida E, Jiménez-Garrudo A, Gil-Mur FJ, Manero JM, Punset-Fuste M, et al. Mechanical Characterisation and Biomechanical and Biological Behaviours of Ti-Zr Binary-Alloy Dental Implants. BioMed Research International. 2017;2017:10.
117. Seki Y, Bessho K, Sugatani T, Kageyama T, Inui M, Tagawa T. Clinicopathological study on titanium miniplates. J Oral Maxillofac Surg. 1994;40:892-6.
118. Frączek T, Olejnik M, Tokarz A. Evaluation of plasma nitriding efficiency of titanium alloys for medical applications. METABK. 2009;48(2):83-6.
119. Textor M, Sittig C, Frauchiger V, Tosatti S, Brunette DM, Tengvall P, et al. Properties and Biological Significance of Natural Oxide Films on Titanium and Its Alloys. The Effect of Hydrogen and Hydrides on the Integrity of Zirconium Alloy Components: Springer Science and Business Media LLC; 2001. p. 171-230.
120. Jorge JR, Barao VA, Delben JA, Faverani LP, Queiroz TP, Assuncao WG. Titanium in dentistry: historical development, state of the art and future perspectives. J Indian Prosthodont Soc. 2013;13(2):71-7.
121. Kuphasuk C, Oshida Y, Andres CJ, Hovijitra ST, Barco MT, Brown DT. Electrochemical corrosion of titanium and titanium-based alloys. J Prosthet Dent. 2001;85(2):195-202.
122. Grandin HM, Berner S, Dard M. A review of titanium zirconium (TiZr) alloys for use in endosseous dental implants. Materials. 2012;5:1348-60.
123. Correa DR, Vicente FB, Donato TA, Arana-Chavez VE, Buzalaf MA, Grandini CR. The effect of the solute on the structure, selected mechanical properties, and biocompatibility of Ti-Zr system alloys for dental applications. Mater Sci Eng C Mater Biol Appl. 2014;34:354-9.
124. Bressan E, Ferroni L, Gardin C, Bellin G, Sbricoli L, Sivolella S, et al. Metal Nanoparticles Released from Dental Implant Surfaces: Potential Contribution to Chronic Inflammation and Peri-Implant Bone Loss. Materials (Basel). 2019;12(12).
125. Barrak F, Li S, Muntane A, Bhatia M, Crossthwaite K, Jones J. Particle release from dental implants immediately after placement - An ex vivo comparison of different implant systems. Dent Mater. 2022.
126. Cundy WJ, Mascarenhas AR, Antoniou G, Freeman BJ, Cundy PJ. Local and systemic metal ion release occurs intraoperatively during correction and instrumented spinal fusion for scoliosis. J Child Orthop. 2015;9(1):39-43.
127. Hallab NJ, Jacobs JJ. Chemokines Associated with Pathologic Responses to Orthopedic Implant Debris. Front Endocrinol (Lausanne). 2017;8:5.
128. Landgraeber S, Jager M, Jacobs JJ, Hallab NJ. The pathology of orthopedic implant failure is mediated by innate immune system cytokines. Mediators Inflamm. 2014;2014:185150.
129. Kaar SG, Ragab AA, Kaye SJ, Kilic BA, Jinno T, Goldberg VM, et al. Rapid repair of titanium particle-induced osteolysis is dramatically reduced in aged mice. J Orthop Res. 2001;19(2):171-8.

130. Shin DK, Kim MH, Lee SH, Kim TH, Kim SY. Inhibitory effects of luteolin on titanium particle-induced osteolysis in a mouse model. Acta Biomater. 2012;8(9):3524-31.
131. Senna P, Antoninha Del Bel Cury A, Kates S, Meirelles L. Surface Damage on Dental Implants with Release of Loose Particles after Insertion into Bone. Clin Implant Dent Relat Res. 2015;17(4):681-92.
132. Ribeiro AR, Gemini-Piperni S, Travassos R, Lemgruber L, Silva RC, Rossi AL, et al. Trojan-Like Internalization of Anatase Titanium Dioxide Nanoparticles by Human Osteoblast Cells. Sci Rep. 2016;6:23615.
133. Sierra MI, Valdes A, Fernandez AF, Torrecillas R, Fraga MF. The effect of exposure to nanoparticles and nanomaterials on the mammalian epigenome. Int J Nanomedicine. 2016;11:6297-306.
134. Geetha M, Singh AK, Asokamani R, Gogia AK. Ti based biomaterials, the ultimate choice for orthopaedic implants – A review. Progress in Materials Science. 2009;54(3):397-425.
135. Khadija G, Saleem A, Akhtar Z, Naqvi Z, Gull M, Masood M, et al. Short term exposure to titanium, aluminum and vanadium (Ti 6Al 4V) alloy powder drastically affects behavior and antioxidant metabolites in vital organs of male albino mice. Toxicol Rep. 2018;5:765-70.
136. Kim KT, Eo MY, Nguyen TTH, Kim SM. General review of titanium toxicity. Int J Implant Dent. 2019;5(1):10.
137. Kohal RJ, Schwindling FS, Bachle M, Spies BC. Peri-implant bone response to retrieved human zirconia oral implants after a 4-year loading period: A histologic and histomorphometric evaluation of 22 cases. J Biomed Mater Res B Appl Biomater. 2016;104(8):1622-31.
138. Cossellu G, Motta V, Dioni L, Angelici L, Vigna L, Farronato G, et al. Titanium and Zirconium Levels Are Associated with Changes in MicroRNAs Expression: Results from a Human Cross-Sectional Study on Obese Population. PLoS One. 2016;11(9):e0161916.
139. Zhang Y, Guo L, Li Y, Feng GH, Teng F, Li W, et al. MicroRNA-494 promotes cancer progression and targets adenomatous polyposis coli in colorectal cancer. Mol Cancer. 2018;17(1):1.
140. Baino F, Novajra G, Miguez-Pacheco V, Boccaccini AR, Vitale-Brovarone C. Bioactive glasses: Special applications outside the skeletal system. Journal of Non-Crystalline Solids. 2016;432:15-30.
141. Guillen-Romero LD, Oropeza-Guzmán MT, López-Maldonado EA, Iglesias AL, Paz-González JA, Ng T, et al. Synthetic hydroxyapatite and its use in bioactive coatings. Journal of Applied Biomaterials & Functional Materials. 2019;17(1):2280800018817463.
142. Mohammad NF, Othman R, Abdullah NA, Yeoh FY. In vitro Evaluation of Mesoporous Carbonated Hydroxyapatite in MC3T3-E1 Osteoblast Cells. Procedia Chemistry. 2016;19:259-66.
143. Fagerlund S, Massera J, Moritz N, Hupa L, Hupa M. Phase composition and in vitro bioactivity of porous implants made of bioactive glass S53P4. Acta Biomaterialia. 2012;8(6):2331-9.
144. Bruckner R, Tylkowski M, Hupa L, Brauer DS. Controlling the ion release from mixed alkali bioactive glasses by varying modifier ionic radii and molar volume. J Mater Chem B. 2016;4(18):3121-34.
145. Shih S-J, Chen C-Y, Lin Y-C, Lee J-C, Chung R-J. Investigation of bioactive and antibacterial effects of graphene oxide-doped bioactive glass. Advanced Powder Technology. 2016;27(3):1013-20.
146. Sepulveda P, Jones JR, Hench LL. In vitro dissolution of melt-derived 45S5 and sol-gel derived 58S bioactive glasses. J Biomed Mater Res. 2002;61(2):301-11.
147. Wallace KE, Hill RG, Pembroke JT, Brown CJ, Hatton PV. Influence of sodium oxide content on bioactive glass properties. J Mater Sci Mater Med. 1999;10(12):697-701.
148. Orefice R, Hench L, Brennan A. Evaluation of the interactions between collagen and the surface of a bioactive glass during in vitro test. J Biomed Mater Res A. 2009;90(1):114-20.

149. Stolz M, Raiteri R, Daniels AU, VanLandingham MR, Baschong W, Aebi U. Dynamic Elastic Modulus of Porcine Articular Cartilage Determined at Two Different Levels of Tissue Organization by Indentation-Type Atomic Force Microscopy. Biophysical Journal. 2004;86(5):3269-83.
150. Weitz-Schmidt G, Chreng S. Cell adhesion assays. Methods Mol Biol. 2012;757:15-30.
151. Buxboim A, Ivanovska IL, Discher DE. Matrix elasticity, cytoskeletal forces and physics of the nucleus: how deeply do cells 'feel' outside and in? J Cell Sci. 2010;123(Pt 3):297-308.
152. Venugopal B, Mogha P, Dhawan J, Majumder A. Cell density overrides the effect of substrate stiffness on human mesenchymal stem cells' morphology and proliferation. Biomater Sci. 2018;6(5):1109-19.
153. Klinge B, Klinge A, Bertl K, Stavropoulos A. Peri-implant diseases. Eur J Oral Sci. 2018;126 Suppl 1:88-94.
154. Witherel CE, Sao K, Brisson BK, Han B, Volk SW, Petrie RJ, et al. Regulation of extracellular matrix assembly and structure by hybrid M1/M2 macrophages. Biomaterials. 2021;269:120667.
155. Miron RJ, Bosshardt DD. OsteoMacs: Key players around bone biomaterials. Biomaterials. 2016;82:1-19.
156. Day RM, Boccaccini AR. Effect of particulate bioactive glasses on human macrophages and monocytes in vitro. J Biomed Mater Res A. 2005;73(1):73-9.
157. Arcos D, Vallet-Regí M. Sol–gel silica-based biomaterials and bone tissue regeneration. Acta Biomaterialia. 2010;6(8):2874-88.
158. Obata A, Iwanaga N, Terada A, Jell G, Kasuga T. Osteoblast-like cell responses to silicate ions released from 45S5-type bioactive glass and siloxane-doped vaterite. Journal of Materials Science. 2017;52(15):8942-56.
159. Zhou Z, Shi Q, Wang J, Chen X, Hao Y, Zhang Y, et al. The unfavorable role of titanium particles released from dental implants. Nanotheranostics. 2021;5(3):321-32.
160. Noronha Oliveira M, Schunemann WVH, Mathew MT, Henriques B, Magini RS, Teughels W, et al. Can degradation products released from dental implants affect peri-implant tissues? J Periodontal Res. 2018;53(1):1-11.
161. Přikrylová J, Procházková J, Podzimek Š. Side Effects of Dental Metal Implants: Impact on Human Health (Metal as a Risk Factor of Implantologic Treatment). BioMed Research International. 2019;2019:2519205.
162. Vijayaraghavan V, Sabane AV, Tejas K. Hypersensitivity to titanium: a less explored area of research. J Indian Prosthodont Soc. 2012;12(4):201-7.
163. Zwolak I. Vanadium carcinogenic, immunotoxic and neurotoxic effects: a review of in vitro studies. Toxicol Mech Methods. 2014;24(1):1-12.
164. Leinfelder KF, Lemons JE. Clinical restorative materials and techniques. Philadelphia: Lea & Febiger; 1988. p. 139-59.
165. Lucas LC, Lemons JE. Biodegradation of restorative metallic systems. Adv Dent Res. 1992;6:32-7.
166. Stricker A, Bergfeldt T, Fretwurst T, Addison O, Schmelzeisen R, Rothweiler R, et al. Impurities in commercial titanium dental implants–A mass and optical emission spectrometry elemental analysis. Dental Materials. 2022;38(8):1395-403.
167. Nichol T, Callaghan J, Townsend R, Stockley I, Hatton PV, Le Maitre C, et al. The antimicrobial activity and biocompatibility of a controlled gentamicin-releasing single-layer sol-gel coating on hydroxyapatite-coated titanium. Bone Joint J. 2021;103-b(3):522-9.
168. Saiz E, Goldman M, Gomez-Vega JM, Tomsia AP, Marshall GW, Marshall SJ. In vitro behavior of silicate glass coatings on Ti6A14V. Biomaterials. 2002;23(17):3749-56.
169. Barrak FN, Li S, Mohammed AA, Myant C, Jones JR. Anti-inflammatory properties of S53P4 bioactive glass implant material. J Dent. 2022;127:104296.

170. Gomez-Vega JM, Saiz E, Tomsia AP. Glass-based coatings for titanium implant alloys. J Biomed Mater Res. 1999;46(4):549-59.
171. Gomez-Vega JM, Hozumi A, Saiz E, Tomsia AP, Sugimura H, Takai O. Bioactive glass-mesoporous silica coatings on Ti6Al4V through enameling and triblock-copolymer-templated sol-gel processing. J Biomed Mater Res. 2001;56(3):382-9.
172. Brauer DS, Möncke D. Introduction to the structure of silicate, phosphate and borate glasses. Bioactive Glasses: Fundamentals, Technology and Applications: Royal Society of Chemistry; 2016. p. P61-88.
173. Fagerlund S, Hupa L. Melt-derived Bioactive Silicate Glasses. Bioactive Glasses: Fundamentals, Technology and Applications: Royal Society of Chemistry; 2016. p. P1-26.
174. Oku T, Suganuma K, Wallenberg LR, Tomsia AP, Gomez-Vega JM, Saiz E. Structural characterization of the metal/glass interface in bioactive glass coatings on Ti-6Al-4V. J Mater Sci Mater Med. 2001;12(5):413-7.
175. Moritz N, Vallittu PK. Introduction to the structure of silicate, phosphate and borate glasses. Bioactive Silicate Glass in Implantable Medical Devices: From Research to Clinical Applications: Royal Society of Chemistry; 2016. p. P442-70.
176. Kelly CN, Francovich J, Julmi S, Safranski D, Guldberg RE, Maier HJ, et al. Fatigue behavior of As-built selective laser melted titanium scaffolds with sheet-based gyroid microarchitecture for bone tissue engineering. Acta Biomaterialia. 2019;94:610-26.
177. Ataee A, Li Y, Brandt M, Wen C. Ultrahigh-strength titanium gyroid scaffolds manufactured by selective laser melting (SLM) for bone implant applications. Acta Materialia. 2018;158:354-68.
178. Yánez A, Cuadrado A, Martel O, Afonso H, Monopoli D. Gyroid porous titanium structures: A versatile solution to be used as scaffolds in bone defect reconstruction. Materials & Design. 2018;140:21-9.
179. Fernandes JS, Gentile P, Martins M, Neves NM, Miller C, Crawford A, et al. Reinforcement of poly-l-lactic acid electrospun membranes with strontium borosilicate bioactive glasses for bone tissue engineering. Acta Biomater. 2016;44:168-77.
180. Santocildes-Romero ME, Goodchild RL, Hatton PV, Crawford A, Reaney IM, Miller CA. Preparation of Composite Electrospun Membranes Containing Strontium-Substituted Bioactive Glasses for Bone Tissue Regeneration. Macromolecular Materials and Engineering. 2016;301(8):972-81.
181. Paterson TE, Shi R, Tian J, Harrison CJ, De Sousa Mendes M, Hatton PV, et al. Electrospun Scaffolds Containing Silver-Doped Hydroxyapatite with Antimicrobial Properties for Applications in Orthopedic and Dental Bone Surgery. J Funct Biomater. 2020;11(3).
182. Gentile P, Ferreira AM, Callaghan JT, Miller CA, Atkinson J, Freeman C, et al. Multilayer Nanoscale Encapsulation of Biofunctional Peptides to Enhance Bone Tissue Regeneration In Vivo. Adv Healthc Mater. 2017;6(8).